Universidade de São Paulo
Instituto de Física

Universidade de Hasselt
Faculty of Sciences, Theory Lab

Termodinâmica estocástica de máquinas térmicas colisionais e transição de fase.

Carlos Ernesto Fernández Noa

Orientador (USP): Prof. Dr. Carlos Fiore dos Santos

Orientador (UHASSELT): Prof. Dr. Bart Cleuren

Tese de doutorado apresentada ao Instituto de Física da Universidade de São Paulo, como requisito parcial para a obtenção do título de Doutor em Ciências.

Banca Examinadora:
Prof. Carlos Eduardo Fiore dos Santos (Orientador), Universidade de São Paulo (USP), Brasil.
Prof. Bart Cleuren (Orientador), Universidade de Hasselt (UHASSELT), Bélgica.
Prof. Karel Proesmans, Universidade de Copenhague (UCPH), Dinamarca
Prof. Silvio Salinas, Universidade de São Paulo (USP), Brasil.
Profa. Célia Anteonodo, Pontifícia Universidade Católica do Rio de Janeiro (PUC-Rio), Brasil.
Profa. Letícia Paiva, Universidade Federal de São João del-Rei (UFSJ), Brasil.
Profa. Angelica Souza Mata, Universidade Federal de Lavras (UFLA), Brasil.

São Paulo
2023

FICHA CATALOGRÁFICA
Preparada pelo Serviço de Biblioteca e Informação
do Instituto de Física da Universidade de São Paulo

Fernández Noa, Carlos Ernesto

Termodinâmica estocástica de máquinas térmicas colisionais e transição de fase/ Stochastic thermodynamics of collisional thermal machines and phase transitions. São Paulo, 2023.

Tese (Doutorado) - Universidade de São Paulo. Instituto de Física. Depto. de Física Geral.

Orientador: Prof. Dr. Carlos Eduardo Fiore dos Santos

Área de Concentração: Termodinâmica Estocástica

Unitermos: 1. Produção de entropia; 2. Máquinas térmicas; 3. Eficiência; 4. Transições de fase;

USP/IF/SBI-061/2023

University of São Paulo
Physics Institute

Hasselt University
Faculty of Sciences, Theory Lab

Stochastic thermodynamics of collisional thermal machines and phase transition

Carlos Ernesto Fernández Noa

Supervisor (USP): Prof. Dr. Carlos Fiore dos Santos

Supervisor (UHASSELT): Prof. Dr. Bart Cleuren

Thesis submitted to the Physics Institute of the University of São Paulo in partial fulfillment of the requirements for the degree of Doctor of Science.

Examining Committee:
Prof. Carlos Eduardo Fiore dos Santos (Supervisor), University of São Paulo (USP), Brazil.
Prof. Bart Cleuren (Supervisor), Hasselt University (UHASSELT), Belgium.
Prof. Karel Proesmans, University of Copenhagen (UCPH), Denmark.
Prof. Silvio Salinas, University of São Paulo (USP), Brazil.
Prof. Célia Anteonodo, Pontifical Catholic University of Rio de Janeiro (PUC-Rio), Brazil.
Prof. Letícia Paiva, Federal University of São João Del Rei (UFSJ), Brazil.
Prof. Angelica Souza Mata, Lavras Federal University (UFLA), Brazil.

São Paulo
2023

Dedicatory

To my family, especially Luiz Eduardo.

Acknowledgment

Words cannot express my gratitude to my supervisors Bart Cleuren and Carlos E. Fiore, thank you both for your patience and help, mostly during difficult times of the pandemic. This research would not have been possible without the important collaboration of professors Alexandre Rosas and Grabiel T. Landi. I would like to express my deepest appreciation to my postgraduate colleagues Angel L. L. Stable, Bart Winjs, Bruno A. N. Akasaki, Fernando F. S. Filho, Pedro E. Harunari and William G. C. Oropesa. I would like to extend my sincere thanks to my colleagues from Hasselt University who welcomed me very well during my stays in Belgium. In general, many thanks to all those who, in one way or another, supported me in this project, I mean, staff from both universities, friends, family, and especially my wife Andreza. This study was financed in part by the *Coordenação de Aperfeiçoamento de Pessoal de Nível Superior - Brasil* (CAPES) - Finance Code 001. This project was supported in part by the Special Research Fund (BOF) of Hasselt University under Grant No. BOF20BL1. Last but not least, I am extremely grateful to CAPES and BOF-BILA programs for funding.

Abstract

Non-equilibrium thermodynamics has become one of the main areas of modern statistical mechanics and presenting several applications, such as in phase transitions, biological systems, chemical reactions, engineered systems and others. In the context of small-sized systems (nanometric scale) stochastic thermodynamics was developed and describes energy transformations from the framework of Markov process, hence constituting a relevant toolbox in modern statistical physics. In all these cases, entropy production plays a central role, discerning not only the occurrence or not of certain process but also how energy can be converted into useful work and vice-versa. This PHD thesis is aimed at studying such ideas in the framework of stochastic thermodynamics. In the first part of this thesis, we introduce a strategy for optimizing the performance of Brownian engines, based on a collisional approach. General (and exact) expressions for thermodynamic properties and their optimized values are obtained, irrespective of the driving forces, duration of each stage, the temperatures of reservoirs and protocol to be maximized. Distinct routes for the engine optimization, including maximizations of output power and efficiency with respect to the asymmetry, force and both of them are investigated. The idea of conveniently adjusting/choosing intermediate reservoirs as a strategy for optimizing the performance of a quantum-dot machine sequentially exposed to distinct reservoirs at each stage was also studied, whose thermodynamic quantities (including power and efficiency) can be exactly obtained, irrespective to the number of stages and certain advantages about increasing the number of intermediate stages were discussed. Lastly, we show that entropy production not only locates and distinguishes continuous and first-order phase transitions, but their fluctuations are important in the vicinity of first-order phase transitions and depends on the interplay between observation time and inter-phase tunneling times.

Keywords: Entropy production; Thermal machines; Efficiency; Phase transitions.

Resumo

Nos últimos anos, a termodinâmica de não equilíbrio, aqui referida como termodinâmica estocástica, tornou-se uma das principais áreas da mecânica estatística moderna e apresenta diversas aplicações, como seu estudo em transições de fase, sistemas biológicos, reações químicas, sistemas de engenharia e outros. No contexto de sistemas pequenos (escala nanométrica) a termodinâmica estocástica foi desenvolvida e descreve as transformações de energia por meio da abordagem dos processos markovianos. Devido sua generalidade, ela tornou-se uma ferramenta extremamente relevante na área da física estatística moderna. Em todos os casos, a produção de entropia é uma quantidade que desempenha um papel central, discernindo não apenas a ocorrência ou não de determinado processo, mas também como/se a energia dispendida/gerada pode ser convertida em trabalho útil e vice-versa. Esta tese de doutorado visa o estudo dos temas acima no âmbito da termodinâmica estocástica. Na primeira parte, apresentamos uma estratégia para otimizar o desempenho de motores brownianos, baseada em uma abordagem denominada por nós de colisional. Expressões gerais (e exatas) para propriedades termodinâmicas e seus valores otimizados são obtidos, independentemente da força, tempo de duração entre o sistema e o reservatório, temperaturas dos reservatórios e protocolo a ser maximizado. Diferentes rotas para a otimização do motor, incluindo maximizações de potência de saída e eficiência com relação à assimetria, força e ambas foram investigadas. Também estudamos a ideia de ajustar/escolher convenientemente reservatórios intermediários como estratégia para otimizar o desempenho de uma máquina de um "sistema de dois estados" (*quantum-dot*) exposto sequencialmente, cujas grandezas termodinâmicas (incluindo potência e eficiência) podem ser obtidas exatamente independentemente do número de estágios, de onde as certas vantagens sobre o aumento do número dos estágios foram discutidos. Por fim, mostramos que a produção de entropia não apenas localiza e distingue transições de fase contínuas e de primeira ordem, mas que suas flutuações nas proximidades de transições de fase de primeira ordem são importantes e dependem da interação entre tempo de observação e tempos de tunelamento entre fases.

Palavras chaves: Produção de entropia; Mâquinas térmicas; Eficiência; Transições de fase;

Contents

Chapter 1

Introduction

Thermodynamics is traditionally confined to the description of equilibrium states of macroscopic systems or to the transition between such states. It describes how equilibrium (macroscopic) systems are affected by macroscopic properties, such as temperature, that emerge from the behavior of microscopic constituents. The thermodynamic characterization of equilibrium systems is commonly performed via equilibrium statistical mechanics which states that a system in contact with a heat bath is described by the Boltzmann-Gibbs probability distribution. However, a large number of systems in nature are subject to processes that are far from equilibrium, as prominent examples, we cite biological systems [1], chemical reactions [2, 3], quantum systems [4, 5, 6] and others. Due to the lack of a unified probability distribution in such case, several approaches have been considered. The theory of linear irreversible thermodynamics has become one of the cornerstones of modern statistical physics due to the seminal work of primarily Onsager and Prigogine [7, 8, 9], by including microscopic dynamical properties into the far from equilibrium irreversible realm. Close to equilibrium, one can use this framework to determine the thermodynamic fluxes, such as heat and work, and show that they satisfy general properties. As stated previously, beyond this linear response regime, for a long time, no universal exact results were available.

The starting point of stochastic description for thermodynamics comprise entropy and production of entropy. Usually, the macroscopic limit is characterized by a suppression of fluctuations of physical quantities, both in and out of equilibrium. However, these fluctuations are crucial to understanding systems on smaller scales, thus the need for a stochastic treatment. As stated previously, the second law of thermodynamics leads to a positive increase in the entropy of the system, however, an apparent "violation" was reported in the literature starting in the 1990s. Evans [10] discovered numerically and justified heuristically, for a thermostatted shear-driven

fluid in contact with a heat bath, a remarkable symmetry of the probability distribution of entropy production in the steady state. Then, Gallavotti and Cohen [11] proven the now known as the (steady-state) fluctuation theorem (FT) for a large class of systems using concepts from chaotic dynamics, later for driven Langevin dynamics by Kurchan [12] and for driven diffusive dynamics by Lebowitz and Spohn [13]. As a variant, a transient fluctuation theorem valid for relaxation toward the steady state was found by Evans and Searles [14]. Jarzynski proved a remarkable relation which allows one to express the free energy difference between two equilibrium states by a non-linear average over the work required to drive the system in a non-equilibrium (markovian) process from one state to the other [15, 16]. By comparing probability distributions for the work spent in the original process with the time-reversed one, Crooks found a 'refinement' of the Jarzynski relation (JR), now called the Crooks fluctuation theorem [17, 18]. A close analogy to the JR, which relates different equilibrium states, is the Hatano–Sasa relation that applies to transitions between two different non-equilibrium steady states [19]. Therefore, negative values of entropy production on this mesoscopic level are possible, but experimentally less probable than positive ones.

On the other hand, for driven Brownian motion, Sekimoto realized that two central concepts of classical thermodynamics, namely the exchanged heat and the applied work, can be meaningfully defined on the level of individual trajectories [20, 21]. These quantities entering the first law become fluctuating ones giving birth to what he called stochastic energetics. Also, Maes emphasized that entropy production in the medium is related to that part of the stochastic action which determines the weight of trajectories that is odd under time reversal [22, 23]. Finally, Seifert considered that in addition to the fluctuations of the entropy production in the heat bath one should similarly assign a fluctuating, or 'stochastic', entropy to the system proper [24]. Once this is carried out, the key quantities known from classical thermodynamics are defined along individual trajectories where they become accessible to experimental or numerical measurements. This approach of taking both energy conservation, i.e. the first law, and entropy production seriously on this mesoscopic level has been called stochastic thermodynamics.

Over the last few years, it has become clear that stochastic thermodynamics systematically provides a framework for extending the notions of classical thermodynamics such as work, heat and entropy production to the level of individual trajectories of well-defined non-equilibrium ensembles. On the more practical side, the new formulation allows to address new questions, either related to non-equilibrium properties, such as efficiency, efficiency at maximum power, information to work conversion, or relating to the thermodynamic description of small systems. General theories have been derived for periodically driven systems in contact with a single reservoir [25, 26, 27], multiple reservoirs[28], and for steady-state systems in contact with two reservoirs [29, 30], leading to bounds the power and efficiency of thermodynamic engines [31, 32, 33]. Furthermore, this

theory has lead to applications in several other branches of science, such as information theory [34], chemical reaction networks [2], and active matter [35, 36]. A second milestone in stochastic thermodynamics is the establishment of (original) thermodynamic uncertainty relation that was proposed for biomolecular systems described by Markov dynamics [37]. As a final comment, we highlight the role of entropy production rate in stochastic thermodynamics, supporting its regular presence throughout this thesis: It generalizes the second law for non-equilibrium processes, measures irreversibility, distance to equilibrium and energy dissipation and has particular symmetries in its probability distribution. Entropy production rate is a quantity of theoretical and experimental interest, and it will be analyzed in distinct scenarios.

This thesis is aimed at advancing in aforementioned points, including the proposal of distinct strategies for engineered setups. We proposed/considered the idea of "collisional approach" for Brownian and master equation nanoscale setups. In chapter 2 of this thesis a brief synthesis of the most important foundations of the dynamics stochastic theory will be displayed. First, what is a Markovian process will be discussed. Then, a continuous phase space case will be treated, that is, based on the Langevin formulation for a Brownian particle. Next, we will deal with the case of a discrete phase space, where the master equation is used as the basis of the theoretical formulation. Since the construction of efficient thermal engines operating at finite times constitutes a fundamental and timely topic in non-equilibrium thermodynamics. In the chapter 3 , we introduce a strategy for optimizing the performance of Brownian engines, based on a collisional approach for unequal interaction times between the system and thermal reservoirs. General (and exact) expressions for thermodynamic properties and their optimized values are obtained, irrespective of the driving forces, asymmetry, the temperatures of reservoirs and protocol to be maximized. Distinct routes for the engine optimization, including maximizations of output power and efficiency with respect to the asymmetry, force and both of them are investigated. For the isothermal work-to-work converter and/or small difference of temperature between reservoirs, they are solely expressed in terms of Onsager coefficients. Although the symmetric engine can operate very inefficiently depending on the control parameters, the usage of distinct contact times between the system and each reservoir not only can enhance the machine performance (signed by an optimal tuning ensuring the largest gain) but also enlarges substantially the machine regime operation. The present approach can pave the way for the construction of efficient Brownian engines operating at finite times.

Despite aforementioned sequential (or collisional) engines have been put forward as an alternative candidate for the realisation of reliable engine setups, distinct points, such as understanding the role of the different stages and the influence of the intermediate reservoirs is not well understood. In the chapter 4 we exploit the idea of conveniently adjusting/choosing intermediate reservoirs at engine devices as a strategy for optimizing its performance. This is done by considering a minimal model composed of a quantum-dot machine sequen-

tially exposed to distinct reservoirs at each stage, and for which thermodynamic quantities (including power and efficiency) can be obtained exactly from the framework of stochastic thermodynamics, irrespective to the number of stages. Results show that a significant gain can be obtained by increasing the number of stages and conveniently choosing their parameters.

A stochastic treatment also extends the prosperous field of phase transitions, in particular non-equilibrium phase transitions. Discontinuous phase transitions out of equilibrium can be characterized by the behavior of macroscopic stochastic currents. But while much is known about the average current, the situation is much less understood for higher statistics. In chapter 5, we study how relevant fluxes behave during continuous and first-order phase transitions; not only their averages, but also higher-order moments. We address the consequences of the diverging metastability lifetime – a hallmark of discontinuous transitions – in the fluctuations of arbitrary thermodynamic currents, including the entropy production. The behavior of the entropy production rate proves to constitute a powerful tool for localizing and characterizing phase transitions. In particular, we center our discussion on the *conditional* statistics, given which phase the system is in. We highlight the interplay between integration window and metastability lifetime, which is not manifested in the average current, but strongly influences the fluctuations. We introduce conditional currents and find, among other predictions, their connection to average and scaled variance through a finite-time version of Large Deviation Theory and a minimal model. Our results are then further verified in two paradigmatic models of discontinuous transitions: Schlögl's model of chemical reactions, and a 12-states Potts model subject to two baths at different temperatures.

Chapter 2

Theoretical foundations

2.1 Stochastic Dynamics

As described previously, sufficiently small systems, generally on the mesoscopic scale, are significantly affected by fluctuations. In this way, we can consider the magnitudes of the system as random variables, for instance, the velocity of a Brownian particle, the state (occupied or empty) of a quantum dot or the order parameter of a system that presents a discontinuous phase transition within the criticality zone. The dynamics that describe this type of processes becomes Markovian, i.e. the future state of the system depends only on the present one with no memory of the past. If the states are made up by continuous variables (such as position or velocity), the dynamics is commonly described by a Langevin equation for an individual system and a Fokker–Planck equation for the whole ensemble. Sometimes it is more convenient to identify discrete states with transition rates governing the dynamics which, on the ensemble level, leads to a master equation.

In this chapter we briefly present the main aspects of the theory. Firstly, the formulation to describe the systems that present a continuous phase space is illustrated through a collisional model system: a colloidal particle in sequential contact with different thermal reservoirs and subject to the action of an external time-dependent force (or driving force). This model system, also known as Brownian particle, can arguably serve as the paradigm for the field, since the main concepts of stochastic thermodynamics can be introduced using it. This Brownian particle, depending of the set parameters, can be interpreted as an engine that can release work.

Next, thermodynamic relations are derived for systems that present a discrete phase state. To introduce these ideas we use an other collisional model consisting of a quantum dot in sequential contact with different chemical

reservoirs. This system is capable of transporting particles from one reservoir to another, consuming energy supplied from an external source, working like a bomb, or, on the contrary, it can funtionate as a engene, realising work from consuming chemical energy.

2.2 Continuous state

We begin with a brief description of the simplest case of one particle performing a random movement, which we call Brownian motion, and subjected to two forces. One dissipative, which we assume to be proportional to its velocity, and another of random character due to the impact of the particle with the molecules of the medium. The time evolution of the velocity v can be determined using the Langevin equation:

$$\frac{dv}{dt} = -\gamma v + \zeta(t). \tag{2.1}$$

where γ is a viscous constant and $\zeta(t)$ is a stochastic force (interaction between particle and the reservoir), all divided by the mass of the particle. The stochastic force satisfies the white noise properties

$$\langle \zeta(t) \rangle = 0 \qquad \text{and} \qquad \langle \zeta(t)\zeta(t') \rangle = \Gamma \delta(t - t') \tag{2.2}$$

where Γ is a coefficient associated to the reservoir temperature. An important property of the Langevin equation is that the net displacement is due only to the external force, since the random force does not have preferential directions. However, higher-order moments of the position are also related to the temperature, and thus the diffusion depends on it. In reference [38] is shown in detail how to obtain the values for the mean velocity $\langle v \rangle$ and and the mean square velocity $\langle v^2 \rangle$, they are

$$\langle v \rangle = v_0 e^{-\gamma t} \qquad \text{and} \qquad \langle v^2 \rangle = \frac{\Gamma}{2\gamma}(1 - e^{-\gamma t}) \tag{2.3}$$

For large times, that is, in the stationary regime, $\langle v \rangle = 0$ and the mean-square velocity becomes $\langle v^2 \rangle = \frac{\Gamma}{2\gamma}$

Expanding the characteristic function of a discretized version of Eq. (2.1) [38], it is possible to derive the evolution for the probability density, the Fokker-Planck equation

$$\frac{\partial P}{\partial t} = -\frac{\partial J}{\partial v}, \tag{2.4}$$

where P is the probability density function of a particle following a Langevin equation, and J is the probability current

$$J = -\gamma v P - \frac{\Gamma}{2}\frac{\partial P}{\partial v}. \tag{2.5}$$

We suppose that the variable v takes values in the interval $[v_i, v_f]$. If we integrate both sides of Eq. (2.4) in v, we get

$$\frac{\partial}{\partial t}\int_{v_i}^{v_f} P(v,t)dv = J(v_i,t) - J(v_f,t) \tag{2.6}$$

Since the probability density must be normalized at any time, that is

$$\int_{v_i}^{v_f} P(v,t)dv = 1 \tag{2.7}$$

then the left-hand side of Eq. (2.6) should vanish, from which we may conclude that the boundary conditions are such that $J(v_i,t) = J(v_f,t)$. Thus, the conservation of total probability (2.7) is not only consequence of the Fokker-Planck equation but also of the boundary conditions. We will treat in this section only the case in which the probability current vanishes at the ends, $v = v_i$ and $v = v_f$, at any instant t, that is, $J(v_i,t) = J(v_f,t) = 0$. The boundary condition such that the probability current vanishes is called reflecting.

There are other boundary conditions for the Fokker-Planck equation, which we choose according to the problem we wish to solve. The periodic boundary conditions are such that $P(v_i,t) = P(v_f,t)$ and $J(v_i,t) = J(v_f,t)$ so that in this case the total probability is also conserved. However, unlike the reflecting boundary condition, the probability current at the boundaries is, in general, nonzero. The boundary condition, called absorbing, is such that only P vanishes at the boundary. The derivative $\frac{\partial P}{\partial v}$ as well as the probability current are nonzero. If the currents are distinct at the ends, the condition (12.7) is not fulfilled.

A steady state is reached when the probability distribution function is not longer time dependent, this means $\frac{\partial P}{\partial t} = 0$, therefore, as we can verified in equation (2.4), this implies that the current does not depend explicitly on the velocity. On the other hand, since P does not depend on time, we can ensure through equation (2.5) that the current J does not depend on time either. Therefore, it must have the same value for any v. But since it vanishes at the ends of the interval $[v_i, v_f]$, it must be zero in the whole interval, that is,

$$J(v) = 0. \tag{2.8}$$

which is to be understood as the microscopic reversibility condition, in other words, is the detailed balance condition for continuous state-space and the stationary distribution is known as equilibrium. Therefore, the stationary distribution $P(v)$ obeys the equation

$$-\gamma v P - \frac{\Gamma}{2}\frac{dP}{dv} = 0 \qquad \text{or yet} \qquad \frac{d}{dv}\ln P = -\frac{2\gamma v}{\Gamma}. \tag{2.9}$$

from which we obtain the equilibrium probability distribution $P_{eq}(v)$:

$$P_{eq}(v) = Ae^{-\frac{2\gamma v^2}{\Gamma}} \tag{2.10}$$

where A is a normalization constant. The present description can be extended for an arbitrary number of particles by considering a family of Langevin equations with uncorrelated noise functions. The joint probability density $P(v_1, v_2, ..., t)$ will follow a multi-variate Fokker Planck equation that has can be written as

$$\frac{\partial}{\partial t}P(v_1, v_2, ..., t) = -\sum_j \frac{\partial}{\partial v_j}J_j(v_1, v_2, ..., t), \tag{2.11}$$

As we have seen so far, after a long enough time, the system will evolve towards a steady state of equilibrium, provided the system is placed in contact with a single thermal bath and devoid of non-conservative forces [38, 39].

Next, we discuss some fundamental concepts about the system placed in contact with distinct thermal baths and subjected to distinct drivings each stroke. For simplicity, we shall curb ourselves on the case of a Brownian particle with mass m sequentially and cyclically placed in contact with different thermal reservoirs, each at a temperature T_i for a time interval τ_i. Here $i = 1, \ldots, N$ label the reservoirs and also the order of contact between the reservoirs and the particle. The fact of placing the particle sequentially in contact with two or more reservoirs is enough to generate a stationary state out of equilibrium. The interaction time with each reservoir can be the same (symmetric case) or we can assign a different interaction time for each reservoir (asymmetric case), both cases present different results and will be analyzed in more detail in the next chapter. Each reservoir, let's say the i-th one, is associated to a medium with viscous constant γ_i, an external force (or driving force) f_i and stochastic forces (interaction between particle and the reservoir), all divided by the mass of the particle. The external (driving) force is a function of time and is the second ingredient in throwing the system out of equilibrium. There are several driving force dependencies on time , the constant, the linear and the exponential drivings are some examples that we will to study in the next chapter. The time evolution of the velocity v_i can be determined using the Langevin equation:

$$\frac{dv_i}{dt} = -\gamma_i v_i + f_i(t) + \zeta_i(t). \tag{2.12}$$

Where the stochastic force $\zeta_i(t)$ accounts for the interaction between particle and the i-th environment and satisfies the white noise properties

$$\langle \zeta_i(t) \rangle = 0 \qquad \text{and} \qquad \langle \zeta_i(t)\zeta_{i'}(t') \rangle = 2\gamma_i T_i \delta_{ii'}\delta(t - t') \tag{2.13}$$

On the other hand, the system evolves to a non equilibrium steady state regime (*NESS*) characterized by a non-vanishing production of entropy. The probability distribution is governed by the Fokker-Planck equation:

$$\frac{\partial P_i}{\partial t} = -\frac{\partial J_i}{\partial v} - f_i(t)\frac{\partial P_i}{\partial v}, \tag{2.14}$$

where J_i is the probability current

$$J_i = -\gamma_i v P_i - \frac{\gamma_i k_B T_i}{m}\frac{\partial P_i}{\partial v}. \tag{2.15}$$

As can be verified by direct substitution, the non-equilibrium steady state *(NESS)* is characterized by a Gaussian probability distribution $P_i(v,t)$:

$$P_i(v,t) = \frac{1}{\sqrt{2\pi b_i(t)}} e^{-\frac{(v-\langle v_i\rangle)^2}{2b_i(t)}}, \tag{2.16}$$

for which the mean $\langle v_i\rangle(t)$ and the variance $b_i(t) \equiv \langle v_i^2\rangle(t) - \langle v_i\rangle^2(t)$ are time-dependent and obey the following equations of motion

$$\frac{d}{dt}\langle v_i\rangle(t) = -\gamma_i\langle v_i\rangle(t) + f_i(t), \qquad \text{and} \qquad \frac{d}{dt}b_i(t) = -2\gamma_i b_i(t) + \Gamma_i, \tag{2.17}$$

where $\Gamma_i = 2\gamma_i k_B T_i/m$. Obviously, the continuity of the probability distribution must be assured whenever the particle changes its environment, and should use it to calculate $b_i(t)$ and $\langle v_i\rangle(t)$.

2.2.1 Stochastic Thermodynamics

In order to derive explicit expressions for macroscopic quantities, we start from the definitions of the average kinetic energy $U_i = m\langle v_i^2\rangle/2$ and entropy $S_i(t) = -k_B\langle \ln[P_i(v,t)]\rangle$, respectively. In both cases, the time variation can be straightforwardly obtained from the Fokker-Planck equation and applying vanishing boundary conditions for both $P_i(v,t)$ and $J_i(v,t)$ in the infinity speed limit [38]. Differentiating the kinetic energy with respect to time reads

$$\frac{dU_i}{dt} = \frac{m}{2}\frac{d}{dt}\langle v_i^2\rangle = \frac{m}{2}\frac{d}{dt}[b_i(t) + \langle v_i\rangle^2(t)] = \frac{m}{2}\left[\frac{d}{dt}b_i(t) + 2\langle v_i\rangle\frac{d}{dt}\langle v_i\rangle(t)\right] \tag{2.18}$$

Using the expressions (2.17) and simplifying reads

$$\frac{dU_i}{dt} = -\left[-m\langle v_i\rangle(t)f_i(t) + m\gamma_i\left(\langle v_i^2\rangle(t) - \frac{\Gamma_i}{2\gamma_i}\right)\right] \tag{2.19}$$

The first term is related to the average power dissipated $\dot{W}_i$ and the second term is the heat dissipation during the same period $\dot{Q}_i$ through the first law of thermodynamics relation:

$$\frac{dU_i}{dt} = -[\dot{W}_i(t) + \dot{Q}_i(t)], \tag{2.20}$$

where $\dot{W}_i(t)$ and $\dot{Q}_i(t)$ are given by the following expressions:

$$\dot{W}_i(t) = -m\langle v_i\rangle(t)f_i(t) \qquad \text{and} \qquad \dot{Q}_i(t) = m\gamma_i\left(\langle v_i^2\rangle(t) - \frac{\Gamma_i}{2\gamma_i}\right). \tag{2.21}$$

Similarly, differentiating the entropy $S_i(t)$ with respect to time, the rate of variation of the entropy can be written as [30, 40]:

$$\frac{dS_i}{dt} = \Pi_i(t) - \Phi_i(t), \tag{2.22}$$

where $\Pi_i(t)$ and $\Phi_i(t)$ denote the entropy production rate and the flux of entropy, respectively, which expressions are given by,

$$\Pi_i(t) = \frac{2k_{\mathrm{B}}}{\Gamma_i} \int_{\tilde{\tau}_{i-1}}^{t} \frac{J_i^2}{P_i} dv, \tag{2.23}$$

and

$$\Phi_i(t) = -\frac{2\gamma_i k_B}{\Gamma_i} \int_{\tilde{\tau}_{i-1}}^{t} v J_i dv = \frac{2\gamma_i k_{\mathrm{B}} \dot{Q}_i(t)}{m\Gamma_i} = \frac{\dot{Q}_i(t)}{T_i}, \tag{2.24}$$

respectively, where $\tilde{\tau}_i = \sum_{j=1}^{i} \tau_j$ (with $\tau_0 \equiv 0$). Both expression are valid during the contact of the Brownian particle with the i-th reservoir. Above relations are the starting point for obtaining averages over a complete cycle, providing the calculation of power, efficiency and others.

2.3 Discrete state

When the system in question presents a discrete phase space we used a different formulation. In this case, the time evolution of the probability distribution function is determined by the master equation

$$\frac{d}{dt} P_m = \sum_{m'} \omega_{m,m'} P_{m'}. \tag{2.25}$$

Here $\omega_{m,m'}$ is the probability per unit time to make a transition from state m' to m. We use the shorthand notation with diagonal elements defined as

$$\omega_{m,m} = -\sum_{m \neq m'} \omega_{m,m'}. \qquad \text{Alternatively} \qquad \sum_{m} \omega_{m,m'} = 0 \tag{2.26}$$

a property that guarantees the conservation of normalization. The transition rates have to satisfy an additional property. In the steady state, the system is at equilibrium with the reservoir. Statistical physics prescribes that the steady state distribution is given by the grand canonical equilibrium distribution P_m^{eq}

$$P_m^{eq} = \exp\{-\beta(\epsilon_m - \mu n_m - \Omega^{eq})\} \tag{2.27}$$

The (equilibrium) grand potential Ω^{eq} follows from the normalization of P_m^{eq}

$$\exp\{-\beta\Omega^{eq}\} = \sum_{m} \exp\{-\beta(\epsilon_m - \mu n_m)\} \tag{2.28}$$

The crucial property that is required from the rates is the so-called condition of detailed balance, i.e., at equilibrium every transition, say from m to m', and its inverse, from m' to m, have to be equally likely

$$\omega_{m,m'} P_{m'}^{eq} = \omega_{m',m} P_m^{eq}. \tag{2.29}$$

Combined with the explicit expression of the equilibrium distribution, this gives:

$$k_B \ln\left(\frac{\omega_{m',m}}{\omega_{m,m'}}\right) = \frac{\epsilon_m - \epsilon_{m'} - \mu(n_m - n_{m'})}{T} = \frac{Q_{m',m}}{T}. \tag{2.30}$$

is the "elementary" heat absorbed by the system to make the transition from m' to m. We stress that in the presence of driving, which is shifting the energy levels in time, this relation is supposed to hold at each moment in time, hence the rates also become time-dependent. This condition will be crucial to obtain the correct formulation of the second law.

In order to illustrate above ideas, we consider a collisional model consisting in a quantum dot (QD) in sequential contact with different reservoirs. This system can be in two possible states, if an electron is absorbed while the QD is in contact with the i-th reservoir, then it pass to be from an "empty" state with energy zero to be in an "occupied" state with energy ϵ_i. We call the probability of the system to be in the occupied state as $p_i(t)$ and as $1 - p_i(t)$ the probability to be in the empty state. The time evolution of $p_i(t)$ at the i-th stroke is determined by the master equation

$$\dot{p}_i(t) = [1 - p_i(t)]\,\omega_{01}^{(i)} - p_i(t)\omega_{10}^{(i)}, \tag{2.31}$$

where the rates $\omega_{01}^{(i)}$ and $\omega_{10}^{(i)}$ account to filling up ($0 \to 1$) and vice versa ($1 \to 0$) respectively. These rates depend on ϵ_i and the chemical potential μ_i and are given by

$$\omega_{01}^{(i)} = \frac{\Gamma_0}{1 + e^{A_i}} \qquad \text{and} \qquad \omega_{10}^{(i)} = \frac{\Gamma_0 e^{A_i}}{1 + e^{A_i}}, \tag{2.32}$$

where Γ_0 quantifies the coupling strength between the system and thermal bath (for simplicity taken equal in all cases) and $A_i = \frac{1}{T}(\epsilon_i - \mu_i)$ for the i-th stroke. The Perron-Frobenius theorem states certain properties that transition rates should satisfy in order to ensure system evolution to a unique steady state. An important relation to be considered is the detailed balance condition (DBC), in our quantum dot this is

$$[1 - p_i(t)]\,\omega_{01}^{(i)} = p_i(t)\omega_{10}^{(i)}, \tag{2.33}$$

in others words, the probability of the system transitioning from state empty to occupied state is the same as the reverse transition from occupied state to empty state. This condition implies a microscopic reversibility of the system, it means that Eq (2.33) is only valid when the probability $p_i(t)$ is the equilibrium probability. Therefore, if it is satisfied, the system converges to equilibrium steady state, it would happen if our system remained in contact with only one reservoir, but sequential switching with other reservoirs implies a temporal dependence on the transition rates (given by ϵ_i and μ_i) that break the detailed balance. When the detailed balance is broken the system converges to a non equilibrium steady state (NESS).

2.3.1 Stochastic Thermodynamics of collisonal setups

Thermodynamic relations are derived starting from the system energy given by $E(t) = \epsilon(t)p(t)$ where we introduce $\epsilon(t)$ / $p(t)$ as the energy level / occupation probability of the QD at time t. The time derivative of $E(t)$ gives two contributing terms:

$$\dot{E}(t) = \underbrace{\dot{\epsilon}(t)p(t)}_{\text{“direct drive"}} + \underbrace{\epsilon(t)\dot{p}(t)}_{\text{“exchange"}} \tag{2.34}$$

the former identified as direct driving and appearing only during the external driving phases (during which $\dot{\epsilon}(t) \neq 0$). It can also be identified as the *direct work* $\dot{W}_{\mathrm{d}}$ given by

$$\dot{W}_{\mathrm{d}}(t) = \sum_{i=1}^{N} (\epsilon_{i+1} - \epsilon_i)\, \delta\left(t - \frac{i\tau}{N}\right) p_i(t), \tag{2.35}$$

where periodic boundary conditions for the index i, i.e. $\epsilon_{i+N} = \epsilon_i$ have been employed. We stress that $\dot{W}_{\mathrm{d}}(t) > 0$ according to whether the energy of the QD increases. By averaging it over one full period, one has that

$$\overline{\dot{W}}_{\mathrm{d}} \equiv \frac{1}{\tau}\int_0^{\tau} \dot{W}_{\mathrm{d}}(t)dt = \frac{1}{\tau}\sum_{i=1}^{N} (\epsilon_{i+1} - \epsilon_i)\, p_i\left(\frac{i\tau}{N}\right). \tag{2.36}$$

The second term $\epsilon(t)\dot{p}(t)$ appears during the exchange phases and it is different from zero provided an exchange of particles takes place. From the integration of $\dot{p}(t)$ from $\tau_{i-1} = (i-1)\tau/N$ to τ_i, one can re-express it as $\overline{J}_i \equiv dN_i/\tau$ as the average net number of particles exchanged during stage i per period, given by

$$\overline{J}_i = \frac{1}{\tau}\left[p_i\left(\frac{i\tau}{N}\right) - p_i\left(\frac{(i-1)\tau}{N}\right)\right]. \tag{2.37}$$

The *total* energy exchange dE_i during the exchange phase of stage i is rewritten as

$$dE_i \equiv \int_{\frac{(i-1)\tau}{N}}^{\frac{i\tau}{N}} \epsilon(t)\dot{p}_i(t)dt = \epsilon_i dN_i. \tag{2.38}$$

From the reservoir viewpoint, above expression can be split in two parts: $dE_i = (\epsilon_i - \mu_i)\, dN_i + \mu_i dN_i$, the former and latter terms identified as heat and chemical work respectively, counted positive when *delivered to* the QD, i.e. when the energy of the QD increases. By averaging Eqs. (2.34) and (2.38) over one full period and using Eq. (2.37), it follows that $\overline{\dot{W}}_{\mathrm{d}} + \overline{\dot{Q}} + \overline{\dot{W}}_{\mathrm{ch}} = 0$, where $\overline{\dot{Q}}$ and $\overline{\dot{W}}_{\mathrm{ch}}$ are given by

$$\overline{\dot{Q}} = \sum_{i=1}^{N} (\epsilon_i - \mu_i)\, \overline{J}_i\ ; \tag{2.39}$$

$$\overline{\dot{W}}_{\mathrm{ch}} = \sum_{i=1}^{N} \mu_i \overline{J}_i\ ; \tag{2.40}$$

$$\overline{\dot{W}}_{\mathrm{d}} = -\sum_{i=1}^{N} \epsilon_i \overline{J}_i. \tag{2.41}$$

Defining the nonequilibrium entropy for a discrete space phase by $S(t) = -k_B \sum_m P_m(t) \ln P_m(t)$ we will show that this definition is a proper choice that reduces to the standard thermodynamic entropy at equilibrium, but with the additional advantage that it preserves – in nonequilibrium – the basic features of the second law, namely the relation between heat and entropy exchange and the positivity of the entropy production. Explicitly, we will arrive at the same expression (2.22) obtained for the continuous phase space, where $\Phi(t) = \frac{\dot{Q}(t)}{T}$ and $\Pi \geq 0$. We start differentiating S respect to time

$$\frac{dS}{dt} = -k_B \sum_m (\ln P_m + 1)\frac{dP_m}{dt} = -k_B \sum_{m,m'} \omega_{m,m'} P_{m'} \ln P_m \tag{2.42}$$

where we used the fact that $\sum_m \frac{dP_m}{dt} = \frac{d}{dt}\sum_m P_m = 0$ due to the probability conservation and then, at the second step, we used the master equation. By making small readjustments we can transform expression 2.42 to the form:

$$\begin{aligned} \frac{dS}{dt} &= \frac{k_B}{2} \sum_{m,m'} (\omega_{m,m'} P_{m'} - \omega_{m',m} P_m) \ln \frac{P_{m'}}{P_m} \\ &= \frac{k_B}{2} \sum_{m,m'} (\omega_{m,m'} P_{m'} - \omega_{m',m} P_m) \ln \frac{\omega_{m,m'} P_{m'}}{\omega_{m',m} P_m} + \frac{k_B}{2} \sum_{m,m'} (\omega_{m,m'} P_{m'} - \omega_{m',m} P_m) \ln \frac{\omega_{m',m}}{\omega_{m,m'}} \end{aligned} \tag{2.43}$$

The first term is the entropy production rate Π, this expression is known as Schnakenberg's formula [41]. Check that it is always non negative because $(x-y)\ln(x/y) \geq 0$, vanishing when the detailed balance is fulfilled. Thus it distinguishes equilibrium from nonequilibrium systems. On the other hand, the second term is a microscopic relation for the flux

$$\Phi(t) = k_B \sum_{m,m'} \omega_{m,m'} P_{m'} \ln \frac{\omega_{m,m'}}{\omega_{m',m}}. \tag{2.44}$$

Returning to our quantum dot model, once NESS has been reached, the value of the time derivative of entropy, averaged over a period, must equal zero. That is

$$\overline{\dot{S}} = 0 \qquad \text{which implies that} \qquad \overline{\Phi} = \overline{\Pi} \tag{2.45}$$

then the Schnakenberg's formula reads

$$\overline{\Phi} = \overline{\Pi} = \frac{k_B}{2\tau} \sum_{i=1}^{N} \int_{\frac{(i-1)\tau}{N}}^{\frac{i\tau}{N}} [\omega_{01}^{(i)}(1 - p_i(t)) - \omega_{10}^{(i)} p_i(t)] \ln \frac{\omega_{01}^{(i)}(1 - p_i(t))}{\omega_{10}^{(i)} p_i(t)} \mathrm{d}t, \tag{2.46}$$

Taking into account the periodicity of $p_i(t)$ and the first law of thermodynamics, this expression can be rewritten in the following form:

$$\overline{\Phi} = -\frac{\overline{\dot{Q}}}{T} = \frac{\overline{\dot{W}}_{\mathrm{d}} + \overline{\dot{W}}_{\mathrm{ch}}}{T}, \tag{2.47}$$

consistent to the ratio between the total average heat and the system temperature, as expected. Note that Eq. (2.44) constitutes an alternative (and advantageous) formula for evaluating the steady entropy production, since it corresponds to an average that can be evaluated from the transition rates.

2.4 Entropy production at phase transitions: An overview

Despite the recent advances of stochastic thermodynamics, a fundamental question is whether entropy production can be used as a reliable tool for typifying nonequilibrium phase transitions. In this section, we present the main aspects about the entropy behavior at phase transition regime. More details can be found in [42]. Here I shall describe the main details.

As equilibrium phase transitions, nonequilibrium ones can be typified by the usage of an order parameter. By focusing ourselves in the case "up-down" Z_2 symmetry, but very common in statistical mechanic systems, a continuous phase transition in such class of models is, heuristically, described by the general logistic order-parameter equation:

$$\frac{d}{dt}m = a(q - q_c)m - bm^3, \tag{2.48}$$

where q denotes the control parameter and a and b are positive constants. It has two steady solutions: $m^{(D)} = 0$ (disordered phase) and $m^{(S)} = \pm\sqrt{a(q - q_c)/b}$ (ordered phase), stable for low and large values of q, respectively. The phase transition follows the mean-field exponent $\beta_{mf} = 1/2$ and m vanishes as $m \sim e^{a(q-q_c)t}$ for $q < q_c$ when $m \ll 1$. In a similar fashion, discontinuous phase transitions can also be treated under a mean-field point of view, but in such a case one requires the inclusion of an additional term $+cm^5$ for reporting them [43]:

$$\frac{d}{dt}m = a(q_b - q)m - bm^3 + cm^5, \tag{2.49}$$

where $c > 0$. It exhibits three steady state solutions m: $m^{(D)} = 0$, $m^{(S)}$ and $m^{(U)}$. At $q = q_f = (b^2/4ac) - q_b$, m jumps from $m_1 \equiv m^{(S)}(q_f)$ to $m^{(D)} = 0$. For $q > q_f$, m behaves as $m \sim e^{a(q_b-q)t}$ for $m_0 \ll 1$ irrespective the initial condition $m_0 > 0$. The frontier $q = q_b$ separates the exponential vanishing of $m \sim e^{a(q_b-q)t}$ $(q > q_b)$ from the convergence to a well definite $m_2 \equiv m^{(S)}(q)$ $(q < q_b)$ when $m_0 \ll 1$. For $q_b < q < q_f$ (hysteretic branch), m behaves as follows: $m(t \to \infty) \to m^{(D)}$ if $m_0 < m^{(U)}$, $m(t \to \infty) \to m^{(S)}$ if $m_0 > m^{(U)}$ and only for $m_0 = m^{(U)}$ one has $m(t \to \infty) \to m^{(U)}$. For this reason $m^{(U)}$ is an unstable solution.

Despite largely studied, above characterization of phase transitions hides the irreversible character of the dynamics as well as its influence on the phase transition properties. In order to describe the entropy production behaviors in aforementioned class of systems, we consider a generic dynamics with up-down symmetry described by a one-site dynamics. In such case, Eq. (2.25) acquires the following form:

$$\frac{d}{dt}P(\sigma, t) = \sum_{i=1}^{N}\{w_i(\sigma^i)P(\sigma^i, t) - w_i(\sigma)P(\sigma, t)\}, \tag{2.50}$$

where each microscopic configuration σ is set by the collection of N individuals $\sigma \equiv (\sigma_1, \sigma_2, ..., \sigma_i, ..., \sigma_N)$, with σ_i being the spin variable of site i which takes the values ± 1 according to whether the spin is “up" or

"down", and $w_i(\sigma)$ comprises the transition rate at which each site i changes its opinion from σ_i to $-\sigma_i$, given by the expression $w(\sigma_i) = \frac{1}{2}[1 - q\sigma_i g(X)]$, with q denoting the control parameter and $g(X)$ expressing the generic dependence on a local neighborhood of k spins. Only two assumptions regarding $g(X)$ are required. The first is that due to the Z_2 symmetry, it depends on the sign of the local spin neighborhood (odd function). Also, taking into account that $w(\sigma_i)$ is constrained between 0 and 1, the product $|qg(X)| \leq 1$ for all values of X. These assumptions allow us to rewrite $g(X)$ as $g(X) = |g(X)|S(X)$, where $S(X)$ denotes the sign function: sign$(X) = 1(-1)$ and 0, according to $X > 0 (< 0)$ and $X = 0$, respectively, where $|g(X)|$ gets restricted between 0 and $|g(k)|$.

From Eq. (2.50), one finds that the time evolution of order parameter $m = \langle\sigma_i\rangle$ is given by

$$\frac{d}{dt}\langle\sigma_i\rangle = -2\langle\sigma_i w(\sigma_i)\rangle. \tag{2.51}$$

In the steady state $m = q\langle|g(X)|S(X)\rangle$. For the evaluation of Π, one requires the calculation of $w_i(\sigma)\ln[w_i(\sigma)/w_i(\sigma^j)]$ given by

$$\frac{1}{2}\left[\sigma_i S(X) - q|g(X)|S^2(X)\right]\ln\frac{1-q|g(X)|}{1+q|g(X)|}. \tag{2.52}$$

The reverse transition rate $w_i(\sigma^j)$ was obtained by performing the transformation $\sigma_i \to -\sigma_i$ resulting in $w_i(\sigma^j) = \frac{1}{2}[1 + q\sigma_i g(X)]$. The one-site Mean Field Theory (MFT) consists of rewriting the joint probability $P(\sigma_i, ..., \sigma_k)$ as a product of one-site probabilities $P(\sigma_i)...P(\sigma_k)$, from which one derives closed relations for the correlations from which we obtain the properties as function of the control parameters. Since the main marks of critical and discontinuous phase transitions are not expected to depend on the particularities of $g(X)$, it is reasonable, within the MFT, to replace the averages in terms of an effective $\bar{g}$ given by

$$m = q\langle|g(X)|S(X)\rangle \to q\bar{g}\langle S(X)\rangle, \tag{2.53}$$

$$\frac{1}{2}\left\langle\sigma_i S(X)\ln\frac{1-q|g(X)|}{1+q|g(X)|}\right\rangle \to \frac{1}{2}\ln\frac{1-q\bar{g}}{1+q\bar{g}}\langle\sigma_i S(X)\rangle, \tag{2.54}$$

and

$$\frac{1}{2}\left\langle|g(X)|S^2(X)\ln\frac{1-q|g(X)|}{1+q|g(X)|}\right\rangle \to \frac{\bar{g}}{2}\ln\frac{1-q\bar{g}}{1+q\bar{g}}\langle S^2(X)\rangle. \tag{2.55}$$

At this level of approximation the steady entropy production then reads

$$\Pi = \frac{1}{2}\ln\frac{1-q\bar{g}}{1+q\bar{g}}\left[m\langle S(X)\rangle - q\bar{g}\langle S^2(X)\rangle\right]. \tag{2.56}$$

Above averages are calculated by decomposing the mean sign function in two parts:

$$\langle S(X)\rangle = \langle S(X_+)\rangle - \langle S(X_-)\rangle, \qquad \text{and} \qquad \langle S^2(X)\rangle = \langle S(X_+)\rangle + \langle S(X_-)\rangle, \tag{2.57}$$

with each term being approximated by

$$\langle S(X_\pm)\rangle = \pm\sum_{n=\lceil k/2\rceil}^{k} C_n^k p_\pm^n p_\mp^{k-n}, \tag{2.58}$$

where $\lceil ... \rceil$ is the ceiling function and for $S(X_+)[S(X_-)]$ the term C_n^k takes into account the number of possibilities of a neighborhood with n spins in the $+1[-1]$ states with associated probabilities $p_\pm = (1 \pm m)/2$. Eqs. (2.57) become simpler in the regime of large connectivities. To see this, we first note that each term of the binomial distribution approaches a Gaussian with mean $kp_\pm$ and variance $\sigma^2 = kp_+p_-$, so that

$$\sum_{n=\lceil k/2 \rceil}^{k} C_n^k p_\pm^n p_\mp^{k-n} \to \frac{1}{\sigma\sqrt{2\pi}} \int_{k/2}^{k} e^{-\frac{(\ell - kp_\pm)^2}{2\sigma^2}} d\ell = \frac{1}{2}\sqrt{\pi}\left\{ \mathrm{erf}\left[\frac{k(1-p_\pm)}{\sqrt{2}\sigma}\right] - \mathrm{erf}\left[\frac{k(1/2-p_\pm)}{\sqrt{2}\sigma}\right]\right\}, \tag{2.59}$$

where $\mathrm{erf(x)} = 2\int_0^x e^{-t^2} dt/\sqrt{\pi}$ denotes the error function. Since for large k, $\mathrm{erf}[k(1-p_\pm)/\sqrt{2}\sigma] \to 1$ ($\langle S^2(X)\rangle \to 1$), the expressions for m and Π read

$$m = q\bar{g}\left[\mathrm{erf}\Big(\sqrt{\frac{k}{2}}m\Big)\right], \qquad \text{and} \qquad \Pi = \frac{1}{2}\ln\frac{1-q\bar{g}}{1+q\bar{g}}\left[\frac{m^2}{q\bar{g}} - q\bar{g}\right], \tag{2.60}$$

respectively. At the vicinity of the critical point m behaves as $m \sim (q-q_c)^{1/2}$. So that, one reaches the following expressions for the entropy production:

$$\Pi \sim \frac{1}{2}\ln\frac{1+q\bar{g}}{1-q\bar{g}}\left[\frac{q_c - q}{q\bar{g}} + q\bar{g}\right], \qquad \text{for } q < q_c, \text{ and} \qquad \Pi = \frac{q\bar{g}}{2}\ln\frac{1+q\bar{g}}{1-q\bar{g}}, \tag{2.61}$$

for $q > q_c$. Hence the entropy production is continuous at the critical point q_c, with $\Pi_c = \frac{q_c\bar{g}}{2}\ln\frac{1+q_c\bar{g}}{1-q_c\bar{g}}$. However, its first derivative is discontinuous, jumping from

$$\Pi' = \frac{q_c\bar{g}^2}{1-q_c^2\bar{g}^2} + \frac{1-q_c\bar{g}^2}{2q_c\bar{g}}\ln\frac{1-q_c\bar{g}}{1+q_c\bar{g}}, \qquad \text{when } q \to q_c^-, \text{ to} \qquad \Pi' = \frac{q_c\bar{g}^2}{1-q_c^2\bar{g}^2} - \frac{\bar{g}}{2}\ln\frac{1-q_c\bar{g}}{1+q_c\bar{g}}, \tag{2.62}$$

when $q \to q_c^+$, whose discontinuity of $-\frac{1}{2q_c\bar{g}}\ln\frac{1-q_c\bar{g}}{1+q_c\bar{g}}$ is associated with the critical exponent $\alpha_{mf} = 0$. Remarkably, having the classical exponents β_{mf} and γ_{mf} (evaluated from the order-parameter variance [38]), we see that the hyperscaling relation $\alpha_{mf} + 2\beta_{mf} + \gamma_{mf} = 2$ is satisfied, reinforcing that the criticality is signed by the jump in the first derivative of Π, in close similarity to the specific heat discontinuity for equilibrium systems.

Above MFT entropy production also predicts correctly the signatures at discontinuous phase transitions. According to Eq. (2.49), m jumps from $m_1 \equiv m^{(S)}(q_f)$ to 0 at $q = q_f = (b^2/4ac) - q_b$ and thereby from Eq. (2.60) the entropy production will jump from

$$\frac{1}{2}\left(q_f\bar{g} - \frac{m_1^2}{q_f\bar{g}}\right)\ln\left[\frac{1+q_f\bar{g}}{1-q_f\bar{g}}\right], \qquad \text{to} \qquad \frac{q_f\bar{g}}{2}\ln\left[\frac{1+q_f\bar{g}}{1-q_f\bar{g}}\right]. \tag{2.63}$$

Conversely m jumps from 0 to $m_2 \equiv m^{(S)}(q_b)$ at $q = q_b$ and hence Π will jump from

$$\frac{q_b\bar{g}}{2}\ln\left[\frac{1+q_b\bar{g}}{1-q_b\bar{g}}\right], \qquad \text{to} \qquad \frac{1}{2}\left(q_b\bar{g} - \frac{m_2^2}{q_b\bar{g}}\right)\ln\left[\frac{1+q_b\bar{g}}{1-q_b\bar{g}}\right]. \tag{2.64}$$

The bistable behavior in the entropy production not only discerns continuous and discontinuous phase transitions but also it properly locates the hysteretic loop. The description beyond the mean field will be given in chapter 5.

Chapter 3

Thermodynamics of collisional models for Brownian particles: General properties and efficiency

3.1 Introduction

A long-standing dilemma in Thermodynamics and related areas concerns the issue of mitigating the impact of thermal noise/wasted heat in order to improve the machine performance. This constitutes a high relevant problem, not only for theoretical purposes but also for the construction of experimental setups [44, 45, 46]. Giving that the machine performance is commonly dependent on particular chemical compositions and operation conditions, notably for small-scale engines, the role of fluctuations being crucial for such engines, distinct approaches have been proposed and investigated in the realm of stochastic and quantum thermodynamics [47, 48]. A second fundamental point concerns that, even if all sources of dissipation could be mitigated, the performance of any thermal machine would still be limited by Carnot efficiency, which requires the occurrence of infinitely slow quasi-static processes and consequently the engine operates at null power. In contrast, realistic systems operate at finite time and power. Such conundrum (control/mitigation of dissipation and engine optimization) has contributed for the discovery of several approaches based on the maximization of power output instead of the efficiency [31, 48, 49, 50, 51, 52, 53, 54, 55, 56, 57, 58, 59, 60, 61, 62].

Thermal machines based on Brownian particles have been successfully studied not only for theoretical purposes

[31, 49, 50, 63] but also for the building of reliable experimental setups [64, 65, 66, 67, 68, 69]. They are also remarkable for depicting the limitations of classical thermodynamics and disclose the scales in which thermal fluctuations become relevant. In several situations, thermal machines involve isothermal transformations [64, 65, 66]. Such class of processes are fundamental in thermodynamic since they are minimally dissipative. However, isothermal transformations are slow, demanding sufficient large number of stages for achieving the desired final state. For this reason, distinct protocols, such as increasing the coupling between system and the thermal bath, have been undertaken for speeding it up and simultaneously controlling the increase of dissipation [70, 71, 72, 73, 74].

Here we introduce a strategy for optimizing the performance of irreversible Brownian machines operating at isothermal parts via the control of interaction time between the system and the environment. Our approach is based on a Brownian particle sequentially placed in contact with distinct thermal baths and subject to external forces [75] for unequal times. Such description, also referred as collisional, has been successfully employed in different contexts, such as systems that interact only with a small fraction of the environment and those presenting distinct drivings over each member of system [34, 76, 77, 78]. Depending on the parameters of the model (period, driving and difference of temperatures), the symmetric version can operate very inefficiently. Our aim is to show that the machine performance improves substantially by tuning properly the interaction time between particle and each reservoir. Besides the increase of the power and/or efficiency, the asymmetry in the contact time also enlarges the regime of operation of the machine substantially. Contrasting with previous works [71, 72, 73, 74], the optimization is solely obtained via the control of interaction time and no external parameters are considered. We derive general relations for distinct kinds of maximization, including the maximization of the efficiency and power with respect to the force, the asymmetry and both of them. For the isothermal work-to-work converter and/or small difference of temperature between reservoirs, they are solely expressed in terms of Onsager coefficients. The present approach can pave the way for the construction of efficient Brownian engines operating at finite times.

3.2 Thermodynamics of asymmetric interaction times

In this section we will return to the study of the Brownian particle model seen in section 2.2. As stated before, the present collisional approach for Brownian machines can be considered for an arbitrary set of reservoirs and external forces, which generic solutions $\langle v_i \rangle(t)$'s and $b_i(t)$'s in the nonequilibrium steady state regime are

$$\langle v_i \rangle(t) = e^{-\gamma_i (t-\tilde{\tau}_{i-1})} a_i + e^{-\gamma_i t} F_i(t), \tag{3.1}$$

and

$$b_i(t) = A_i e^{-2\gamma_i(t-\tilde{\tau}_{i-1})} + \frac{\Gamma_i}{2\gamma_i}, \tag{3.2}$$

where a_i and A_i are integration constants to be determined from the boundary conditions and $F_i(t)$ can be viewed as a "time integrated force", which is related to the external forces through the expression

$$F_i(t) = \int_{\tilde{\tau}_{i-1}}^{t} e^{\gamma_i t'} f_i(t')dt'. \tag{3.3}$$

Here, the variable t is interpreted as the time modulus the period $\tau = \tilde{\tau}_N$.

Since the probability distribution is continuous, the conditions $\langle v_i\rangle(\tau_i) = \langle v_{i+1}\rangle(\tau_i)$ and $b_i(\tau_i) = b_{i+1}(\tau_i)$ must hold for $i = 1, \ldots N-1$. In addition, the steady state condition (periodicity) implies that $\langle v_1\rangle(0) = \langle v_N\rangle(\tau)$ and $b_1(0) = b_N(\tau)$. Hence, the a_i and A_i can be determined as the solution of two uncoupled linear systems of N equations each. Here we shall focus on the case of $N = 2$ reservoirs – the simplest case for tackling the efficiency of a thermal engine, in which the interaction with the first and second reservoirs occur during τ_1 and $\tau_2 = \tau - \tau_1$, respectively. For simplicity, from now on, we consider that the viscous constant are equal $\gamma_1 = \gamma_2 = \gamma$. Therefore, the average velocities and their variances are

$$\begin{aligned} \langle v_1\rangle(t) &= \frac{(e^{\gamma\tau}-1)\,F_1(t) + F_1(\tau_1) + F_2(\tau)}{e^{\gamma t}\,(e^{\gamma\tau}-1)}, \\ \langle v_2\rangle(t) &= \frac{e^{\gamma\tau}F_1(\tau_1) + (e^{\gamma\tau}-1)\,F_2(t) + F_2(\tau)}{e^{\gamma t}\,(e^{\gamma\tau}-1)}, \end{aligned} \tag{3.4}$$

and

$$\begin{aligned} b_1(t) &= -\frac{(\Gamma_1-\Gamma_2)\left(1-e^{-2\gamma\tau_2}\right)}{2\gamma\,(1-e^{-2\gamma\tau})}e^{-2\gamma t} + \frac{\Gamma_1}{2\gamma}, \\ b_2(t) &= \frac{(\Gamma_1-\Gamma_2)\left(1-e^{-2\gamma\tau_1}\right)}{2\gamma\,(1-e^{-2\gamma\tau})}e^{-2\gamma(t-\tau_1)} + \frac{\Gamma_2}{2\gamma}, \end{aligned} \tag{3.5}$$

respectively. The expressions for $\langle v_1\rangle(t)$ and $b_1(t)$ hold for $0 \le t \le \tau_1$, while the expressions for $\langle v_2\rangle(t)$ and $b_2(t)$ are valid for $\tau_1 \le t \le \tau$. It is worth pointing out that the particle will be exposed to the contact with the reservoir 1 and force $f_1(t)$ for a longer (shorter) time than with reservoir 2 and force $f_2(t)$ if $\tau_1 \ge \tau_2$ ($\tau_1 \le \tau_2$). Furthermore, while the average velocities $\langle v_i\rangle(t)$ depend on the external force (but not on the temperature of the reservoirs), its variances $b_i(t)$ depend on the temperatures (but not on the external forces).

Having the expressions for the mean velocities and variances, thermodynamic quantities of interest can be directly obtained. The average work in each part of the cycle is given by

$$\overline{\dot{W}}_1 = \frac{1}{\tau}\int_0^{\tau_1} \langle v_1\rangle(t) f_1(t)dt, \tag{3.6}$$

$$\overline{\dot{W}}_2 = \frac{1}{\tau}\int_{\tau_1}^{\tau} \langle v_2\rangle(t) f_2(t)dt. \tag{3.7}$$

Using Eq. (3.4) and expressing each external force as $f_i(t) = X_i g_i(t)$, with X_i and $g_i(t)$ denoting force strength and its driving, respectively, we finally arrive at the following expressions:

$$\begin{aligned}
\overline{\dot{W}}_1 &= -\frac{m}{\tau\,(e^{\gamma\tau}-1)}\left[X_1^2\left((e^{\gamma\tau}-1)\int_0^{\tau_1} g_1(t)e^{-\gamma t}\,dt\int_0^{t} g_1(t')e^{\gamma t'}\,dt' + \int_0^{\tau_1} g_1(t)e^{-\gamma t}\,dt\int_0^{\tau_1} g_1(t')e^{\gamma t'}\,dt'\right)\right. \\
&+ \left. X_1X_2\int_0^{\tau_1} g_1(t)e^{-\gamma t}\,dt\int_{\tau_1}^{\tau} g_2(t')e^{\gamma t'}\,dt'\right], \qquad (3.8)\\
\overline{\dot{W}}_2 &= -\frac{m}{\tau\,(e^{\gamma\tau}-1)}\left[X_2^2\left(\int_{\tau_1}^{\tau} g_2(t)e^{-\gamma t}\,dt\int_{\tau_1}^{\tau} g_2(t')e^{\gamma t'}\,dt' + (e^{\gamma\tau}-1)\int_{\tau_1}^{\tau} g_2(t)e^{-\gamma t}dt\int_{\tau_1}^{t} g_2(t')e^{\gamma t'}\,dt'\right)\right. \\
&+ \left. X_1X_2e^{\gamma\tau}\int_{\tau_1}^{\tau} g_2(t)e^{-\gamma t}\,dt\int_0^{\tau_1} g_1(t')e^{\gamma t'}\,dt'\right]. \qquad (3.9)
\end{aligned}$$

The expressions above, Eqs. (3.8) and (3.9), are exact and are valid for any kind of drivings $g_1(t)$ and $g_2(t)$ and stage duration τ_1 and τ_2. Usually, in the linear regime, $\overline{\dot{W}}_i$ is written as the product of a flux $\mathcal{J}_i = L_{ii}X_i + L_{ij}X_j$ by a force X_i, that is, $\overline{\dot{W}}_i = -k_{\mathrm{B}}T_i\mathcal{J}_iX_i$. Since in the present case $\overline{\dot{W}}_i$ is always bilinear in the forces X_i, such expression is also valid even far from the linear regime. Thus, the Onsager coefficients L_{ij} may be written as,

$$\begin{aligned}
L_{11} &= \frac{2\gamma}{\Gamma_1\tau\,(e^{\gamma\tau}-1)}\left[(e^{\gamma\tau}-1)\int_0^{\tau_1} g_1(t)e^{-\gamma t}dt\int_0^{t} g_1(t')e^{\gamma t'}\,dt' + \int_0^{\tau_1} g_1(t)e^{-\gamma t}\,dt\int_0^{\tau_1} g_1(t')e^{\gamma t'}\,dt'\right],\\
L_{22} &= \frac{2\gamma}{\Gamma_2\tau\,(e^{\gamma\tau}-1)}\left[\int_{\tau_1}^{\tau} g_2(t)e^{-\gamma t}\,dt\int_{\tau_1}^{\tau} g_2(t')e^{\gamma t'}\,dt' + (e^{\gamma\tau}-1)\int_{\tau_1}^{\tau} g_2(t)e^{-\gamma t}dt\int_{\tau_1}^{t} g_2(t')e^{\gamma t'}\,dt'\right],\\
L_{12} &= \frac{2\gamma}{\Gamma_1\tau\,(e^{\gamma\tau}-1)}\int_0^{\tau_1} g_1(t)e^{-\gamma t}\,dt\int_{\tau_1}^{\tau} g_2(t')e^{\gamma t'}\,dt',\\
L_{21} &= \frac{2\gamma e^{\gamma\tau}}{\Gamma_2\tau\,(e^{\gamma\tau}-1)}\int_0^{\tau_1} g_1(t')e^{\gamma t'}\,dt'\int_{\tau_1}^{\tau} g_2(t)e^{-\gamma t}\,dt.
\end{aligned} \qquad (3.10)$$

Reciprocal relations are verified as follows: Since forces $f_1(t)$ and $f_2(t)$ solely act from 0 to τ_1 and τ_1 to τ, respectively, both upper and lower integral limits in Eqs. (3.6) and Eq. (3.7) can be replaced for τ and 0, respectively and hence all expressions from Eq. (3.6) to Eq. (3.10) can be evaluated over a complete cycle. By exchanging the indexes $1 \leftrightarrow 2$, we verify that $L_{ij} \leftrightarrow L_{ji}$.

Similarly, general expressions can be obtained for the average heat dissipation during the contact of the Brownian particle with each reservoir. Since the heat is closely related to the entropy production rate [see e.g. Eq. (2.24)], we curb our discussion to the latter quantity. The average entropy production over a complete cycle is then given by,

$$\overline{\Pi} = \frac{1}{\tau}\left[\int_0^{\tau_1}\Phi_1(t)\,dt + \int_{\tau_1}^{\tau}\Phi_2(t)\,dt\right]. \qquad (3.11)$$

By inserting Eq. (2.24) into Eq. (3.11) and using the expression for $\dot{Q}_i(t)$ given by Eq. (2.21), $\overline{\Pi}$ can be decomposed in two terms: one associated with the difference of temperature of the reservoirs

$$\overline{\Pi}_T = \frac{k_B}{\tau}\left[\frac{2\gamma^2}{\Gamma_1}\int_0^{\tau_1} b_1(t)\,dt + \frac{2\gamma^2}{\Gamma_2}\int_{\tau_1}^{\tau} b_2(t)\,dt - \gamma\tau\right], \qquad (3.12)$$

and the other coming from the external forces

$$\overline{\Pi}_F = \frac{k_B}{\tau}\left[\frac{2\gamma^2}{\Gamma_1}\int_0^{\tau_1}\langle v_1\rangle^2(t)\,dt + \frac{2\gamma^2}{\Gamma_2}\int_{\tau_1}^{\tau}\langle v_2\rangle^2(t)\,dt\right]. \tag{3.13}$$

Now, from Eqs. (3.5) and (3.12), one obtains the general form for $\overline{\Pi}_T$:

$$\overline{\Pi}_T = k_B\frac{\Gamma_1\Gamma_2}{\tau}\frac{\sinh(\gamma\tau_1)\sinh(\gamma\tau_2)}{\sinh(\gamma\tau)}\left(\frac{1}{\Gamma_1}-\frac{1}{\Gamma_2}\right)^2, \tag{3.14}$$

which it is strictly positive (as expected). The component $(1/\Gamma_1 - 1/\Gamma_2)$ can be regarded as the "thermodynamic force" f_Γ associated with the difference of temperature of the reservoirs. Particularly, in the linear regime ($\Gamma_2 \simeq \Gamma_1 = \Gamma$), $\overline{\Pi}_T$ can be conveniently written down in terms of Onsager coefficient $\overline{\Pi}_T = L_{\Gamma\Gamma} f_\Gamma$, where $L_{\Gamma\Gamma}$ is given by,

$$L_{\Gamma\Gamma} = k_B\frac{\Gamma^2}{\tau}\frac{\sinh(\gamma\tau_1)\sinh(\gamma\tau_2)}{\sinh(\gamma\tau)}. \tag{3.15}$$

Note that $L_{\Gamma\Gamma}$ is strictly positive and it reduces to $k_B\Gamma^2\tanh[\frac{\gamma\tau}{2}]/2\tau$ for $\tau_1 = \tau_2$ (symmetric case). Further, it is straightforward to verify that the dissipation term Π_T is a monotonous decreasing function of τ and it is always larger for the symmetric case ($\tau_1 = \tau_2$). Both properties of $\overline{\Pi}_T$ are illustrated in Fig. 3.1, where $\overline{\Pi}_T$ is shown as a function of τ for various values of the asymmetry parameter $\kappa = \tau_1/\tau_2$ (notice that $\overline{\Pi}_T$ is invariant over the switch of the interaction times $\tau_1 \leftrightarrow \tau_2$ or, equivalently $\kappa \leftrightarrow 1/\kappa$). There is one caveat which concerns the validity of the results of Fig. 3.1. Collisional models usually neglects the time for changing the contact between the system and thermal baths. However, if τ is very small, such approximation can no longer be hold. We shall assume along this chapter that τ is large enough for the collisional approximation to be valid.

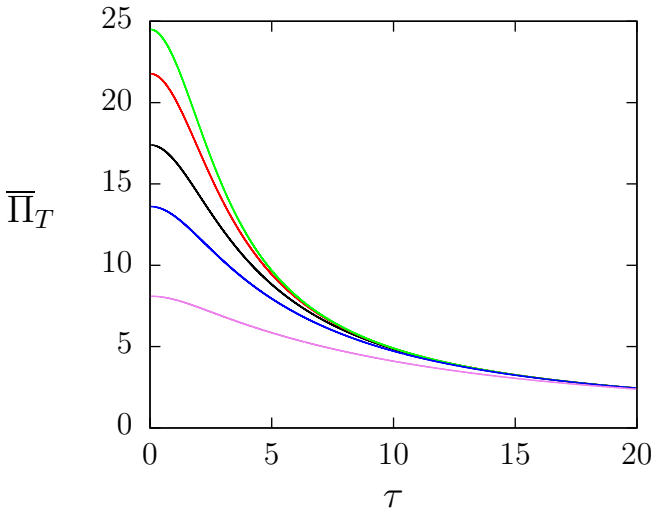

Figure 3.1: Mean entropy production component $\overline{\Pi}_T$ as a function of the period τ for $\gamma = 1$, $\Gamma_1 = 1$ and $\Gamma_2 = 100$ and distinct asymmetries. From top to bottom: $\kappa = 1.0,\ 0.5,\ 0.3,\ 0.2$ and 0.1.

The entropy production component coming from external forces also assumes a general (bilinear) form given

by,

$$\overline{\Pi}_F = \tilde{L}_{11}X_1^2 + (\tilde{L}_{12} + \tilde{L}_{21})X_1X_2 + \tilde{L}_{22}X_2^2. \tag{3.16}$$

The coefficients $\tilde{L}_{ij}$'s are shown in the Appendix A, Eq. (A.2). It should be noticed that Eq. (3.16) is exact for all force regimen (not only in the linear regime). For equal temperatures, they coincide with Onsager coefficients [Eq. (3.10)]. A detailed analysis for distinct linear regimes (low temperature difference and/or low forces) is undertaken in Appendix A. Furthermore, since $\tau_2 = \tau - \tau_1$, the coefficients above fulfill the reciprocal relations $\tilde{L}_{11} \leftrightarrow \tilde{L}_{22}$ and $\tilde{L}_{12} \leftrightarrow \tilde{L}_{21}$ by exchanging $1 \leftrightarrow 2$ for the generic drivings $g_i(t)$'s, the interaction times τ_i's and the temperature of the reservoirs T_i's.

3.3 Efficiency

The optimization of engines, which converts energy (usually heat or chemical work) into mechanical work, constitutes one of the main issues in thermodynamics, engineering, chemistry and others. Here we exploit the role of asymmetric contact times between the Brownian particle and the thermal reservoirs as a reliable strategy for optimizing the machine performance. More specifically, the amount of energy (heat and work) received by the particle is partially converted into output work (or, equivalently, the output power per cycle) $\mathcal{P} = \overline{\dot{W}_2} \geq 0$ during the second half stage. A measure of efficiency is given by the ratio of the amount of output work to the total energy injected

$$\eta = -\frac{\mathcal{P}}{\overline{\dot{W}_1} + \overline{\dot{Q}_i}}, \tag{3.17}$$

where $\overline{\dot{Q}_i}$ is the average heat extracted from the reservoir i ($i = 1$ or 2 whether the reservoir 1 or 2 delivers heat to the Brownian particle), whereas for the other way round (both reservoirs absorbing energy from the particle), $\overline{\dot{Q}_i}$ does not appear in Eq. (3.17), as shall be discussed in Sec. 3.3.1. It is worth mentioning that in the case of more than 2 reservoirs, the numerator of the efficiency should be the total power extracted from the systems (sum of all $\overline{\dot{W}_i} > 0$) and the denominator is the total power injected into the system (sum of all $\overline{\dot{W}_i} < 0$) plus the total heat injected into the system (sum of all $\overline{\dot{Q}_i} < 0$).

Below, we are going to investigate the machine optimization with respect to the loading force X_2 and asymmetry coefficient $\kappa = \tau_1/\tau_2$ for two distinct scenarios: equal and different temperatures.

3.3.1 Isothermal work-to-work converter

Many processes in nature, such as biological systems, operate at homogeneous (or approximately equal) temperatures, in which an amount of chemical work/energy is converted into mechanical work and vice-versa (see e.g. [79, 80]). This highlight the importance of searching for optimized protocols operating at equal temperatures. Here we exploit the present Brownian machine operating at equal temperatures, but subject to distinct external forces. From Eqs. (2.21) and (3.5), it follows that $\overline{\dot{Q}_1} \geq 0$ and $\overline{\dot{Q}_2} \geq 0$ and therefore no heat is delivered to the particle. Such engine reduces to a work-to-work converter: the particle receives input power $\overline{\dot{W}_1} < 0$ which is partially converted into output power $\mathcal{P} \geq 0$. From Eq. (3.10), the output power and efficiency can expressed in term of the Onsager coefficients according to the following expressions:

$$\mathcal{P} = \overline{\dot{W}}_2 = -k_{\mathrm{B}}T\left[L_{22}(\kappa)X_2^2 + L_{21}(\kappa)X_1X_2\right]. \tag{3.18}$$

and

$$\eta = -\frac{L_{21}X_1X_2 + L_{22}X_2^2}{L_{11}X_1^2 + L_{12}X_1X_2}, \tag{3.19}$$

Both of them can be expressed in terms of the ratio X_2/X_1 between forces, the output power being a function of such ratio multiplied by X_1^2. As mentioned previously, there are three routes to be considered with respect to the engine optimization (holding X_1 and τ fixed): the time asymmetry optimization (conveniently carried out in terms of ratio $\kappa = \tau_1/\tau_2$), the output force X_2 optimization and both optimizations together. We shall analyze all cases in the following subsections.

1. Maximization with respect to the asymmetry

Since the Brownian particle must be in contact with the first reservoir long enough for the injected energy to be larger than the energy dissipated by the viscous force, for any set of X_1 and X_2 there is a minimum value κ_m for which $\mathcal{P} \geq 0$. On the other hand, depending on the kind of driving, it can extend up $\kappa \to \infty$, for which L_{21} and L_{22} vanishes [see Eq. (3.10)].

The choice of optimal asymmetries are expected to be dependent of the quantity chosen to be maximized. Usually, there are two quantities of interest: maximum efficiency or maximum power output. Starting with the latter case, the optimal asymmetry κ_{MP} which maximizes $\mathcal{P}$ is the solution of following equation

$$\frac{L'_{21}(\kappa_{MP})}{L'_{22}(\kappa_{MP})} = -\frac{X_2}{X_1}, \tag{3.20}$$

where $L'_{ij}(\kappa) \equiv \partial L_{ij}(\kappa)/\partial\kappa$ and in this section L_{ij}'s (together their derivatives) have been expressed in terms of κ for specifying which quantity ($\mathcal{P}$ or η) has been maximized. In general, Eq. (3.20) may have more than one

solution for each choice of the ratio X_2/X_1 and one should be careful to identify the global maximum. However, in the following discussion (as in the examples presented in Section 3.3.1), we consider the cases which present a single maximum.

Similarly, from Eq. (3.19), we obtain the value of the asymmetry that maximizes the efficiency $\kappa_{M\eta}$ from the transcendental equation

$$\begin{aligned}\Delta_{2212}(\kappa_{M\eta})X_2^2 + \Delta_{2111}(\kappa_{M\eta})X_1^2 \\ + \left[\Delta_{2211}(\kappa_{M\eta}) + \Delta_{2112}(\kappa_{M\eta})\right] X_1X_2 = 0,\end{aligned} \tag{3.21}$$

where $\Delta_{ijkl}(\kappa) = L'_{ij}(\kappa)L_{kl}(\kappa) - L'_{kl}(\kappa)L_{ij}(\kappa)$. Although exact, for a given choice of the drivings $g_i(t)$ and the strengths X_i, Eqs. (3.20) and (3.21), in general, have to be solved numerically for κ_{MP} and $\kappa_{M\eta}$, respectively. After these values are obtained, we can evaluate the power $\mathcal{P}_{MP,\kappa}$ and efficiency $\eta_{MP,\kappa}$ at maximum power as

$$\mathcal{P}_{MP,\kappa} = \frac{k_{\rm B}TL'_{21}(\kappa_{MP})}{L'^2_{22}(\kappa_{MP})}[L_{21}(\kappa_{MP})L'_{22}(\kappa_{MP}) - L_{22}(\kappa_{MP})L'_{21}(\kappa_{MP})]X_1^2, \tag{3.22}$$

and

$$\eta_{MP,\kappa} = \frac{L'_{21}(\kappa_{MP})[L'_{22}(\kappa_{MP})L_{21}(\kappa_{MP}) - L_{22}(\kappa_{MP})L'_{21}(\kappa_{MP})]}{L'_{22}(\kappa_{MP})[L_{11}(\kappa_{MP})L'_{22}(\kappa_{MP}) - L_{12}(\kappa_{MP})L'_{21}(\kappa_{MP})]}. \tag{3.23}$$

Analogously, we can write the power at maximum efficiency $\mathcal{P}_{M\eta,\kappa}$ and maximum efficiency $\eta_{M\eta,\kappa}$ as

$$\mathcal{P}_{M\eta,\kappa} = -k_{\rm B}T\left[L_{22}(\kappa_{M\eta})X_2^2 + L_{21}(\kappa_{M\eta})X_1X_2\right], \tag{3.24}$$

and

$$\eta_{M\eta,\kappa} = -\frac{L_{22}(\kappa_{M\eta})X_2^2 + L_{21}(\kappa_{M\eta})X_1X_2}{L_{11}(\kappa_{M\eta})X_1^2 + L_{12}(\kappa_{M\eta})X_1X_2}, \tag{3.25}$$

respectively. In Sec 3.3.1, we will exemplify our exact expressions for maximum efficiencies and powers for two kinds of drivings.

2. Maximization with respect to the output force

For given asymmetry and drivings, the Onsager coefficients are constant. Hence, the maximization of the output power and the efficiency turn out to be similar to the approach from Refs. [58, 75]. Below, we recast the main results.

As previously, the engine regime ($\mathcal{P} > 0$) also imposes boundaries to optimization with respect to the force strength. Here, the output force X_2 must lie in the interval $X_m \leq X_2 \leq 0$, where $X_m = -L_{21}X_1/L_{22}$. In general, X_m is different from the value of the output force that minimizes the entropy production X_{2mS} (for X_1 and κ

constants). According to Eq. (3.16), such difference is given by $X_{2m} - X_{2mS} = (L_{12} - L_{21})X_1/2L_{22}$. Note that they coincide $X_m = X_{2mS}$ for symmetric Onsager coefficients $L_{12} = L_{21}$, but they are different when $L_{12} \neq L_{21}$. Similarly to the previous subsection, the optimization can be performed to ensure maximum power $\mathcal{P}_{MP,X_2}$ (with efficiency η_{MP,X_2}) or maximum efficiency $\eta_{M\eta,X_2}$ (with power $\mathcal{P}_{M\eta,X_2}$), by adjusting the output forces to optimal values X_{2MP} and $X_{2M\eta}$, respectively. These optimal output forces can be expressed in terms of the Onsager coefficients as

$$X_{2M\eta} = \frac{L_{11}}{L_{12}}\left(-1 + \sqrt{1 - \frac{L_{12}L_{21}}{L_{11}L_{22}}}\right)X_1, \tag{3.26}$$

and

$$X_{2MP} = -\frac{1}{2}\frac{L_{21}}{L_{22}}X_1, \tag{3.27}$$

respectively. Hence, the maximum efficiency $\eta_{M\eta,X_2}$ and the efficiency at maximum power η_{MP,X_2} are given by,

$$\eta_{M\eta,X_2} = -\frac{L_{21}}{L_{12}} + \frac{2L_{11}L_{22}}{L_{12}^2}\left(1 - \sqrt{1 - \frac{L_{12}L_{21}}{L_{11}L_{22}}}\right), \tag{3.28}$$

and

$$\eta_{MP,X_2} = \frac{L_{21}^2}{4L_{11}L_{22} - 2L_{12}L_{21}}, \tag{3.29}$$

while the power at maximum efficiency $\mathcal{P}_{M\eta,X_2}$ and the maximum power $\mathcal{P}_{MP,X_2}$ can obtained by inserting $X_{2M\eta}$ or X_{2MP} into the expression for $\mathcal{P}$. In fact, these quantities are not independent of each other, instead they are related as

$$\eta_{MP,X_2} = \frac{P_{MP,X_2}}{2P_{MP,X_2} - P_{M\eta,X_2}}\eta_{M\eta,X_2}. \tag{3.30}$$

Furthermore, for symmetric Onsager coefficients $L_{12} = L_{21}$, there two additional simple relations given by,

$$\eta_{MP,X_2} = \frac{\eta_{M\eta,X_2}}{1 + \eta_{M\eta,X_2}^2} \qquad \text{and} \qquad \frac{\mathcal{P}_{M\eta,X_2}}{\mathcal{P}_{MP,X_2}} = 1 - \eta_{M\eta,X_2}^2. \tag{3.31}$$

As shown in Appendix B, $L_{12} = L_{21}$ for constant drivings for any value of κ. Conversely, they are in general different ($L_{12} \neq L_{21}$) for linear drivings (see Appendix C). For the symmetric time case ($\kappa = 1$), however, the equality holds also for linear drivings [75].

3. Constant and linear drivings

In order to access the advantages of the asymmetry in the time spent by the Brownian particle in contact with each reservoir, we consider two different driving models. In the first model, the drivings are constant and the external forces can be written as

$$f_1(t) = X_1, \quad \text{for } 0 \leq t < \tau_1 \tag{3.32}$$

$$f_2(t) = X_2, \quad \text{for } \tau_1 \leq t < \tau. \tag{3.33}$$

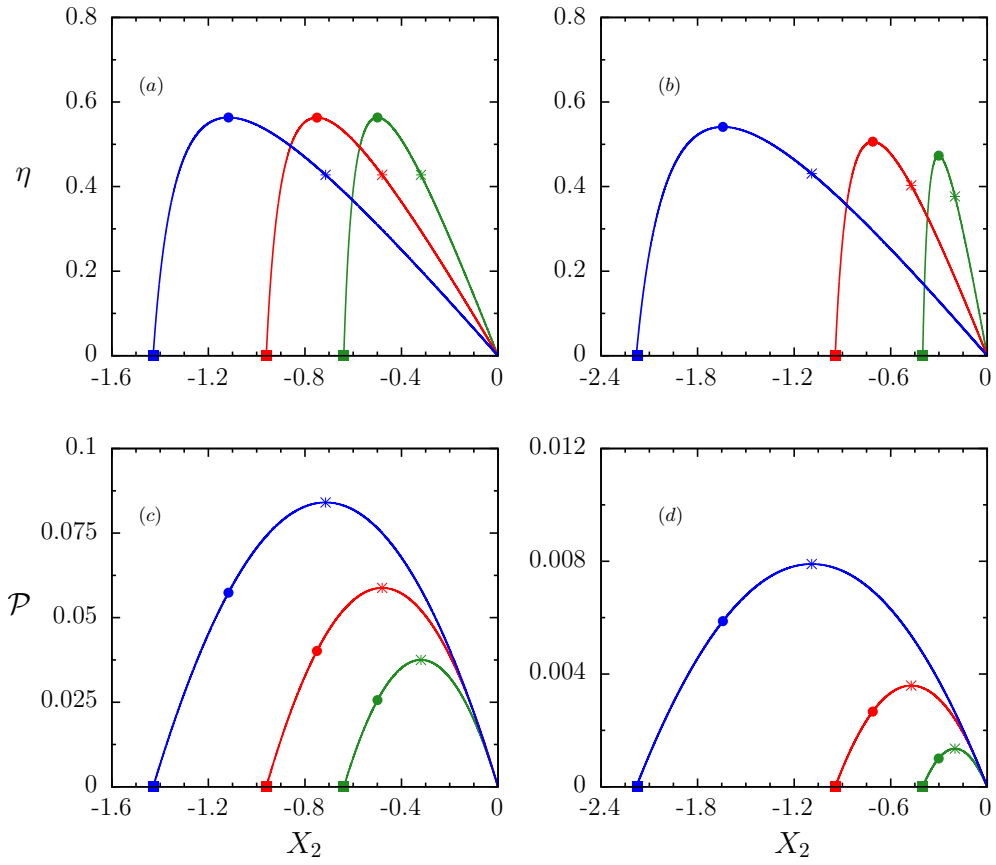

Figure 3.2: Efficiency [panels (a) and (b)] and output power [panels (c) and (d)] (averaged over one period) for the isothermal work-to-work converter with $X_1 = 1$, $\tau = 1$, $\gamma = 1$ and different asymmetries κ doing $\kappa = 1.50,\ 1.00$ and 0.67 for the lines blue, red and green respectively. Panels (a) and (c) depict the results for constant drivings, whereas (b) and (d) for the linear drivings one. In all panels, squares, circles and stars denote X_{2mS}, $X_{2M\eta}$ and X_{2MP}, respectively.

In Appendix B, we present explicit expressions for the average velocities $\langle v_i \rangle(t)$ and Onsager coefficients L_{ij} (which coincides with the coefficients $\tilde{L}_{ij}$ for isothermal reservoirs). The second class of Brownian engines deals with drivings evolving linearly in time and given by the following expressions

$$f_1(t) = X_1 \gamma t, \quad \text{for } 0 \leq t < \tau_1 \tag{3.34}$$

$$f_2(t) = X_2 \gamma (t - \tau_1), \quad \text{for } \tau_1 \leq t < \tau. \tag{3.35}$$

The main expressions for such case are listed in Appendix C. Figs. 3.2 and 3.3 depict typical plots of the efficiency and power output for both force models as a function of the output force X_2 and asymmetry κ, respectively.

As discussed above, the engine regime operates for $X_{2m} < X_2 < 0$. An immediate advantage of the time asymmetry concerns the minimum output forces X_{2m} which decreases with κ, implying that the engine regime

interval increases with the asymmetry (see Fig. 3.2). Such trend is consistent with the absorption of energy (average work rate $\overline{\dot{W}_1}$) for longer and longer time as κ increases. Furthermore, the minimum entropy production (represented by the squares in the figure) coincides with the minimum loading force (vanishing power output and efficiency) for constant drivings, but not for the linear case (although, for the values of the parameters used in Fig. 3.2, X_{2mS} is so close to X_m that the difference is not discernible – it is of the order of 10^{-3}).

The maximum efficiencies are almost constant for the constant force model [Fig. 3.2(a)] and slightly increase with κ [Fig. 3.2(b)] for the linear force model. However, for small $|X_2|$, the efficiency is larger for the smaller values of κ. The effect of the time asymmetry for the output power is more pronounced. For both force models, the maximum power output clearly increases with κ.

Fig. 3.4 depicts, for constant and linear drivings, a heat map for the power output and efficiency as a function of both the asymmetry and loading forces. For aesthetic reasons, they have been expressed in terms $1/\kappa$ (instead of κ) in the vertical axis. Noteworthy, the maximum efficiency curves, represented by the dashed (full) line for the maximization with respect to κ (loading force), are close to each other. Consequently, the choice of the parameter to maximize the efficiency is not important for both models presented here. Moreover, as previously discussed, the maximum efficiency is almost constant for the constant drivings model, but increases with κ for the linear drivings one. In contrast to the maximum efficiencies, maximum power curves (panels 3.4(a) and 3.4(c) for constant and linear drivings, respectively) present rather different behaviors depending on the optimization parameter. The $\mathcal{P}_{MP,\kappa}$ curves (dashed lines) always lie below the $\mathcal{P}_{MP,X_2}$ (full lines) ones and they approach each other as $\kappa \to \infty$. Finally, it is worth pointing out that while both drivings provide similar efficiencies, the constant driving case is clearly more advantageous than the linear one in terms of the output power.

4. Simultaneous maximization of the asymmetry and the force

One may also raise the relevant issue of maximizing the power output and efficiency with respect to the asymmetry and output force strength simultaneously. Although this is not possible in some cases (as explained below), we will proceed presenting the framework assuming that such maximization is possible. As before, we shall restrict the analysis to drivings presenting a single physical solution for Eqs. (3.20) and (3.21). If this is not the case, each maximum of these equations should be analyzed individually to assert which is the global maximum in each case.

Under the assumption above, the maximum power output must satisfy simultaneously Eqs. (3.20) and (3.27),

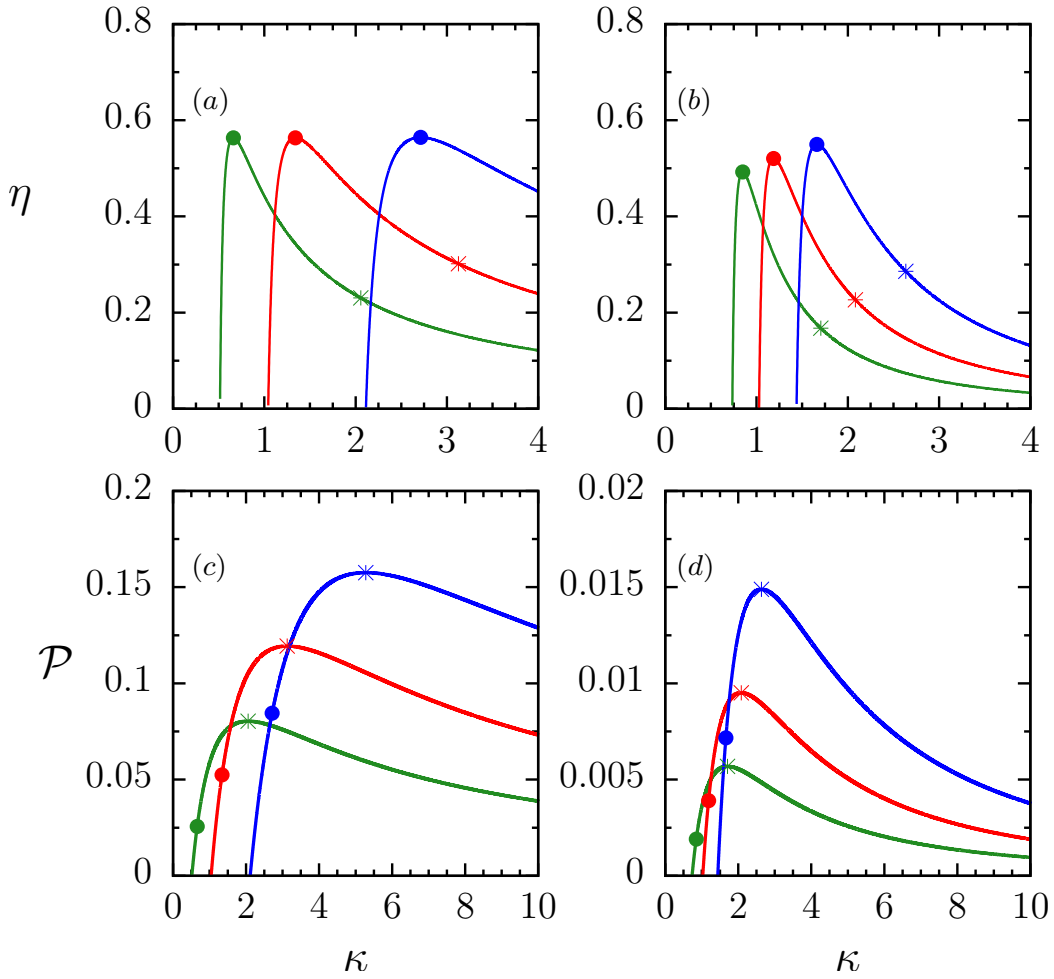

Figure 3.3: Efficiency [panels (a) and (b)] and output power [panels (c) and (d)] (averaged over one period) for the isothermal work-to-work converter with $X_1 = 1$, $\tau = 1$, $\gamma = 1$ and different values of X_2, doing $X_2 = -0.5, -1.0$ and -2.0 for the lines green, red and blue respectively. Panels (a) and (c) depict the main results for the constant drivings model while (b) and (d) the linear drivings one. In all panels, circles and stars denote $\kappa_{2M\eta}$ and κ_{2MP}, respectively. For such set of parameters, the associate κ_{2mS}'s are out of the engine regime.

that is, we must find the optimal value of the asymmetry κ^*_{MP} which satisfy the following condition:

$$\frac{L'_{21}(\kappa^*_{MP})}{L'_{22}(\kappa^*_{MP})} = \frac{1}{2}\frac{L_{21}(\kappa^*_{MP})}{L_{22}(\kappa^*_{MP})}. \tag{3.36}$$

Once the optimal asymmetry κ^*_{MP} is obtained, the optimal force X^*_{2MP} is calculated from Eq. (3.27) and given by

$$X^*_{2MP} = -\frac{1}{2}\frac{L_{21}(\kappa^*_{MP})}{L_{22}(\kappa^*_{MP})}X_1. \tag{3.37}$$

Graphically, the condition above is precisely the crossing point between lines for which the power (or efficiency) is maximized with respect to X_2 and κ. However, in some cases, (as illustrated by the constant and linear

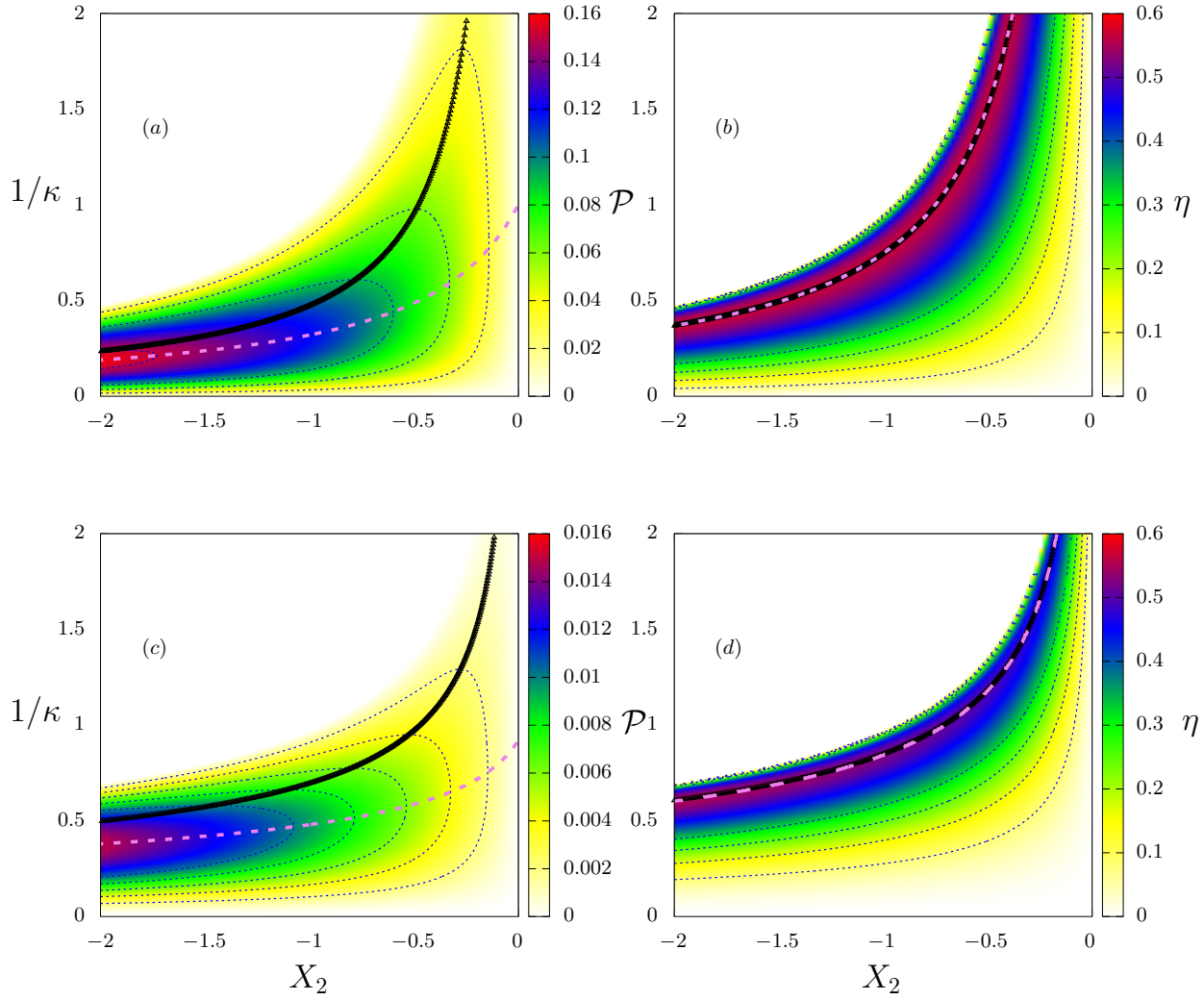

Figure 3.4: For the isothermal work-to-work converter, the output power (left panels) and efficiency (right panels) for the constant [(a) and (b)] and linear [(c) and (d)] drivings models as a function of the inverse of the asymmetry parameter κ and loading forces X_2. Dotted lines represent constant value loci, dashed and full lines represent maximization with respect to κ and X_2, respectively. Parameters: $\tau = 1,\ \gamma = 1,\ X_1 = 1$.

drivings presented above) these two lines do not cross at all. The physical reason is that the power output keeps growing as $\kappa \to \infty$ (with an appropriate choice of a value of X_2 for each κ). In other words, for such models, it is advantageous to apply a very large output force (in modulus) for a short period. Conversely, if the force model involves a rapidly decaying input driving $g_1(t)$ and growing output driving $g_2(t)$, an optimal output power may be found. In such case, the power and efficiency at maximum power are readily evaluated as

$$\mathcal{P}^* = \frac{k_B T}{4} \frac{L_{21}^2(\kappa^*_{MP})}{L_{22}(\kappa^*_{MP})} X_1^2, \tag{3.38}$$

and

$$\eta^* = \frac{L_{21}^2(\kappa^*_{MP})}{4L_{11}(\kappa^*_{MP})L_{22}(\kappa^*_{MP}) - 2L_{21}(\kappa^*_{MP})L_{12}(\kappa^*_{MP})}. \tag{3.39}$$

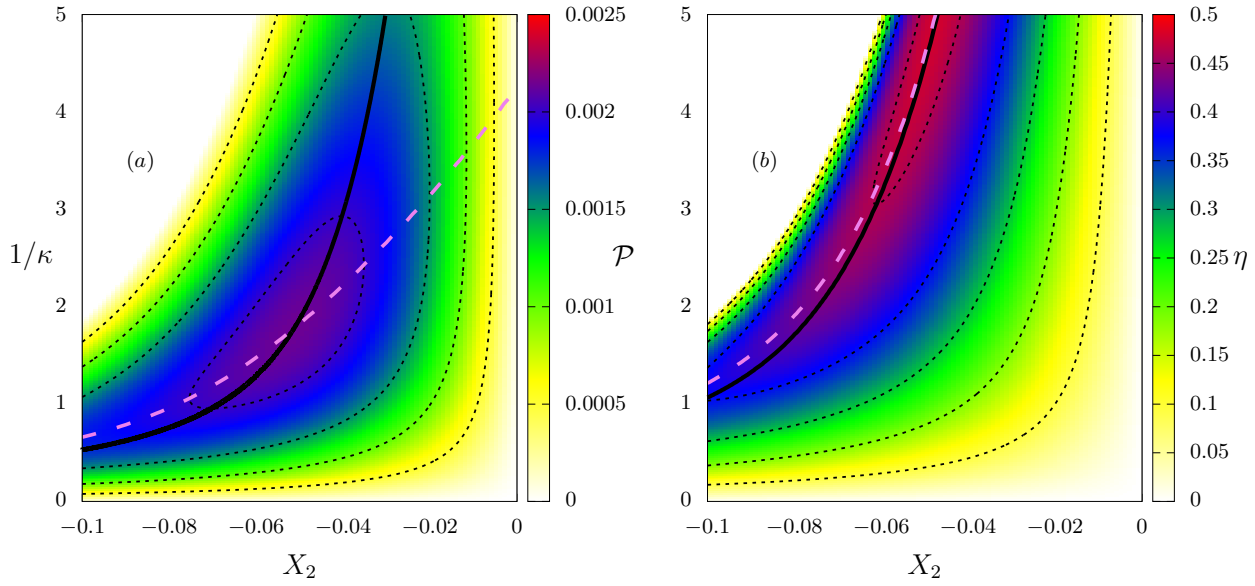

Figure 3.5: For the exponential driving, depiction of output power (a) and efficiency (b) versus the inverse of the asymmetry coefficient κ and the output force X_2 for $\tau = 1$, $\gamma = 1$ and $X_1 = 1$. Dotted lines represent constant value loci, dashed and solid lines represent maximization with respect to κ and X_2, respectively.

Thereby, the optimal output power increases quadratically with the input force while the efficiency is completely determined by the driving force model. It is noteworthy that, despite the apparent temperature dependency of the power output in Eq. (3.38), the temperature cancels out when we use the expressions for the Onsager coefficients [see e.g. Eq. (3.10)]. Similar expressions can be obtained for the simultaneous maximization of efficiency [by equaling the ratio X_2/X_1 from Eqs. (3.21) and (3.26)]. Since expressions are more involved, we abstain to present them here. In order to illustrate the previous ideas, we consider an exponential driving given by

$$f_1(t) = X_1 e^{-9\gamma t}, \quad \text{for } 0 \leq t < \tau_1 \tag{3.40}$$

$$f_2(t) = X_2 e^{\gamma(t-\tau_1)}, \quad \text{for } \tau_1 \leq t < \tau. \tag{3.41}$$

Figs. 3.5 (a) and (b) depict, for above exponential drivings, the heat maps of the output power and efficiency as functions of κ and X_2, respectively. Contrasting to the previous models, the crossing between maximum power lines are evident for the exponential drivings model above and thereby the global optimization is possible. Although for the exponential model given by Eqs. (3.40) and (3.41) the crossing between maximum efficiency curves is absent, it does appear for other exponential drivings choices (e.g. for $f_1(t) = X_1 e^{-7\gamma t}$ and $f_2(t) = X_2 e^{3\gamma(t-\tau_1)}$) and follow theoretical prescription above.

3.3.2 Thermal engine

In this section, we derive general findings for thermal engines in which the particle is also exposed to distinct thermal baths in each stage. Although the power output $\mathcal{P}$ is the same as before (it does not depend on the temperatures), the efficiency may change because of the appearance of heat flow. Hence, in addition to the input energy received as work, the engine may also receive energy from the hot reservoir. Consequently, the maximization of power output with respect to the output force X_{2MP} or the asymmetry κ_{MP} is the same as before, but the corresponding efficiencies may differ (if $\overline{\dot{Q}}_1 < 0$ or $\overline{\dot{Q}}_2 < 0$) from such case, following Eq. (3.17) instead. Anyhow, the efficiency of the engine for reservoirs with different temperatures is always smaller or equal than for isothermal reservoirs.

From Eq. (2.21), the average heat dissipated by the Brownian particle per cycle while in contact with the i-reservoir $\overline{\dot{Q}}_i$ can be obtained as

$$\overline{\dot{Q}}_1 = \frac{m\gamma}{\tau}\left[\int_0^{\tau_1}\langle v_1\rangle^2 dt - C(\tau_1)(\Gamma_1-\Gamma_2)\right], \tag{3.42}$$

$$\overline{\dot{Q}}_2 = \frac{m\gamma}{\tau}\left[\int_{\tau_1}^{\tau}\langle v_2\rangle^2 dt + C(\tau_1)(\Gamma_1-\Gamma_2)\right], \tag{3.43}$$

where $C(\tau_1) = \mathrm{csch}(\gamma\tau)\sinh(\gamma\tau_1)\sinh(\gamma\tau_2)/2\gamma^2$ is strictly positive. Therefore, since the first term on the right-hand side of Eqs. (3.42) and (3.43) are positive, heat always flow into the colder reservoir. As about the hot reservoir, the heat may flow from or into the reservoir. For simplicity, we shall restrict our analysis to the case $\Gamma_1 > \Gamma_2$, that is, the first reservoir being the hot one, but it is worth pointing out that all the discussion below holds valid for $\Gamma_1 < \Gamma_2$ if we analyze Eq. (3.43) instead of Eq. (3.42).

For $\Gamma_1 > \Gamma_2$, Eq. (3.42) ensures that heat flows into the system if $\int_0^{\tau_1}\langle v_1\rangle^2 dt < C(\tau_1)(\Gamma_1-\Gamma_2)$. Physically, this condition is a balance between kinetic energy that flows into the system due to the forces and the dissipation. If X_1 is strong enough (or if the difference of temperature of the reservoirs is small enough), energy flows into both reservoirs. Thereby, the engine effectively reduces to an isothermal work-to-work converter, so that the efficiency is still described by Eq. (3.19) and all results and findings from Section 3.3.1 regarding the efficiency optimization hold. Moreover, for small enough temperature differences, the engine efficiency is larger the Carnot efficiency. This is possible because work-to-work conversion is not bounded by the thermodynamics laws the same way heat-to-work conversion is [81]. Otherwise, the inequality above is satisfied and energy flows from the first reservoir into the engine. For $\Gamma_1 < \Gamma_2$, the same energy balance occurs, but we need to assert the positiveness or negativeness of Eq. (3.43).

Furthermore, although exact, the achievement of general expressions for optimized efficiencies outside the

isothermal work-to-work regime is more cumbersome than the ones obtained for such regime, making a general analysis unfeasible. Nevertheless, the discussion of a simple asymptotic limit is instructive. If the second term on the right-hand side of Eq. (3.42) [or Eq. (3.43)] is the dominant one, $|\Gamma_1 - \Gamma_2| \gg 1$ and $|\overline{\dot{Q}}_1| \gg |\overline{\dot{W}}_1|$ [or $|\overline{\dot{Q}}_2| \gg |\overline{\dot{W}}_1|$]. Therefore, the efficiency becomes $\eta \approx -\mathcal{P}/\overline{\dot{Q}}_1$ [or $\eta \approx -\mathcal{P}/\overline{\dot{Q}}_2$], which maximization, with respect to X_2, yields $X_{2M\eta} \approx X_{2MP}$ and follows Eq. (3.27). Hence, the corresponding $\eta_{M\eta}$ approaches to the following expression

$$\eta_{M\eta,X_2} \approx \frac{T_2}{8\gamma^2 T_i C(\tau_1)} \frac{L_{21}^2}{L_{22}} \tau X_1^2 \ll 1, \tag{3.44}$$

where T_i is the temperature of the hot reservoir. When the hot bath is the first reservoir, the fact that the efficiency is small is direct since the factor $T_2/T_1 << 1$. However, when the second reservoir is the hotter one, the temperature ratio becomes 1 and the smallness of the efficiency comes from the Onsager coefficients: $L_{21}^2/L_{22} \propto 1/T_2$. It is also worth mentioning that the apparent dependence on the period cancels out because the Onsager coefficients are proportional to $1/\tau$ [see Eq. (3.10)]. Therefore, for high temperature differences, the engine efficiency is very small for any value of the asymmetry.

In order to illustrate our findings for reservoirs with different temperatures, we consider the constant and linear drivings models presented above. Fig. 3.6 exemplifies, for distinct temperature reservoirs, the efficiency for the same values of κ used in Fig. 3.2 for constant [panels (*a*) and (*b*)] and linear drivings [panels (*c*) and (*d*)], respectively. In panels (*a*) and (*c*) the temperature of the first reservoir is larger than that of the second reservoir, while panels (*b*) and (*d*) depict the other way around.

In accordance with general findings from Sec. 3.3.2, for constant drivings there are two regimes (the vertical lines in the figure denotes the value of X_2 which separates them) for which the heat exchanged between the Brownian particle and the hot reservoir changes sign. Conversely, they are not present for the linear drivings model – panels (c) and (d) – because the heat exchange with the hot reservoir does not change sign for the parameters used in the figures. Since $\langle v_i \rangle^2$ increases with X_2^2, the term coming from the difference of temperatures in Eq.(3.42) dominates over it when $|X_2|$ is small and hence the machine is less efficient than the isothermal work-to-work converter. Conversely, for large $|X_2|$ the engine may become as efficient as the isothermal work-to-work converter if the exchanged heat with the hot reservoir change sign – left of the line in panels (*a*) and (*b*). Anyhow, by comparing the performance of isothermal with the different temperature case, we see that the decay of efficiency for linear drivings is more pronounced than for constant drivings.

As for isothermal reservoirs, the machine performance always improves as κ increases, encompassing not only an extension of its operation regime X_{2m} but it also presents a more pronounced increase of efficiencies, again, more substantial for linear drivings. Moreover, the asymmetry may be used to mitigate the drop in the efficiency

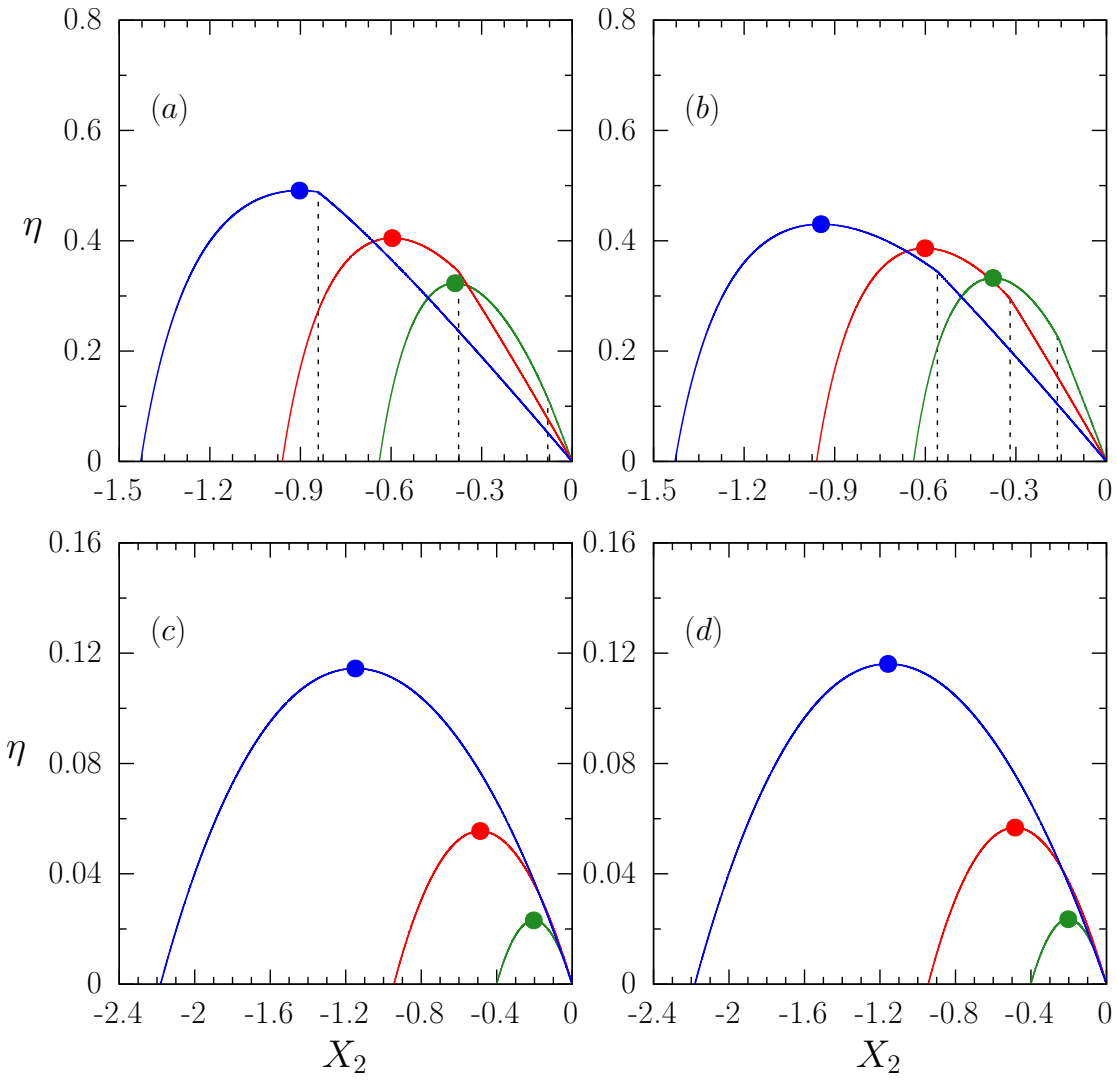

Figure 3.6: Efficiency as a function of the force strength X_2 for the constant [(a) and (b)] and linear [(c) and (d)] drivings, respectively. Parameters: $\tau = 1$, $\gamma = 1$ and $X_1 = 1$ and distinct temperatures [$\Gamma_1 = 2.0$ and $\Gamma_2 = 1.5$ in panels (a) and (c) and $\Gamma_1 = 1.5$ and $\Gamma_2 = 2.0$ in panels (b) and (d)]. Circles denote maximum efficiencies and their X_{2MP}'s are the same as in Fig. 3.2. From left to right, $\kappa = 1.50,\ 1.00$ and 0.67). Dashed vertical lines stands for the value of X_2 for which $\overline{\dot{Q}}_i$ changes sign (i being the index of the hot reservoir).

produced by the different temperatures of the thermal reservoirs.

In Fig. 3.7, we show the efficiency as a function of the asymmetry for various values of X_2. Similarly to the previous figure, the vertical lines denote the values of κ for which the heat from the hot reservoir change sign and delimits the isothermal work-to-work converter regime. The discussion whether the isothermal work-to-work converter regime lies to the left or right of the vertical lines is not so obvious because both $C(\tau_1)$ and $\langle v_1 \rangle$

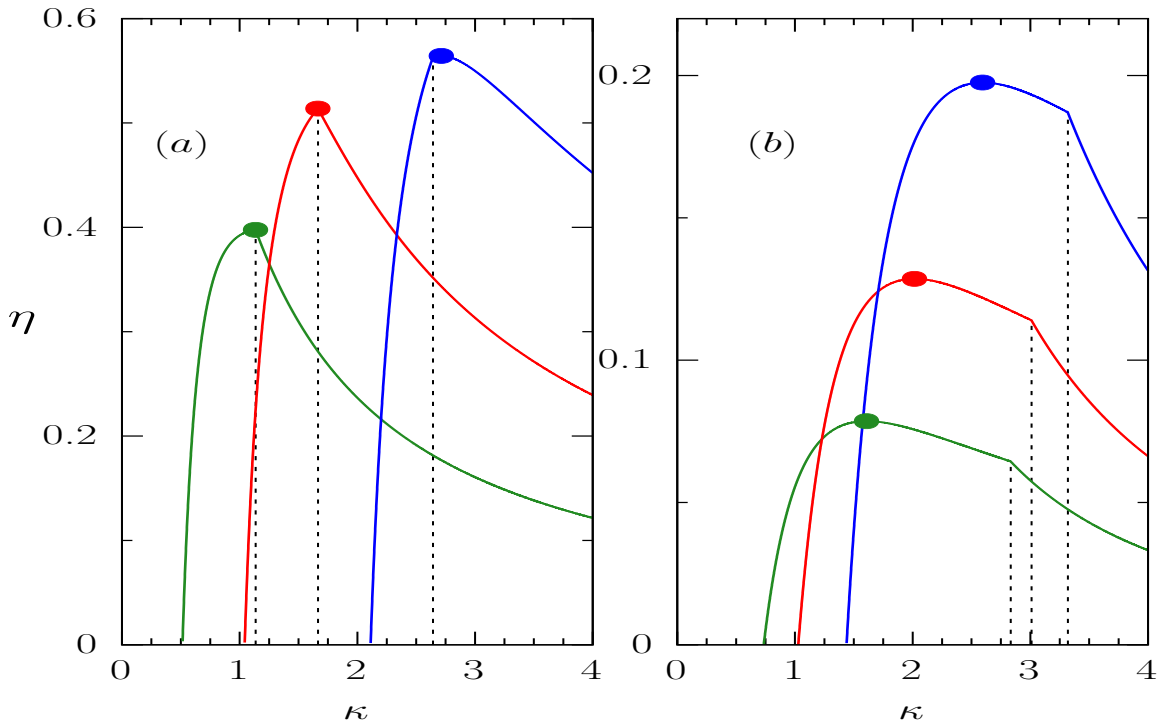

Figure 3.7: Efficiency versus the time asymmetry κ for the (a) constant and (b) and linear drivings, respectively, for $\tau = 1$, $\gamma = 1$ and $X_1 = 1$ and different temperatures [$\Gamma_1 = 2.0$ and $\Gamma_2 = 1.5$]. Circles denote maximum efficiencies and their X_{2MP}'s are the same as in Fig. 3.3. From left to right, $X_2 = -0.5, -1.0$ and -2.0. Dashed vertical lines stands for the value of κ for which $\overline{\dot{Q}}_1$ changes sign. For such set of parameters κ_{2mS} are out of the engine regime.

depend on the asymmetry. However, the work-to-work regime lies to the right of the lines, since the function $C(\tau_1)$ reaches its maximum for $\kappa = 1(\tau_1 = \tau/2)$ and the first term on the right-hand side of Eq. (3.42) is expected to increase giving that its limit of integration increases with κ.

Fig. 3.8 presents heat maps of the efficiency for different temperature reservoirs as a function of the output force and asymmetry. By drawing a comparison with the isothermal work-to-work converter (Fig. 3.4), it reveals that the difference of temperature makes the choice of the optimization parameter (force strength or time asymmetry) more relevant. While both optimized lines lie almost on top of each other for the isothermal case, Fig. 3.8 shows that they are clearly distinct, particularly for the linear drivings. Another point to be addressed concerns that high efficiencies are restricted to larger $|X_2|$'s for constant drivings when temperatures are different. This contrasts to its extension to smaller values for isothermal reservoirs [the hot (red) region in Fig. 3.4(b) is more spread than in Fig. 3.8(a)]. Conversely, for linear drivings, the decrease of the efficiency extends for all values of κ and X_2 when compared with the isothermal work-to-work converter [note that efficiency in Fig. 3.4(d) is 3

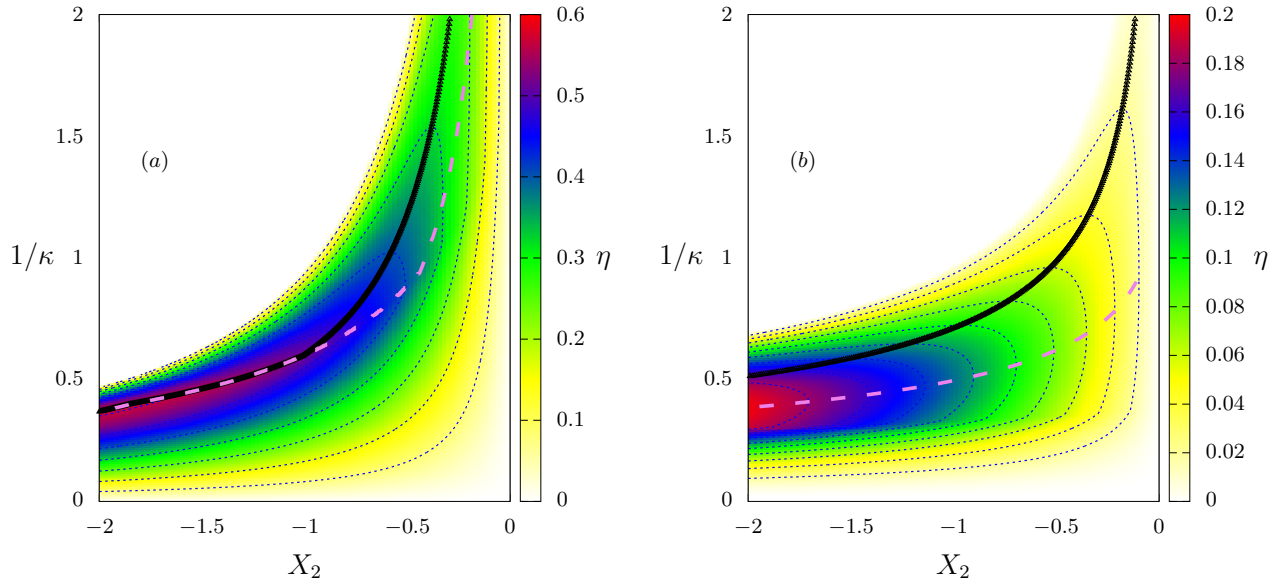

Figure 3.8: Depiction of efficiency as a function of the inverse of the asymmetry coefficient κ and the output force X_2, for constant (a) and linear (b) drivings, respectively. Solid and dashed lines denote the maximization with respect to X_2 and κ, respectively. Parameters: $\Gamma_1 = 2.0$ and $\Gamma_2 = 1.5$, $\tau = 1$, $\gamma = 1$ and $X_1 = 1$.

times larger than Fig. 3.8(b)]. However, larger efficiencies in such case is obtained solely for larger values of $|X_2|$ under a certain range of κ.

3.4 Symmetric case and $\Delta\Gamma \ll 1$

Finally, we will limit our study to the symmetric case $\kappa = 1$ (that is, $\tau_1 = \tau_2$). This particular case allows obtaining approximate expressions when the system operates at small temperature differences ($\Delta\Gamma \ll 1$) since under these conditions we can assume the symmetry relation $L_{12} \approx L_{21}$. To this end, we will propose an alternative definition for efficiency (described below) based on the ratio of entropy production flows [75]. This definition, although it is in qualitative agreement with previous results (section 3.3.1.3) and is approximately correct when reservoir temperatures are close ($\Delta\Gamma \to 0$ or $\Delta\Gamma << 1$), it overestimates the efficiency of the machine as $\Delta\Gamma$ increases. The alternative expression is defined as

$$\eta = -\frac{\mathcal{J}_1 X_1}{\mathcal{J}_2 X_2 + \mathcal{J}_T X_T} = -\frac{L_{11}X_1^2 + L_{12}X_1X_2}{L_{21}X_2X_1 + L_{22}X_2^2 + L_{TT}X_T^2}. \tag{3.45}$$

where $X_T = f_\Gamma$ and we use Eq. (3.16) to relate the flows with the Onsager coefficients.

The values of load forces X_{1mP}, X_{1mE} and X_{1mS} can be obtained straightforwardly from expressions for $\mathcal{P}$ and Eq. (3.45), respectively. Due to the present symmetric relation between Onsager coefficients (in both cases),

they acquire simpler forms and read $2X_{1mP} = -L_{12}X_2/L_{11}$,

$$X_{1mE} = \frac{1}{L_{11}L_{12}X_2}\left[-L_{11}(L_{22}X_2^2 + L_{TT}X_T^2) + A(X_2, X_T)\right], \tag{3.46}$$

with $A(X_2, X_T)$ being given by

$$A(X_2, X_T) = \sqrt{L_{11}(L_{22}X_2^2 + L_{TT}X_T^2)}\sqrt{[L_{11}(L_{22}X_2^2 + L_{TT}X_T^2) - L_{12}^2X_2^2]} \tag{3.47}$$

and $X_{1mS} = -L_{12}X_2/L_{11} = 2X_{1mP}$, respectively.

The efficiencies at minimum dissipation, maximum power and its maximum value become $\eta_{mS} = 0$,

$$\eta_{mP} = \frac{L_{12}^2X_2^2}{2(2L_{22}L_{11} - L_{12}^2)X_2^2 + 4L_{TT}L_{11}X_{TT}^2}, \tag{3.48}$$

and

$$\eta_{mE} = \frac{1}{L_{12}^2X_2^2}[2L_{11}(L_{22}X_2^2 + L_{TT}X_{TT}^2) - L_{12}^2X_2^2 - 2A(X_2, X_T)], \tag{3.49}$$

respectively, and finally their associated power outputs read $\mathcal{P}_{mS} = 0$, $\mathcal{P}_{mP} = \Gamma_1 L_{12}^2X_2^2/4L_{11}$ and

$$\mathcal{P}_{mE} = \frac{\Gamma_1}{L_{11}L_{12}^2X_2^2}\left[L_{11}(L_{22}X_2^2 + L_{TT}X_T^2) - A(X_2, X_T) - L_{12}^2X_2^2\right]\left[L_{11}(L_{22}X_2^2 + L_{TT}X_T^2) - A(X_2, X_T)\right], \tag{3.50}$$

respectively.

We pause to make a few comments: First, above expressions extend the findings from Ref. [58] for a couple of driving forces. Second, both efficiency and power vanish when $X_1 = X_{1mS}$ and $X_1 = 0$ and are strictly positive between those limits. Hence the physical regime in which the system can operate as an engine is bounded by the lowest entropy production $\overline{\Pi}_{mS} = L_{TT}X_T^2 + (L_{22} - L_{12}^2/L_{11})X_2^2$ and the value $\overline{\Pi}^* = L_{TT}X_T^2 + L_{22}X_2^2$. Third, despite the long expressions for Eqs. (3.49) and (3.50), powers $\mathcal{P}_{mP}, \mathcal{P}_{mE}$ and efficiencies η_{mP}, η_{mE} are linked through a couple of simple expressions (3.31) and they imply that $0 \leq \eta_{mP} < \eta_{mE}$ (with $0 \leq \eta_{mE} \leq 1$ and $0 \leq \eta_{mP} \leq 1/2$) and $0 \leq \mathcal{P}_{mE} \leq \mathcal{P}_{mP}$. Fourth and last, the achievement of most efficient machine $\eta_{mE} = 1$ implies that the system has to be operated at null power $\mathcal{P}_{mE} = 0$ and hence the projection of a machine operating for finite $\mathcal{P}_{mP}/\mathcal{P}_{mE}$ will imply at a loss of its efficiency. Onsager coefficients become simpler in the limit of fast switchings, $\tau \to 0$ and L_{11}, L_{22}, L_{12} approach to $(\Gamma_1 + \Gamma_2)/(4\Gamma_1\Gamma_2)$. Some remarkable quantities then approach to the asymptotic values $f_{1mS} \to -f_2 = 2f_{1mP}$ and

$$\eta_{mP} \to \frac{f_2^2(\Gamma_1 + \Gamma_2)}{2[f_2^2(\Gamma_1 + \Gamma_2) + 2\Delta\Gamma^2]}, \tag{3.51}$$

respectively. For $\Gamma_1 \approx \Gamma_2$, $\eta_{mP} \to 1/2$, $\eta_{mE} \to 1$ and $\mathcal{P}_{mP}$ reads $\mathcal{P}_{mP} \to f_2^2/8$ and thereby the limit of an ideal machine is achieved for low periods and equal temperatures.

Similar features are verified for the linear driving, including increasing efficiencies as both τ and $\Delta\Gamma$ decreases. However, they are marked by a reentrant behavior for $\tau << 1$ and $\Delta\Gamma \neq 0$ (see e.g. Fig. 3.10). It moves for lower τ's as $\Delta\Gamma$ goes down and the limit of ideal machine, $\eta_{mP} \to 1/2$ and $\eta_{mE} \to 1$, is also recovered when both $\tau \to 0$ for $\Delta\Gamma \to 0$.

Other differences between protocols are appraised in Figs. 3.9 and 3.10. For finite difference of temperatures, the constant driving is always more efficient than the linear one and their power outputs are also superior. The maximum efficiency curves (linear drivings) are also reentrant, whose maxima values increase and deviate for lower τ's as $\Delta\Gamma$ decreases.

We close this section by remarking that although short periods indicates a general route for optimizing the efficiency of thermal machines in contact to sequential reservoirs, the present description provides to properly tune the period and forces in order to obtain the desirable compromise between maximum efficiency and power.

3.5 Conclusions

We introduced an alternative strategy for optimizing the performance of Brownian engines, based on the idea of asymmetric interaction time between the system (Brownian particle) and the thermal baths. Exact expressions for thermodynamic quantities and their maximized values were obtained, irrespective the kind of driving and asymmetry. The time asymmetry can always be tuned to obtain a gain larger than in the symmetric case. In addition to the improvement of the power output and efficiency, the time asymmetry also enlarges the range of forces for which the system operates as an engine. Another advantage of asymmetric times is that they can be conveniently chosen for compensating part of the limitations due the machine design, such as its operation period and the driving considered. Results for constant and linear drivings confirm that the appropriate tuning of the asymmetry produce gains for the efficiency substantially larger than those achieved for the symmetric case. It is important to point out that the symmetric engine does not necessarily operate inefficiently, as exemplified in Fig. 3.2. However, the tuning of the asymmetry, for given values of the other parameters (output force and period), provides a reliable route for enhancing the engine performance.

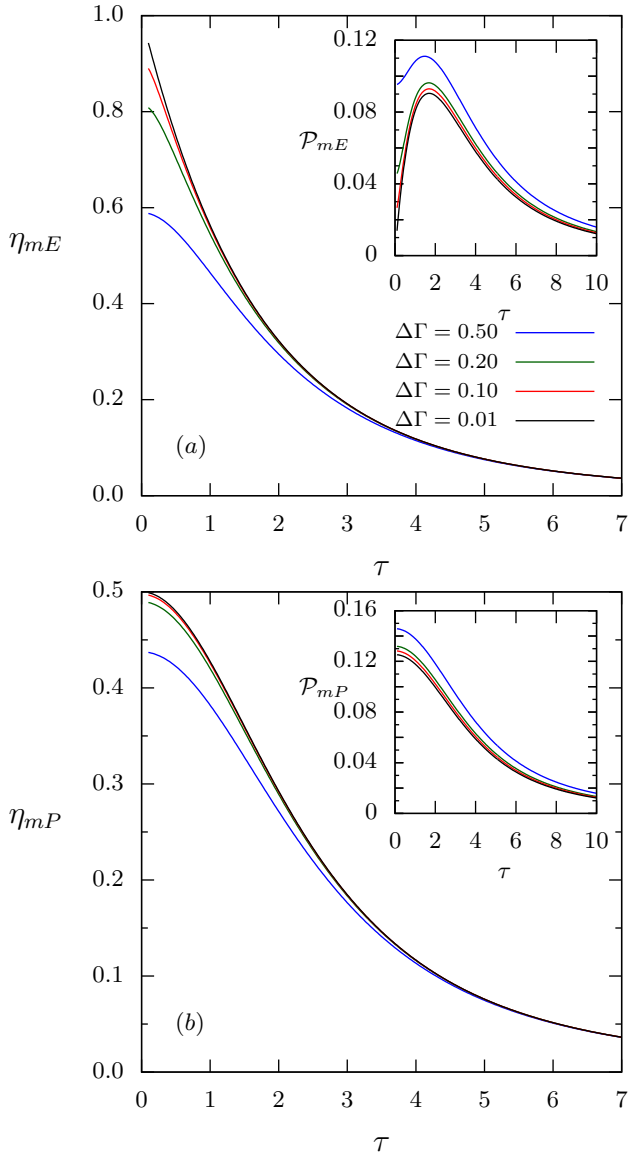

Figure 3.9: For $\Gamma_1 = 2$, $X_2 = 1$ and distinct $\Delta\Gamma$'s, the comparison between maximum efficiency (panel (a)) and efficiency at maximum power (panel (b)) for constant drivings. Insets: The corresponding power outputs $\mathcal{P}$'s versus τ.

Contrariwise to usual machines, for which the heat flow due to the gradient of temperature is fundamental for the power extraction and enhancing the efficiency, in the present case the efficiency is higher for isothermal reservoirs. The reason for such behavior concerns that the energy exchange between the Brownian particle and the different thermal reservoirs occurs in different stages. Since the heat transfer and the output force are uncoupled, the heat flux can not be converted into useful work. For instance, one would require drivings dependent of the velocity in order to be able to extract work from heat in the present model. Although the robustness of our findings has been verified for a few examples of drivings, our approach can be straightforwardly extended for other thermal machines, where in principle similar findings are expected. This is reinforced for

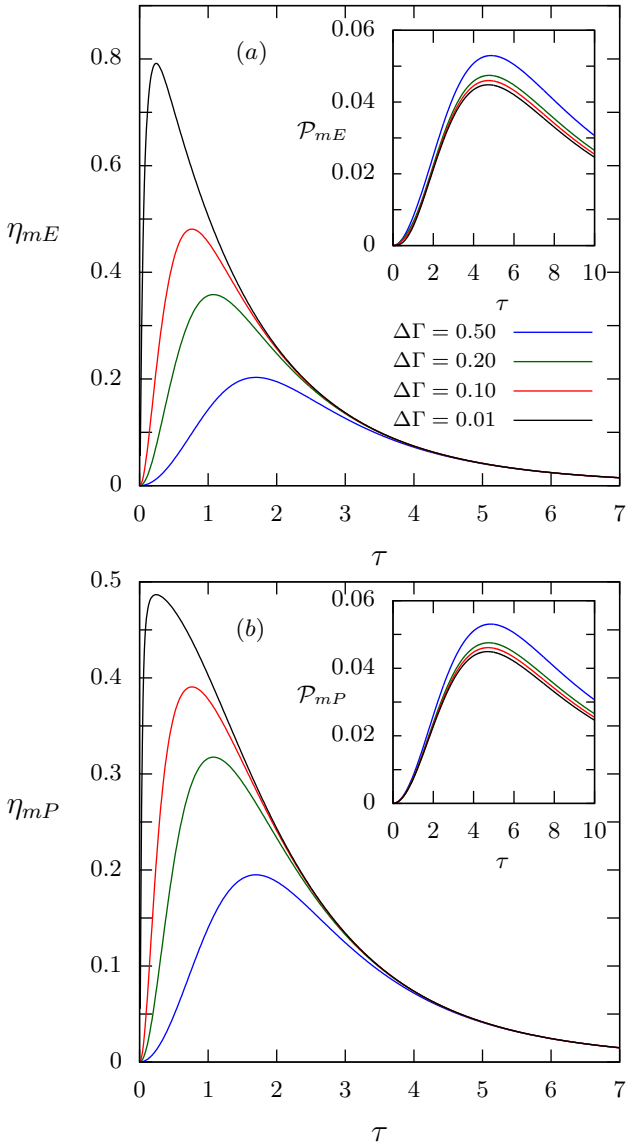

Figure 3.10: For $\Gamma_1 = 2$, $X_2 = 1$ and distinct $\Delta\Gamma$'s, the comparison between maximum efficiency (panel (a)) and efficiency at maximum power (panel (b)) for linear drivings. Insets: The corresponding power outputs $\mathcal{P}$'s versus τ.

recent results unveiling the importance of asymmetric times for optimizing the efficiency at maximum power of a quantum-dot thermal machine, which gain provides efficiencies larger than Curzon-Ahlborn [82].

We finish this chapter highlighting a couple of perspectives. While in the present work we analyzed the maximization of the output power and efficiency with respect to the time asymmetry and the output force strength, keeping the other parameters of the machine fixed, it might be worth to study the maximization under different physical conditions, such as holding the dissipation or efficiency fixed. Finally, it might also be interesting to extend the role of asymmetric times for other kinds of drivings (e.g. velocity dependent drivings providing

extraction of useful work from heat) as well as for massive Brownian particles (underdamped case) in order to compare their performances.

Chapter 4

Thermodynamics of a collisional quantum-dot machine: The role of stages.

4.1 Introduction

Stochastic engines are devices that convert a given amount of energy, say heat**,** into work or vice-versa. In contrast to macroscopic engines, they operate at the nanoscale and consequently the relevant thermodynamic quantities are subjected to fluctuations at the microscopic level, above all in power and efficiency. Although an ideal engine is always desired to operate at high power, high efficiency and low (power) fluctuations, these conditions can never be satisfied simultaneously. For this reason the development of distinct approaches/trade-offs has been strongly levered in the last years, such as by including the variation of external parameters [83], cyclic operations under quasistatic conditions [84], interaction between particles [85, 86], dynamics based on control via shortcuts to adiabaticy [72, 87, 88], to isothermality [89], maximization of power [31, 48, 50, 52, 53, 54, 55, 56, 57, 59, 60, 61, 62] and efficiency [58, 86] and more recently the strategies based on synchronized operation under ordered arrangements [90] or Pareto optimal cycles for power, efficiency and fluctuations [91].

Sequential (or collisional) engines have been put forward as an alternative candidate for the realisation of reliable thermal engines [92, 93] and novel engine setups [75, 82, 94, 95]. They consist of sequentially placing the system/engine in contact with distinct thermal reservoirs and subjected to external driving forces during each stage (stroke) of the cycle. Each stage is characterized by the connected thermal reservoir. The time needed to switch between the thermal baths at the beginning/end of each stage is neglected. Despite its reliability in

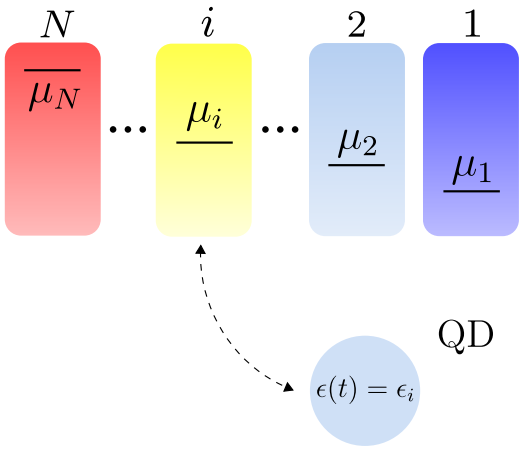

Figure 4.1: Sketch of a Quantum-dot setup sequentially exposed to N distinct thermal baths, each one at the interval $\tau_{i-1} \leq t < \tau_i = i\tau/N$ characterized by chemical potential μ_i and temperature $T_i = T$.

distinct situations [34, 76, 77, 78], the conditions to be imposed in order to provide a better performance have not been fully understood and for this reason distinct (and recent) approaches for enhancing its performance have been proposed and analyzed. Among them, we cite the convenient choices of the duration of each stroke [82, 94] and driving [86, 95].

In this contribution, we address a less explored strategy for improving the performance of collisional engines: the number of stages and the reservoir parameters for each stage. The system we consider is a particle pump model introduced in references [92, 93], consisting of a two-level system sequentially brought into contact with distinct reservoirs allowing for the exchange of particles among reservoirs and the generation of a power output. Quantum dot devices are one of the most prominent system in the realm of stochastic and quantum thermodynamics, as in theoretical [96, 97, 98, 99] and experimental [100] studies. Due to its simplicity, it presents several advantages such as an exact solution irrespective of the number of strokes and model parameters [96, 97, 98, 99]. And so it provides full access to all relevant quantities. Another advantage concerns that they can be projected to function either as heat or pump engines rather than Brownian engines, which only can be operated as work-to-work converters depending on the kind of external driving used as the work source [75, 86, 94, 95]. A careful analysis over the space of parameters for distinct intermediate stages reveals that a remarkable gain can be obtained by increasing the number of stages and a suitable choice of parameters.

4.2 Collisional engines

In this section we will study in more detail the collisional model briefly explained in section 2.3. The model we consider consists of a quantum dot (QD) and N thermal reservoirs. During operation, the QD is connected sequentially to each of the reservoirs, and this for a time duration τ/N. The total time to complete one cycle is τ. The QD has a single energy level which is either filled or empty. At stage i when the QD is connected to reservoir i we write $p_i(t)$ for the probability for the QD to be filled. The cycle is started at time $t = 0$ and the QD is connected to reservoir 1 which is characterised by the temperature T_1 and chemical potential μ_1. The energy level of the QD is set to ϵ_1. After a time duration τ/N, it is disconnected and reconnected to reservoir 2 with μ_2 and T_2. Furthermore, the energy level is changed from ϵ_1 to ϵ_2. This process of connecting/deconnecting is repeated until the N-th stage, marking a full cycle of period τ, after which the process starts all over. For simplifying matters we set all $T_i = T$ so that we obtain an isothermal operation. Figure 4.1 sketches the actual setup. For each stage i, we distinguish two *phases*:

- an *exchange* phase during which the QD is connected to reservoir i (chemical potential μ_i). During this phase the energy level of the QD is ϵ_i.
- an *external driving* phase during which the QD is uncoupled from any reservoir and its energy level is changed from ϵ_i to ϵ_{i+1}. Since the duration of this driving phase is irrelevant for the thermodynamic discussion we effectively set it equal to zero, so that the energy level change is instantaneous.

The time evolution of $p_i(t)$ at the i-th stroke is determined by the master equation

$$\dot{p}_i(t) = \left[1 - p_i(t)\right] \omega_{01}^{(i)} - p_i(t)\omega_{10}^{(i)}, \tag{4.1}$$

where the rates $\omega_{01}^{(i)}$ and $\omega_{10}^{(i)}$ account to filling up ($0 \to 1$) and vice versa ($1 \to 0$) respectively. These rates depend on ϵ_i and μ_i and are given by

$$\omega_{01}^{(i)} = \frac{\Gamma_0}{1 + e^{A_i}} \qquad \text{and} \qquad \omega_{10}^{(i)} = \frac{\Gamma_0 e^{A_i}}{1 + e^{A_i}}, \tag{4.2}$$

where Γ_0 quantifies the coupling strength between the system and thermal bath (for simplicity taken equal in all cases) and $A_i = \frac{1}{T}(\epsilon_i - \mu_i)$ for the i-th stroke.

In section 2.3.1 are introduced stochastic definitions for the heat rate (2.39), the chemical work rate (2.40), direct work rate (2.41) and entropy production (2.47), all averaged in one period.

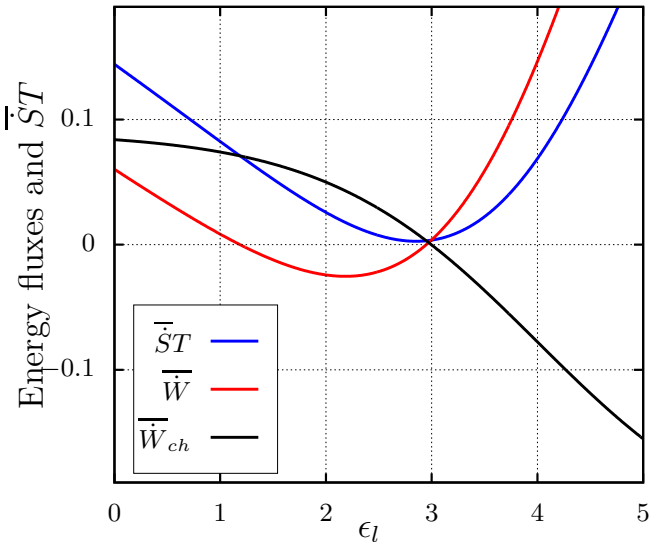

Figure 4.2: In the case of three stages, the entropy production times temperature $\overline{\dot{S}T}$ (blue), direct work $\overline{\dot{W}}_{\rm d}$ (red) and chemical work $\overline{\dot{W}}_{\rm ch}$ (black) vs ϵ_l. Parameters: $T = 1$, $\tau = 0.1$, $\Gamma_0 = 1$, $\epsilon_r = 1$, $\mu_r = 2$, $\epsilon_m = 1.7$, $\mu_m = 3$ and $\mu_l = 4$.

4.2.1 General expressions for the probability distribution and average flux

Although the QD evolves to the equilibrium regime when it is in contact with only one thermal bath, this is no longer true when it is periodically connected to different reservoirs. From Eq. (4.1) together with the continuity of $p_i(t)$ at each reservoir switching and taking into account that the system returns to the initial state after a complete period, one obtains the following (generic) expression for $p_i(t)$ for the i-th stage and N strokes [99]:

$$p_i(t) = p_i^{\rm eq} + \left[p\left(\frac{(i-1)\tau}{N}\right) - p_i^{\rm eq} \right] e^{-(\omega_{01}^{(i)}+\omega_{10}^{(i)})(t-\frac{(i-1)\tau}{N})}, \tag{4.3}$$

where $p_i^{eq} = \omega_{01}^{(i)}/(\omega_{01}^{(i)} + \omega_{10}^{(i)}) = (1 + e^{\frac{1}{T}(\epsilon_i - \mu_i)})^{-1}$ is obtained from transition rates $\omega_{01}^{(i)}$ and $\omega_{10}^{(i)}$ at the stage i for $(i-1)\tau/N \leq t < i\tau/N$. By expressing $p\left((i-1)\tau/N\right)$ in terms of probabilities from previous strokes, we finally arrive at the generic form for $p_i(t)$:

$$p_i(t) = p_i^{\rm eq} + e^{-(\omega_{01}^{(i)}+\omega_{10}^{(i)})(t-\frac{(i-1)\tau}{N})} \left\{ \sum_{m=2}^{i} \xi_{m,i-1}\Delta_{m-1,m} \; + \frac{\xi_{1,i-1}}{1-\xi_{1,N}} \left[\Delta_{N,1} + \sum_{n=2}^{N} \xi_{n,N}\Delta_{n-1,n} \right] \right\}, \tag{4.4}$$

solely expressed in terms of quantities $\Delta_{i,j} \equiv p_i^{\rm eq} - p_j^{\rm eq}$ and $\xi_{i,j} \equiv \exp\{-\frac{\tau}{N}\sum_{n=i}^{j}(\omega_{01}^{(i)} + \omega_{10}^{(i)})\}$. It is worth pointing out that $p_i(t)$ is the exact time-periodic occupation probability of the quantum dot at the i-th stage. We stress that since the system is ergodic and is periodically driven periodically, the relation $p_i(t+\tau) = p_i(t)$ holds for any stroke i. Having $p_i(t)$, average fluxes can be obtained. From Eqs. (2.37) and (4.3) the average flux $\overline{J}_i$ during

stage i reads

$$\overline{J}_i = \frac{1}{\tau}\left\{\frac{\xi_{1,i-1}}{1-\xi_{1,N}}\left[\Delta_{N,1} + \sum_{n=2}^{N}\xi_{n,N}\Delta_{n-1,n}\right] + \sum_{m=2}^{i}\xi_{m,i-1}\Delta_{m-1,m}\right\}(\xi_{i,i}-1). \tag{4.5}$$

From Eq. (4.5), the mean flux and thermodynamic quantities can be obtained for a generic N.

4.2.2 Two (N=2) and three (N=3) stages collisional engine

The simplest collisional engine is constituted by $N = 2$ strokes, in which at the first stage ($0 < t < \tau^*$) the system in contact with the right reservoir (and disconnected from the left reservoir), whereas in the second stage ($\tau^* < t < \tau$) the system is connected to the left reservoir (and disconnected from the right reservoir). Despite the simplicity, distinct aspects comprising the role of parameters for equal [92] and asymmetric switchings and distinct maximization routes [95] have been considered. By curbing our analysis to the the simplest symmetric case $\tau^* = \tau/2$, Eq. (4.5) reduces to:

$$\overline{J}_l = \frac{1}{2\tau}\left[\tanh\left(\frac{A_r}{2}\right) - \tanh\left(\frac{A_l}{2}\right)\right]\tanh\left(\frac{\Gamma_0\tau}{4}\right), \tag{4.6}$$

where $\overline{J}_r = -\overline{J}_l$ and indexes $i = r, l$ are associated with right or left reservoir respectively. From Eq. (2.39), the total heat exchanged $\overline{\dot{Q}} = \overline{\dot{Q}}_r + \overline{\dot{Q}}_l$ is given by

$$\overline{\dot{Q}} = (\epsilon_r - \mu_r - \epsilon_l + \mu_l)\overline{J}_l, \tag{4.7}$$

whereas chemical work and direct work, obtained from Eq. (2.40) and (2.41) respectively, read $\overline{\dot{W}}_{\rm chem} = (\mu_l - \mu_r)\overline{J}_r$ and $\overline{\dot{W}}_{\rm d} = (\epsilon_r - \epsilon_l)\overline{J}_r$.

Since the main goal of this chapter is to tackle the role of intermediate stages, we present a detailed analysis about the simplest setup with an intermediate stage, namely a cycle composed out of $N = 3$ stages. More

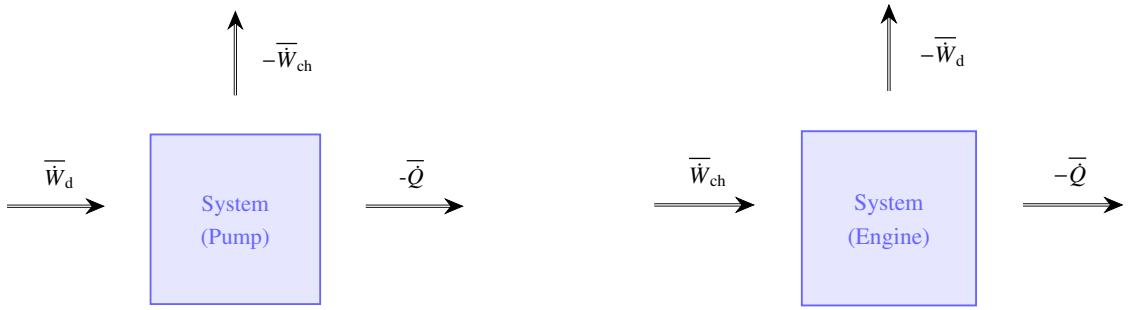

Figure 4.3: Sketch of a pump (left) and engine (right) working operation.

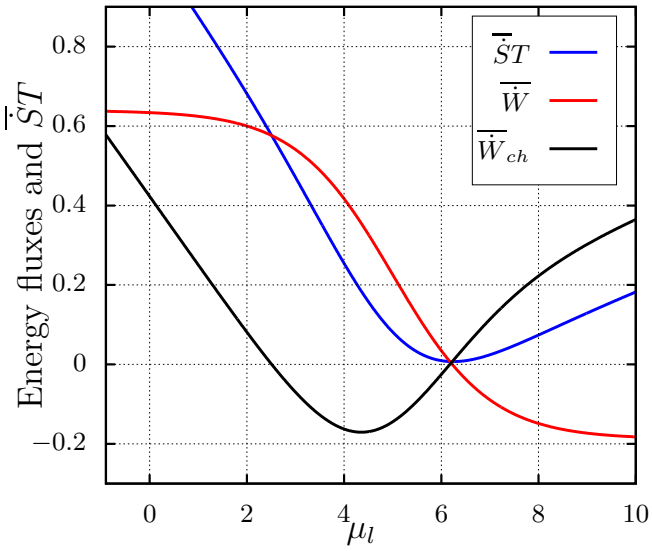

Figure 4.4: In the case of three stages, the entropy production times temperature $\overline{\dot{S}T}$ (blue), direct work $\overline{\dot{W}}_{\rm d}$ (red) and chemical work $\overline{\dot{W}}_{\rm ch}$ (black) vs μ_l. Parameters: $T = 1$, $\tau = 0.1$, $\Gamma_0 = 1$, $\epsilon_r = 1$, $\mu_r = 2$, $\epsilon_m = 1.7$, $\mu_m = 3$ and $\epsilon_l = 5$.

concretely, the system is placed in contact with the right reservoir during the first third of time, to the middle reservoir in the second stage, and to the left reservoir at the final stage, completing a periodic cycle after τ. From Eq. (4.3), the probability distribution $p_i(t)$ at the i-th stage reduces to the following expression

$$p_i(t) = \frac{1}{e^{A_i}+1} - \frac{e^{\Gamma_0(\frac{i\tau}{3}-t)}}{\phi}\left(\frac{1+e^{\frac{\Gamma_0\tau}{3}}}{e^{A_i}+1} - \frac{1}{e^{A_{i+1}}+1} - \frac{e^{\frac{\Gamma_0\tau}{3}}}{e^{A_{i+2}}+1}\right) \tag{4.8}$$

respectively, where $\phi = 1 + e^{\frac{\Gamma_0\tau}{3}} + e^{\frac{2\Gamma_0\tau}{3}} \geq 3$. From Eq. (4.5) for $N = 3$, each mean flux $\overline{J}_i$ reduces to the following expression:

$$\overline{J}_i = \Omega\Big[\left(1+e^{A_{i+1}}\right)\left(e^{A_i}-e^{A_{i-1}}\right)e^{\frac{\Gamma_0\tau}{3}} + \left(e^{A_{i-1}}+1\right)\left(e^{A_i}-e^{A_{i+1}}\right)\Big], \tag{4.9}$$

where

$$\Omega = \frac{e^{\frac{\Gamma_0\tau}{3}}-1}{(e^{A_r}+1)(e^{A_m}+1)(e^{A_l}+1)\phi\tau} > 0. \tag{4.10}$$

Quantities $\overline{\dot{W}}_{\rm chem}$ and $\overline{\dot{W}}_{\rm d}$ are straightforwardly obtained from Eqs. (2.40), (2.41) and (4.9), given by $\overline{\dot{W}}_{\rm chem} = (\mu_l-\mu_m)\overline{J}_l + (\mu_r-\mu_m)\overline{J}_r$ and $\overline{\dot{W}}_{\rm d} = (\epsilon_m-\epsilon_l)\overline{J}_l + (\epsilon_m-\epsilon_r)\overline{J}_r$, respectively.

A first insight into the behavior of thermodynamic quantities ($T\overline{\dot{S}}$, $\overline{\dot{W}}_{\rm d}$ and $\overline{\dot{W}}_{\rm ch}$) is depicted in Figs. 4.2 and 4.4 upon varying the energy ϵ_l and chemical potential μ_l respectively. In the former case, there is a closed region delimited by approximately $1 < \epsilon_l < 3$ in which $\overline{\dot{W}}_{\rm d} < 0$ and $\overline{\dot{W}}_{\rm ch} > 0$, consistent to an engine operation (as

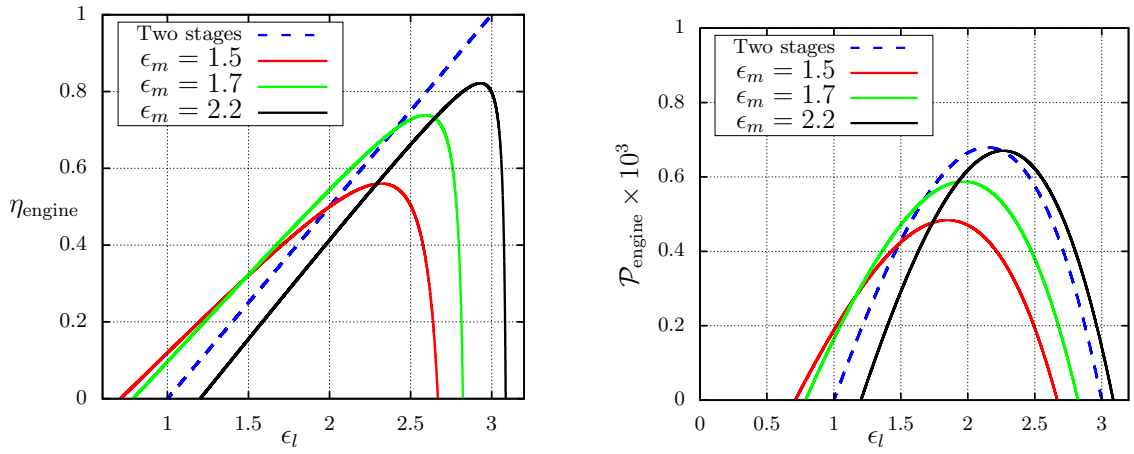

Figure 4.5: For the engine operation mode and distinct ϵ_m's, the depiction of efficiency η (left) and power $\mathcal{P}_{engine}$ (right) versus ϵ_l for $N = 2$ and $N = 3$ stages. Parameters: $\tau = 15$, $\Gamma_0 = 1$, $\epsilon_r = 1$, $\mu_r = 2$, $\mu_m = 3$ and $\mu_l = 4$.

shall be explained further). Conversely, for $\epsilon_l > 3$, one has that $\overline{\dot{W}}_{\rm d} > 0$ and $\overline{\dot{W}}_{\rm ch} < 0$, consistent to a pump regime operation. Similar findings are depicted in Fig. 4.4, but as μ_l is varied the pump regime is delimited by a closed region $2.5 < \mu_l < 6$, whereas the engine mode operation extends to $\mu_l > 6.2$.

4.3 Efficiency

Having introduced the main features of the model and obtained expressions for the relevant thermodynamical quantities, we are now in position to describe the operation of our collisional system as engine or as pump, together with the existence of distinct optimization routes. To start, a short comment about the sign of thermodynamic quantities in each regime is useful in order to establish a reliable definition of the efficiency. A particle pump typically consumes direct work $\overline{\dot{W}}_{\rm d}$ in order to move a particle from a lower to a higher chemical potential, which is consistent with $\overline{\dot{W}}_{\rm ch} < 0$ and $\overline{\dot{W}}_{\rm d} > 0$ (see e.g. left panel of Fig. 4.3). Since there is no particle accumulation in the QD, such delivered chemical work can only be the result of transferring particles from reservoirs at lower to those to higher chemical potentials. A reliable definition of power is given by $\mathcal{P}_{\rm pump} = -\overline{\dot{W}}_{\rm ch}$ with associated efficiency $\eta_{\rm pump}$ given by

$$\eta_{\rm pump} = \frac{\mathcal{P}_{\rm pump}}{\overline{\dot{W}}_{\rm d}}, \tag{4.11}$$

respectively. By construction, the above efficiency definition implies that $0 \leq \eta_{\rm pump} \leq 1$.

With an appropriate choice of parameters the system can also operate as an engine ($\overline{\dot{W}}_{\rm d} < 0$ and $\overline{\dot{W}}_{\rm ch} > 0$),

as sketched in right panel of Fig. 4.3. The dynamics are similar, but in this case the power output is given by $\mathcal{P}_{\text{engine}} = -\overline{\dot{W}}_{\text{d}} \geq 0$ according to the efficiency definition:

$$\eta_{\text{engine}} = \frac{\mathcal{P}_{\text{engine}}}{\overline{\dot{W}}_{\text{ch}}}, \tag{4.12}$$

where $0 \leq \eta_{\text{engine}} \leq 1$. It is worth pointing out that such efficiency definitions state that $\eta_{\text{pump}} = 1/\eta_{\text{engine}}$. For the two simplest $N = 2$ and $N = 3$ cases, efficiencies are given by

$$\eta_{\text{engine},N=2} = (\epsilon_l - \epsilon_r)/(\mu_l - \mu_r), \tag{4.13}$$

and

$$\eta_{\text{engine},N=3} = \frac{(\epsilon_l - \epsilon_m)\overline{J}_l + (\epsilon_r - \epsilon_m)\overline{J}_r}{(\mu_m - \mu_l)\overline{J}_l + (\mu_m - \mu_r)\overline{J}_r}, \tag{4.14}$$

due to the fact that $\overline{J}_l = -\overline{J}_r$, respectively. While the former solely depends on $\epsilon_l, \epsilon_r, \mu_l$ and μ_r, and the ideal regime $\eta_{\text{engine},N=2} = 1$ implies that $\overline{\dot{W}}_{\text{chem}} = -\overline{\dot{W}}_{\text{d}}$ and $\overline{\dot{S}} = 0$, the latter is more revealing and efficiencies depend on the interplay with intermediate parameters (μ_m, ϵ_m) and the period τ.

Analogous expressions are straightforwardly obtained for $N > 3$. Giving that they are longer (and less instructive), they will be omitted here. Below we investigate the influence of adding stages on the performance, cf efficiency and power. Our motivation for doing so is twofold. First, there is a fundamental difference between the $N = 2$ and $N > 2$ setup. As follows from the previous analysis, the $N = 2$ setup is a so-called thermodynamical strongly coupled system, cf [101]. It is well know that in the regime of linear thermodynamics, the efficiency can be made optimal for such systems (see for example [48, 52]). Yet, beyond the linear regime is it not at all clear whether these strongly coupled systems always do better than loosely coupled systems (as is the case for systems with $N > 2$). Second, the performance of any setup is the result of an intricate play between thermodynamics and dynamics (due to the periodic driving). Inserting additional stages makes the corresponding gradients (for example in chemical energy) smaller and hence might reduce the strong fluxes and corresponding dissipation/entropy production. The downside is of course that the number of steps increases, adding to the overall complexity. It is far from obvious how this influences the performance.

respectively. While the former solely depends on $\epsilon_l, \epsilon_r, \mu_l$ and μ_r, due to the fact that $\overline{J}_l = -\overline{J}_r$, the latter is more revealing and efficiencies depend on the interplay with intermediate parameters (μ_m, ϵ_m) and the period τ.

Analogous expressions are straightforwardly obtained for $N > 3$. Giving that they are longer (and less instructive), they will be omitted here.

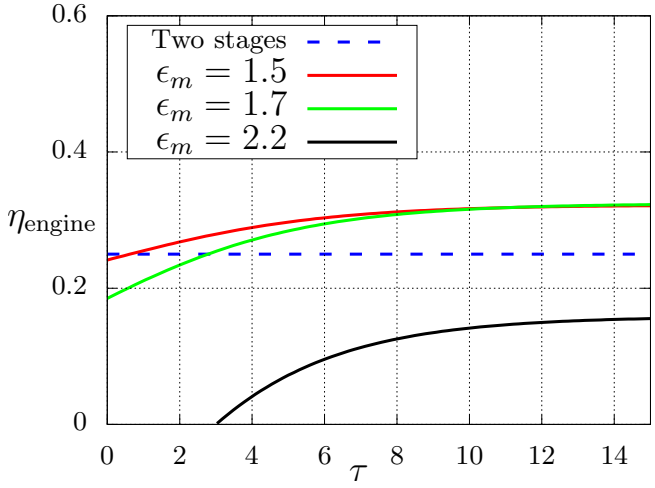

Figure 4.6: For ϵ_l fixed and distinct ϵ_m's, the depiction of efficiency η versus period τ for $N = 2$ and $N = 3$. Parameters: $\Gamma_0 = 1$, $\epsilon_r = 1$, $\epsilon_l = 1.5$, $\mu_r = 2$, $\mu_m = 3$ and $\mu_l = 4$.

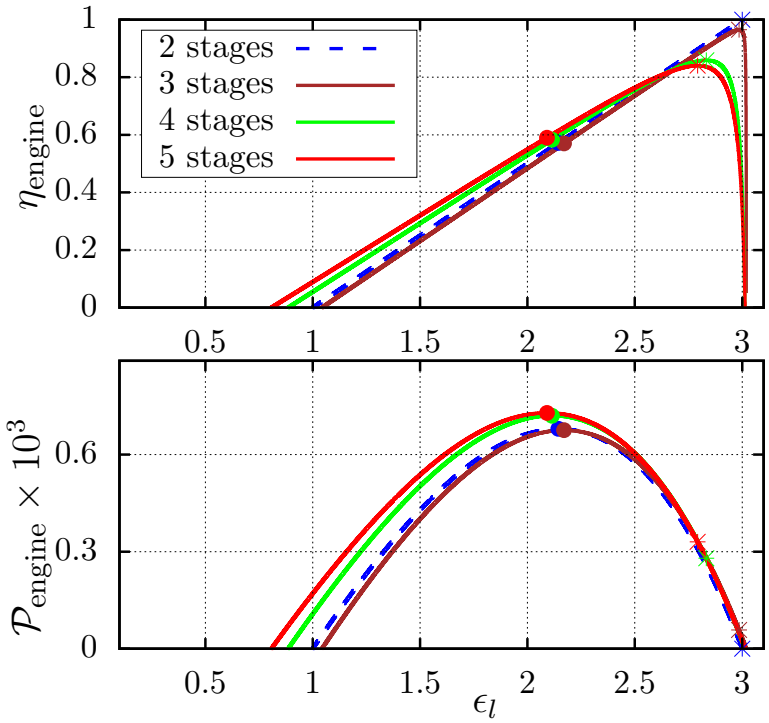

Figure 4.7: For the engine regime operation mode, the comparison between the efficiencies η's (top) and power outputs $\mathcal{P}$'s (bottom) for the two stages system (blue) and the three stages system (brown), four stages (green) and five stages (red) at engine regime vs. ϵ_l. Symbols $*$ and $\bullet$ correspond the maximization of η and $\mathcal{P}$, respectively. Parameters: $\alpha = 0.68$, $\tau = 15$, $\Gamma_0 = 1$, $\epsilon_r = 1$, $\mu_r = 2$ and $\mu_l = 4$.

4.3.1 Influence of intermediate reservoirs

As the number of stages increases, so to do the number of parameters. Below we optimise each setup by fine-tuning a number of these parameters. This is a relevant situation in an experimental context, in which adjusting each and every parameter continuously in order to reach a global optimisation may not always be feasible nor realisable. For this reason, our analysis will be undertaken by means of distinct strategies, as described throughout Secs. 4.3.1 and 4.3.2. In order to get a first insight about the influence of model parameters (N, ϵ_i's, μ_i's and τ) is depicted in Figs. 4.5 and 4.6 for three different values of ϵ_m by varying ϵ_l and τ respectively, and the parameters ϵ_r, μ_r, μ_m and μ_l held fixed (for simplicity). In the former case (fixed τ), the system efficiency is solely improved via adjustment of ϵ_l (or ϵ_r) and hence η exhibits a linear dependence on ϵ_l for $N = 2$, reaching the maximum (ideal) limit $\eta_{ME} = 1$ with $\mathcal{P}_{ME} = 0$, consistent with the reversible operation mode. Conversely, distinct routes for optimization become feasible for $N = 3$, such as by varying ϵ_m and ϵ_l and as a consequence, there are some regions in the set of parameters in which the inclusion of stages can confer a larger performance. However, maximum efficiency η_{ME} and power $\mathcal{P}_{M\mathcal{P}}$ for $N = 2$ is somewhat superior than for $N = 3$. Likewise, Fig. 4.6 reinforces such advantages for $N = 3$ by illustrating that efficiencies η's become superior as the duration τ of cycle increases.

Fig. 4.7 extends the above analysis by tackling number of strokes for N ranging from 2 to 5 by depicting η and $\mathcal{P}$ for distinct values of ϵ_l and ϵ_r, μ_r, μ_l held fixed. Due to the existence of several parameters, we adopt a simple criterion for choosing intermediate μ_m's, by changing them by a fixed amount $\mu_m = \mu_{m-1} + \Delta\mu$, where $\Delta\mu = (\mu_l - \mu_r)/(N-1)$ and corresponding ϵ_m values as proportional to them $\epsilon_m = \alpha\mu_m$ for all (intermediate) m. As for $N = 3$, the system performance can be improved by suitable choice of parameters and properly increasing the number of stages. Also like $N = 3$, associate maximum power and efficiencies are somewhat lower than for $N = 2$.

In Figure 4.8 we compare both power and efficiency of a $N = 3$ and $N = 4$ setup against the power and efficiency of a $N = 2$ setup which has been optimised for maximum power. That is, for $N = 2$ and the parameters μ_l, ϵ_r and μ_r held fixed, ϵ_l is determined by maximizing $\mathcal{P}$. In the (α, μ_l)-space shown in Figure 4.8 the blue and red areas are those for which respectively the power and efficiency for ther $N = 3$ and $N = 4$ setups are improved compared to the $N = 2$ setup. Furthermore, in case $N = 4$ there is an overlap between these regions (indicated in purple) for which both performance indicators are higher. This again supports our claim that the addition of stages improves the performance.

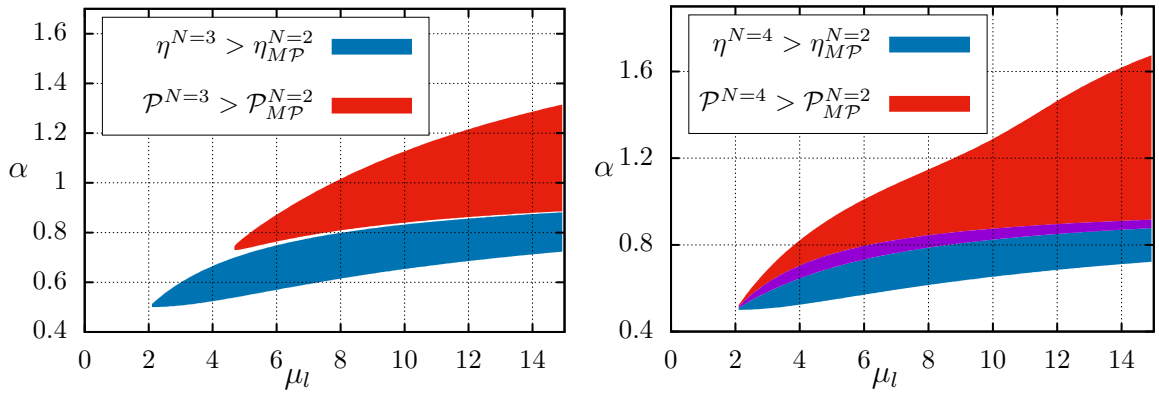

Figure 4.8: Top (bottom) panels depict, for the engine regime operation mode, the set of α values for which $\mathcal{P}$ (red area) and η (blue area) are for $N = 3(N = 4)$ greater than two stages power and efficiency at maximum power regime versus μ_l. Purple area (bottom) shows the intersection between red and blue ones. Parameters: $\tau = 15, \Gamma_0 = 1, \epsilon_r = 1, \mu_r = 2$.

4.3.2 Optimal parameter choices and maximizations for $N = 3$ stages

Due to the existence of more than one independent fluxes, the system optimization for $N > 2$ is rather different from $N = 2$ and it is closely dependent on the number of stages (mainly the efficiency). In this section, we exploit some optimization routes for $N = 3$, in which ϵ_m and μ_m are treated independently from each other. Our analysis will be carried out for $N = 3$ for the following choice of parameters: (ϵ_r, μ_r) always held fixed and by varying (ϵ_l, ϵ_m) [for (μ_l, μ_m) fixed] and the other way around. Despite the exactness of all results, expressions for maximized quantities are quite cumbersome and have to be found numerically by solving transcendental equations. In particular, maximal powers $\mathcal{P}_{M\mathcal{P}}$'s yield at ϵ_m^* (fixed ϵ_l) and ϵ_l^* (for fixed ϵ_m) and obey the following expressions:

$$\overline{J}_r(\epsilon_m^*) + \overline{J}_l(\epsilon_m^*) = (\epsilon_l - \epsilon_m^*)\overline{J}_l'(\epsilon_m^*) + (\epsilon_r - \epsilon_m^*)\overline{J}_r'(\epsilon_m^*), \tag{4.15}$$

in the former case (ϵ_l fixed), with maximum power

$$\mathcal{P}_{M\mathcal{P}} = (\epsilon_l - \epsilon_m^*)\overline{J}_l(\epsilon_m^*) + (\epsilon_r - \epsilon_m)\overline{J}_r(\epsilon_m^*) \tag{4.16}$$

and

$$\overline{J}_l(\epsilon_l^*) = \frac{1}{\epsilon_m}[\epsilon_l^*\overline{J}_l'(\epsilon_l^*) + (\epsilon_r - \epsilon_m)\overline{J}_r'(\epsilon_l^*)], \tag{4.17}$$

in the latter case (for fixed ϵ_m) with maximum power $\mathcal{P}_{M\mathcal{P}} = (\epsilon_l^* - \epsilon_m)\overline{J}_l(\epsilon_l^*) + (\epsilon_r - \epsilon_m)\overline{J}_r(\epsilon_l^*)$. Here $\overline{J}_X'(\epsilon_Y^*) \equiv \partial\overline{J}_X/\partial\epsilon_X$ evaluated at ϵ_Y^* and the notation $\overline{J}_Y(\epsilon_X)$ has been adopted here in order to state which energy was taken into account in the calculation of the derivative. Remarkably, the locus of maximum ϵ_m^* (fixed ϵ_l) and ϵ_l^* (fixed ϵ_m) intersect at a single point $(\bar{\epsilon}_m, \bar{\epsilon}_l)$, marking the existence of a global maximization of power, given by

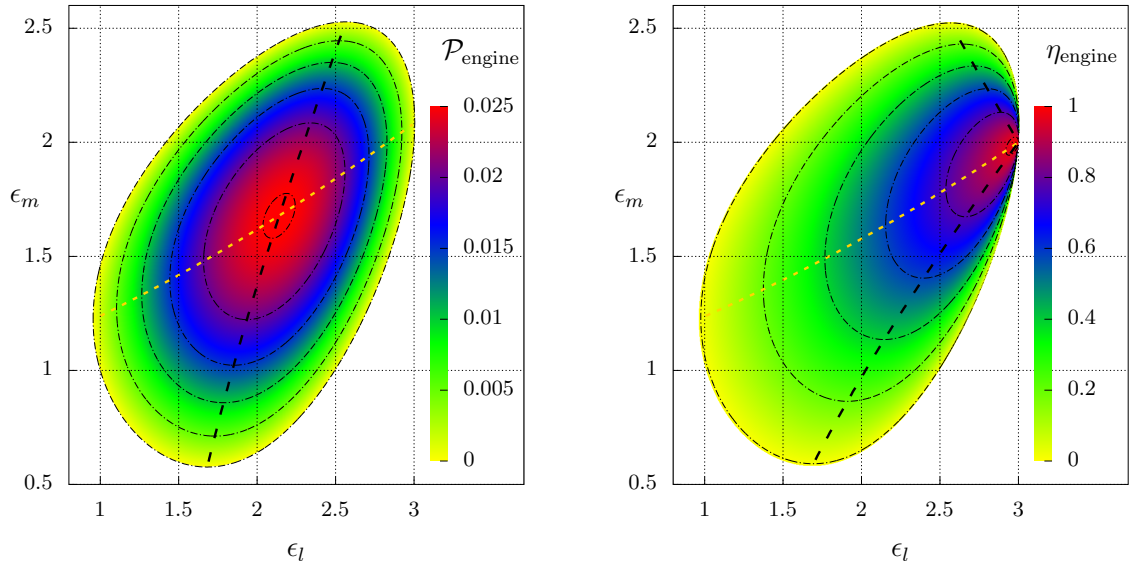

Figure 4.9: For the engine operation mode and $N = 3$, the power and efficiency heat maps for several values of ϵ_l and ϵ_m. White zones correspond to the dud regime. Parameters: $\tau = 1$, $\Gamma_0 = 1$, $T = 1$, $\epsilon_r = 1$, $\mu_r = 2$, $\mu_m = 3$ and $\mu_l = 4$.

$\mathcal{P}^*_{M\mathcal{P}} = (\bar{\epsilon}_l - \bar{\epsilon}_m)\bar{J}_l(\bar{\epsilon}_l) + (\bar{\epsilon}_r - \bar{\epsilon}_m)\bar{J}_r(\bar{\epsilon}_l)$. Analogous expressions are obtained for the pump regime operation just by replacing $\epsilon_X \to \mu_X$. It is worth mentioning that results are different for $N = 2$. While $\eta_{ME} = 1$, maximization of power at ϵ_l^* (ϵ_r fixed) fulfills the relation $\mathcal{P}_{MP} = (\epsilon_r - \epsilon_l^*)^2 \bar{J}_l'(\epsilon_l^*)$, which is different from expressions for $N = 3$.

Figs. 4.9 and 4.10 summarize our main findings for engine and pump regimes, respectively. Firstly, both $\mathcal{P}$ and η can be optimized under suitable choice of intermediate parameters ϵ_m^* and μ_m^* (dashed lines fulfill Eq. (4.15)). The former also being simultaneously maximized with respect to ϵ_l (or μ_l), characterized by a central region and given by the intersection between above lines. Efficiency heat maps are similar to power-output ones, but regions of larger efficiencies are shifted to larger values of ϵ_l/μ_l. Unlike $\mathcal{P}$, maximum efficiency lines do not intersect but they merge at the ideal limit operation $\eta \to 1$, consistent with zero dissipation $\bar{\dot{S}} = 0$. Once again, it is instructive to compare $N = 2$ and $N = 3$ efficiencies for the same sets of parameters $(\epsilon_l, \epsilon_r, \mu_l, \mu_r)$. While optimal ϵ_m^*'s (ϵ_l held fixed) provide larger efficiencies (dotted lines) than for $N = 2$ when ϵ_l is small, values of η_{MP} approach each other as ϵ_l's increases. Similar findings have been verified for the pump regime in Fig. 4.10 when μ_l is small and large. We close this section by drawing a comparison between heat maps from Fig. 4.9 for the opposite case, $\mu_r = 4 > \mu_l = 2$ (not shown). Although heat maps are akin, optimal power and efficiency regions move for lower sets of (ϵ_l, ϵ_m), including negative values. The ideal operation regime yields at $\epsilon_l = -1$ and $\epsilon_m \approx 0$. Conversely, the global maximum power $\mathcal{P}^*_{M\mathcal{P}}$ in such case is approximately half from that in Fig. 4.9.

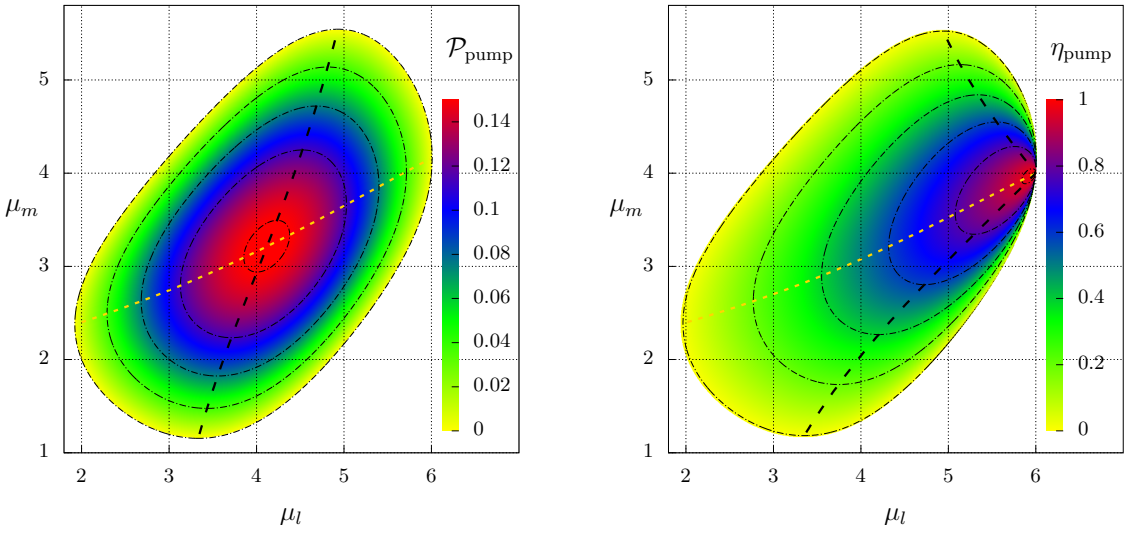

Figure 4.10: For the pump operation mode and $N = 3$, the power and efficiency heat maps for several values of μ_l and μ_m. White zones correspond to the dud regime. Parameters: $\tau = 1$, $\Gamma_0 = 1$, $T = 1$, $\epsilon_r = 1$, $\mu_r = 2$, $\epsilon_m = 3$ and $\epsilon_l = 5$.

4.4 Conclusions

We addressed an alternative route for optimizing the performance of a collisional nonequilibrium setup composed of a quantum-dot, exposed sequentially to distinct reservoirs. Quantum-dot engines have been broadly investigated in the realm of nonequilibrium and quantum thermodynamics and the present system yields an exact solution, irrespective of its projection (energy, chemical potential, period and number of strokes). Despite this, its behavior is rich enough and allows for distinct operations, such as a work-to-work transducer, engine, heat engine and pump. As we demonstrate, the number of stages is a highly relevant parameter which has a significant impact on the performance. Adjusting the number of stages therefor is a highly relevant strategy that allows to enhance the performance. The main point concerning our findings is that a suitable choice of number of stages can provide a better system performance than fewer strokes, above all when the period τ is longer (see e.g. Fig. 4.5). Thereby, a better performance of QD setups for large N and τ might be not only more feasible but also more advantageous from the experimental point of view. It is instructive to compare with collisional Brownian engines [75, 94], which operate less efficiently for large τ. As potential perspectives, we highlight to extend the idea of splitting the dynamics into distinct strokes for other engine setups, such as those presenting collective effects [85, 90, 102].

Chapter 5

Current fluctuations in nonequilibrium discontinuous phase transitions

5.1 Introduction

In microscopic systems, currents of heat, work and entropy production must be treated as random variables, which fluctuate over different runs of an experiment [47, 103]. This represents a paradigm shift in thermodynamics, and has already led to fundamental advancements in the field, such as fluctuation theorems [104, 15, 10, 11, 105, 106] and, more recently, the discovery of thermodynamic uncertainty relations [37, 107, 108, 109, 110]. It also entails practical consequences, e.g. in the design of Brownian engines [27, 65, 66, 67], molecular motors [79, 111, 112, 113], information-driven devices [114, 115], and bacterial baths [68]. In these systems, both the output power [116, 117] and the efficiency [49, 118, 119, 120] may fluctuate significantly, leading to possible violations of macroscopic predictions, such as the Carnot limit. [65].

A scenario of particular interest is that of non-equilibrium steady-states (NESSs), which occur when a system is placed in contact with multiple reservoirs at different temperatures T_i and/or chemical potentials μ_i. NESSs are characterized by finite currents of energy and matter, and thus also a finite entropy production rate σ_t [30, 40, 47, 121, 122]. At the stochastic level, these become fluctuating quantities, associated to a probability distribution. Understanding the behavior of said distributions constitutes a major area of research, as they form the basis for extending the laws of the thermodynamics towards the microscale, providing insights in non-trivial properties of non-equilibrium physics. Of particular interest is their behavior across non-equilibrium

phase transitions [123]. Most of our understanding, however, is centered on the average current. For instance, the average entropy production rate has been found to be always finite around the transition point, with the first derivative either diverging, in continuous transitions [29, 42, 124, 125, 126, 127, 128], or presenting a jump in discontinuous ones [42, 129, 128]. These clear signatures suggest, in fact, that the average entropy production could even be used to classify the type of transition. Conversely, the behavior of higher order statistics, such as the variance, is much less understood.

Cumulants of thermodynamic currents are usually assessed via numerical approaches, such as Monte Carlo simulations [42], or large deviation theory (LDT) [104, 130, 131, 132, 133, 134]. In both cases, cumulants are computed from long-time sample averages, integrated over a time window τ. Ultimately, one is interested in taking $\tau \to \infty$, at least in principle. But in systems presenting discontinuous transitions this can become an issue, since the phase coexistence is characterized by states with very long metastability lifetimes τ_m. In fact, τ_m increases exponentially with the system volume V, which is a consequence of the discontinuous nature of the transition (for continuous transitions these divergences are algebraic). As a consequence, the order of the limits $\tau \to \infty$ and $V \to \infty$ becomes non-trivial [135].

In this chapter we approach this issue by introducing the idea of conditional currents, given which phase the system is in. We focus, in particular, on the diffusion coefficient (scaled variance). We formulate a finite-time large deviation theory, which neatly highlights the non-trivial interplay between τ and τ_m. This is then specialized to a minimal 2-state model, that is able to capture the key features of the problem and also provides useful predictions. These are then tested on two paradigmatic examples of discontinuous transitions: Schlögl's model of chemical kinetics, and a 12-states Potts model subject to two baths at different temperatures. In this thesis we only shown results associated to Potts model, in order to know the results associated to Schlögl's model see Ref. [136].

5.2 Discontinuous phase transitions

For describing the entropy production behavior beyond the mean-field case, we also resort to the ideas from Refs. [42, 43, 137], they have attested that discontinuous phase transitions yield stark differences in regular and complex networks.

5.2.1 Beyond the mean-field: Regular lattices

As described previously, such behavior stems from sudden changes of $|m|$, its variance $\chi = N[\langle m^2\rangle - |m|^2]$ and other quantities whose scaling behavior goes with the system volume N. Both of them, together previous expressions in Sec. 2.4 can be described from the generic assumption in which at the vicinity of an arbitrary discontinuous phase transition point q_0, in which the correlation length is finite, the probability distribution can be approximately written down as a sum of two independent Gaussians, from which one extracts a scaling behavior with the system volume. Here I obtain them in more details. More specifically, the probability distribution is given by $P_N(m) = P_N^{(o)}(m) + P_N^{(d)}(m)$, where $P_N^{(\alpha)}(m)$ is associated to the phase α (with order-parameter m_α):

$$P_N^{(\alpha)}(m) = \frac{\sqrt{N}}{\sqrt{2\pi}} \frac{\exp[N\{\Delta q m - (m-m_\alpha)^2/(2\chi_\alpha)\}]}{[F'_o(\Delta q;N) + F'_d(\Delta q;N)]}. \tag{5.1}$$

Parameters χ_α and $\Delta q \equiv q_N - q_0$ correspond to the distribution width and the "distance" to the coexistence point q_0, respectively. Although in principle the assumption of two independent Gaussians can not describe properly a "weak" discontinuous phase transition, in which an overlap between $P_N^{(o)}(m)$ and $P_N^{(d)}(m)$ is expected, its reliability has been verified in several examples of nonequilibrium phase transitions with distinct properties, even in some cases in which the overlap is observed.

Despite the steady entropy production displaying a non-trivial dependence on the system features and on generic correlations of type $\langle\sigma_i\rangle$, $\langle\sigma_i\sigma_{i+1}\rangle$, $\langle\sigma_i\sigma_{i+1}\sigma_{i+2}\rangle$ and so on, Eq. (2.44) depicts it as the ensemble average of a fluctuating quantity, enabling resorting to the central limit theorem ideas. The generality of order-parameter distribution for tackling the phase coexistence and Eq. (2.44) setting up Φ as an ensemble average suggests the extension of a similar relationship for the steady entropy production. More concretely, we assume that $P_N(\phi) = P_N^{(o)}(\phi) + P_N^{(d)}(\phi)$, where $P_N^{(\alpha)}(\phi)$ is given by

$$P_N^{(\alpha)}(\phi) = \frac{\sqrt{N}}{\sqrt{2\pi}} \frac{\exp[N\{\Delta q\phi - (\phi-\mu_\alpha)^2/(2\bar{\chi}_\alpha)\}]}{[F_o(\Delta q;N) + F_d(\Delta q;N)]},$$

where each Gaussian is centered at μ_α with $\bar{\chi}_\alpha$ being the width of the $\alpha-$th peak. Given that $P_N(\phi)$ is normalized, each term $F_{o(d)}$ then reads $F_{o(d)}(\Delta q;N) = \sqrt{\bar{\chi}_{o(d)}}\,\exp\{N\Delta q\,[\mu_{o(d)} + \bar{\chi}_{o(d)}\Delta q/2]\}$. The steady entropy production $\Pi = \Phi$ is straightforwardly calculated from $P_N(\phi)$, $\Phi = \int_{-\infty}^{\infty}\phi P_N(\phi)d\phi$, reading

$$\Pi = \sum_{\sigma=o,d} \frac{(\mu_\sigma + \bar{\chi}_\sigma\Delta q)\,F_\sigma(\Delta q;N)}{F_o(\Delta q;N) + F_d(\Delta q;N)}. \tag{5.2}$$

According to the finite-size scaling (FSS) theory, at the vicinity of the critical point q_c, a given quantity X [$X \in (|m|, \chi$ and $\Pi' \equiv d\Pi/dq)$] will behave as $X = N^{y_x/\nu} f_x(N^{1/\nu}|\epsilon|)$, where q_x is a scaling function, $\epsilon = (q-q_c)/q_c$ is the distance to the criticality and y_x is the critical exponent obtained from ($y_x = -\beta, \gamma$ and α)[138]. The last exponent is similar to the relationship between the thermal derivative of the entropy, S, and specific heat,

C, in equilibrium phase transitions (recalling that $C = N^{\alpha/\nu} f_c(N^{1/\nu}|\epsilon|)$ [138], illustrating that the connection between entropy production and exchanged heat presented here introduces a physical argument for such scaling behavior. For discontinuous transitions, let us consider a generic ensemble average X, the starting point consists of assuming a bimodal Gaussian distribution, centered at μ_o and μ_d (with associated variances χ_o and χ_d). In the case of the steady entropy production at the vicinity of $\epsilon = q - q_c$, a bimodal entropy production probability distribution centered at μ_o and μ_d (with associate variances χ_d and χ_o) leads to the approximate expression for Π:

$$\Pi \approx \frac{\mu_o + \overline{\alpha}\mu_d e^{-N[(\mu_o-\mu_d)\epsilon]}}{1 + \overline{\alpha} e^{-N[(\mu_o-\mu_d)\epsilon]}}, \tag{5.3}$$

where $\overline{\alpha} = \sqrt{\chi_d/\chi_o}$. We note that the ordered and disordered phases are favored as $\epsilon < 0$ and $\epsilon > 0$ (assuming that $\mu_o < \mu_d$), respectively, and $\Pi^* = (\mu_o + \overline{\alpha}\mu_d)/(1 + \overline{\alpha})$ at $\epsilon = 0$, indicating that all entropy production curves, simulated for distinct N's, will cross at the transition point q_c. The crossing point clearly discerns continuous and discontinuous phase transitions and can be used as an indicator of the phase coexistence. Having Π, its derivative in respect to f behaves at the vicinity of q_c as:

$$\Pi' \approx \frac{N(\mu_o - \mu_d)^2 e^{N(\mu_o-\mu_d)\epsilon}}{\overline{\alpha}\left(1 + \overline{\alpha} e^{N(\mu_o-\mu_d)\epsilon}\right)^2}, \tag{5.4}$$

showing that Π' scales with N at the coexistence $\epsilon = 0$, in agreement with the above finite size expression for the quantity X.

5.2.2 Beyond the mean-field: Complex networks

Distinct works have stated that in contrast to regular structures, the phase coexistence in complex networks is akin to the MFT, whose behavior is generically characterized by the existence of a hysteretic loop and bistability. The order parameter will present a spinodal line in which along the hysteretic loop the system will converge to one of the possible steady states depending on the initial configuration. For locating the "forward transition" point q_f, the system is initially placed in an ordered configuration and the tuning parameter q is increased by an amount δ, whose final state at q is used as the initial condition at $q + \delta$ until the order-parameter discontinuity is viewed. Conversely, the "backward transition" point q_b is pinpointed by starting from the disordered phase and decreasing q (also by the increment δ) until the order-parameter jump takes place. Entropy production also captures these features, which can be viewed through a general argument for order-disorder phase transitions. The order-parameter behaves as $\langle\sigma_i\rangle \sim N^{-1/2}$ in the disordered phase and then a $n-$th correlation will behave as $\langle\sigma_i\sigma_{i+1}...\sigma_{i+n}\rangle \approx \langle\sigma_i\rangle\langle\sigma_{i+1}\rangle...\langle\sigma_{i+n}\rangle = N^{-n/2}$. Hence in the thermodynamic limit, all correlations will vanish in the disordered phase and Π will depend solely on control parameters. Contrariwise, $\langle\sigma_i\sigma_{i+1}...\sigma_{i+n}\rangle$ presents a well defined (nonzero) value in the ordered phase and Π depends not only on the control parameters but also on

correlations. So that, the jumps at q_f (from $m_1 \equiv m(q_f) \neq 0$ to 0) and q_b (from 0 to $m_2 \equiv m(q_b) \neq 0$), commonly viewed in terms of order-parameter, will also be present in the entropy production. The presence of bistability implies that $\Phi(t)$ will converge to one of the two well defined values, since along the hysteretic branch the system behaves just like the disordered or the ordered phase, depending on the initial condition. Although the above argument is valid for a generic order-disorder phase transition, it is expected to describe phase transitions different from the order-disorder ones, provided the order-parameter and correlations also present a hysteretic behavior. Thereby, both cases reveal that the entropy production behavior also embraces phase coexistence traits commonly treated in terms of the order-parameter.

5.3 Model and assumptions.

We consider a stochastic system $X(t)$ undergoing Markovian evolution. For simplicity, we assume continuous-time and a discrete (possibly infinite) set of states $X(t) \in \mathcal{S}$. The system probability $p_x(t)$ is assumed to evolve according to the master equation [139]

$$\dot{p}_x(t) = \sum_y \{W_{xy}p_y - W_{yx}p_x\} := \sum_y \mathbb{W}_{xy}p_y, \tag{5.5}$$

where $W_{xy} \equiv W_{y\to x}$ denotes the transition rates from y to x and $\mathbb{W}_{xx} \equiv -\sum_{y\neq x} W_{yx}$. The dynamics is taken to be ergodic, and such that $W_{xy} > 0$ whenever $W_{yx} > 0$, ensuring the system will relax to a unique steady state p^*_x. In general, p^*_x will be a non-equilibrium steady-state (NESS).

This NESS is also assumed to undergo a discontinuous transition by changing a certain control parameter λ to a threshold value λ_c. This means that in the vicinity of λ_c, there will exist a bistable region characterized by configurations with very long lifetimes. The two phases are labeled as 0 (for $\lambda < \lambda_c$) and 1 (for $\lambda > \lambda_c$). We monitor the phases by defining an indicator random variable $I_t = 0, 1$ (henceforth called the *phase indicator*), which specifies in which phase the system is at time t. This can always be done by partitioning the set of states $\mathcal{S}$ into two subsets, $\mathcal{S}_0$ and $\mathcal{S}_1$, representing each phase. The criteria for doing so is model dependent, and will be discussed further below. The probability of finding the system in phase 1, in the NESS, is then $q \equiv E(I_t) = \Pr(I_t = 1)$. We will also use the notation $q_1 = q$ and $q_0 = 1 - q$, when convenient.

The crucial aspect of discontinuous transitions is that, when the volume V is large, transitions between coexisting phases become extremely rare. The system will thus be governed by two very distinct timescales, one describing fast relaxation *within* each phase and another describing seldom transitions *between* the phases. The latter will be referred to as the metastability lifetime τ_m, and usually grows exponentially with V [140].

We consider the consequences of this type of scaling to the behavior of a generic integrated thermodynamic current. Given a certain time integration window τ, such a current may be defined as [108]

$$\mathcal{J}_\tau = \int_0^\tau dt \sum_{y,z} d_{yz}\delta_{X(t^-),y}\delta_{X(t^+),z}, \tag{5.6}$$

where δ_{ij} is the Kronecker delta, $X(t^\pm)$ is the state of the system immediately before and after a transition and d_{yz} is a function satisfying $d_{yz} = -d_{zy}$, which defines the current in question. In the limit $\tau \to \infty$, such a current will behave according to a large deviation principle [133]. But due to the sensitive interplay between τ and τ_m, we will not assume $\tau \to \infty$, as is customary. Instead, we will analyze the behavior of $\mathcal{J}_\tau$ as a function of τ. More specifically, our interest is in the regime where τ is large compared to the "within-phase" timescales, but not necessarily larger than the metastability lifetime τ_m. We will also focus on both the average J_τ, and diffusion coefficient (scaled variance) D_τ, defined as

$$J_\tau = E(\mathcal{J}_\tau)/\tau, \qquad D_\tau = \left(E(\mathcal{J}_\tau^2) - E(\mathcal{J}_\tau)^2\right)/(2\tau). \tag{5.7}$$

It turns out that $J_\tau \equiv J$ is independent of τ, irrespective of whether τ is large or not [133]. Conversely, for D_τ, this will be the case iff $\tau \gg \tau_m$.

The main feature we introduce in this chapter is the notion of conditional currents, given which phase $i = 0, 1$ the system is in. Inserting the identity $1 = (1 - I_t) + I_t$ inside the integral (5.6) allows us to define the current when the system is in phase 1 as

$$\mathcal{J}_{\tau|1} = \int_0^\tau dt\, I_{t^+} \sum_{y,z} d_{yz}\delta_{X(t^-),y}\delta_{X(t^+),z}. \tag{5.8}$$

The current $\mathcal{J}_{\tau|0}$ is defined similarly, but with $1 - I_t$ instead. There is an ambiguity here as to whether we use I_{t^-} or I_{t^+}. But this only affects those jumps in which $I_{t^-} = 0(1)$ and $I_{t^+} = 1(0)$, which are extremely rare compared to all others. It is important to clarify, at this point, that while the current (5.8) is conditioned on which phase the system is in, the dynamics itself is unconditional; that is, the system is still allowed to transition freely between phases. One could also analyze the currents for a conditional dynamics, where a reflecting barrier is placed between the phases, trapping the system in one phase or another. The relation between these two scenarios is discussed in Sec. 5.4.3.

From Eq. (5.8), the total current (5.6) is then recovered as

$$\mathcal{J}_\tau = \mathcal{J}_{\tau|0} + \mathcal{J}_{\tau|1}, \tag{5.9}$$

an identity which holds at the stochastic level. The conditional first moments are defined as

$$\mu_i = \frac{E(\mathcal{J}_{\tau|i})}{\tau q_i}, \tag{5.10}$$

where the factor of q_i in the denominator is placed to compensate for the varying times the system spends in each phase. The average current is thus decomposed as

$$J = (1-q)\mu_0 + q\mu_1. \tag{5.11}$$

As with J, the conditional averages μ_i will be shown below to also be independent of τ. Similarly, we define conditional diffusion coefficients

$$D_{\tau|i} = \frac{E(\mathcal{J}^2_{\tau|i}) - E(\mathcal{J}_{\tau|i})^2}{2\tau q_i}, \tag{5.12}$$

which represent the fluctuations of the system within each phase. From Eq. (5.9), we therefore see that the diffusion coefficient D_τ in Eq. (5.7) is split in three terms

$$D_\tau = (1-q)D_{\tau|0} + qD_{\tau|1} + C_\tau, \qquad C_\tau := \frac{1}{\tau}\mathrm{cov}(\mathcal{J}_{\tau|0}, \mathcal{J}_{\tau|1}), \tag{5.13}$$

where $\mathrm{cov}(A,B) = E(AB) - E(A)E(B)$ is the covariance between conditional currents A and B, and is expected to be significant only in the vicinity of the transition point.

5.4 Large Deviation Theory (LDT)

To shed light on the behaviour of conditional currents, we consider here a finite-time version of large deviation theory [133, 13, 141, 142]. We being with the unconditional quantities, and then adapt our results to the conditional case. Let $G_\tau(\eta) = E(e^{\eta\mathcal{J}_\tau})$ denote the moment generating function (MGF) associated to the current (5.6). Decomposing it as $G_\tau(\eta) = \sum_x E(e^{\eta\mathcal{J}_\tau}|X_\tau = x)p_x(\tau) = \sum_x G_x(\eta)$, we find that the entries $G_x(\eta)$ will evolve according to equation

$$\frac{dG_x(\eta)}{d\tau} = \sum_y \mathbb{L}_{xy}(\eta)G_y(\eta), \tag{5.14}$$

where the tilted operator $\mathbb{L}(\eta)$ depends on both the transition matrix $\mathbb{W}$ in Eq. (5.5), and the type of current in question, according to

$$\mathbb{L}(\eta)_{xy} = e^{\eta d_{xy}}\mathbb{W}_{xy}, \tag{5.15}$$

where, recall, $d_{xx} = 0$. To evaluate J and D_τ, we only require the series expansion of $\mathbb{L}(\eta)$, which we write as $\mathbb{L}(\eta) = \mathbb{W} + \eta L_1 + \eta^2 L_2$, for matrices $L_{1(2)}$ given by

$$(L_1)_{xy} = W_{xy}d_{xy}, \qquad (L_2)_{xy} = W_{xy}d^2_{xy}/2. \tag{5.16}$$

5.4.1 Unconditional cumulants

We denote by $|\boldsymbol{p}\rangle$ the column vector whose entries are the steady-state distribution p^*_x, and $\langle \mathbf{1}|$ the row vector with all entries equal 1. Then, as discussed further in Appendix D, the first moment can be written, for arbitrary τ, as

$$J_\tau \equiv J = \langle \mathbf{1}|L_1|\boldsymbol{p}\rangle, \tag{5.17}$$

which is independent of τ, as expected. Conversely, the diffusion coefficient is written as

$$D_\tau = \langle \mathbf{1}|L_2|\boldsymbol{p}\rangle + \frac{1}{\tau}\int_0^\tau d\tau' \int_0^{\tau'} d\tau'' \langle \mathbf{1}|L_1 e^{\mathbb{W}(\tau'-\tau'')}L_1|\boldsymbol{p}\rangle - \frac{J^2\tau}{2}. \tag{5.18}$$

We can also obtain a more explicit expression if we assume that $\mathbb{W}$ is diagonalizable, with eigenvalues λ_i, right eigenvectors $\mathbb{W}|\boldsymbol{x}_i\rangle = \lambda_i|\boldsymbol{x}_i\rangle$ and left eigenvectors $\langle \boldsymbol{y}_i|\mathbb{W} = \langle \boldsymbol{y}_i|\lambda_i$. Since the steady-state is unique, one eigenvalue must be zero, say $\lambda_0 = 0$. The corresponding eigenvectors are then $|\boldsymbol{x}_0\rangle = |\boldsymbol{p}\rangle$ and $\langle \boldsymbol{y}_0| = \langle \mathbf{1}|$. Carrying out the integrals one then finds that

$$D_\tau = \langle \mathbf{1}|L_2|\boldsymbol{p}\rangle + \sum_{i\neq 0}\langle \mathbf{1}|L_1|\boldsymbol{x}_i\rangle\langle \boldsymbol{y}_i|L_1|\boldsymbol{p}\rangle\left(\frac{e^{\lambda_i\tau}-1-\lambda_i\tau}{\lambda_i^2\tau}\right), \tag{5.19}$$

where we used the orthogonality relation $\langle \mathbf{1}|\boldsymbol{x}_i\rangle = 0$, for $i \neq 0$. This expression makes it clear that D_τ will depend sensibly on the interplay between τ and all eigenvalues λ_i of $\mathbb{W}$. If $\tau \gg 1/|\lambda_i|$, for all eigenvalues $\lambda_i \neq 0$, then the term $e^{\lambda_i\tau} - 1$ may be neglected, leading to the widely used expression from large deviation

$$D_\tau = \langle \mathbf{1}|L_2|\boldsymbol{p}\rangle - \langle \mathbf{1}|L_1\mathbb{W}^+L_1|\boldsymbol{p}\rangle, \tag{5.20}$$

where $\mathbb{W}^+ = \sum_{i\neq 0}\lambda_i^{-1}|\boldsymbol{x}_i\rangle\langle \boldsymbol{y}_i|$ is the Moore-Penrose pseudoinverse of $\mathbb{W}$ (see Appendix D for more details). Close to the transition point, there will appear a clear separation of time scales in the eigenvalues λ_i. At least one eigenvalue will be very small, of the order $\lambda_i \sim -1/\tau_m$, while all others will be much larger (describing the within-phase dynamics). If τ is large compared to these time scales, but not with respect to τ_m, then the approximation taking Eq. (5.19) to (5.20) will not hold true. And since τ_m scales exponentially with the volume, as we approach the thermodynamic limit, larger and larger values of τ have to be considered. This is a direct illustration of the non-commutativity of the limits $\tau \to \infty$ and $V \to \infty$.

5.4.2 Conditional cumulants

Eqs. (5.17) and (5.18) also apply to the conditional currents (5.8). One simply has to modify accordingly the tilted operator $\mathbb{L}(\eta)$ or, what is equivalent, the matrices L_1 and L_2 in Eq. (5.16). For each conditional current

$\mathcal{J}_{\tau|i}$, we define a projection operator Π^i such that $\Pi^1_{xy} = \delta_{x,y}\sum_{z\in S_i}\delta_{y,z}$; i.e., which projects onto the states $\mathcal{S}_i$ associated to phase $i = 0, 1$. The corresponding tilted operator will then be defined similarly, but with a current of the form $d^i_{xy} = d_{xy}\Pi^i_{yy}$, which means one should use instead matrices $L_1\Pi^i$ and $L_2\Pi^i$.

Eq. (5.17) then yields, taking also into account the factor q_i in the denominator,

$$\mu_i = \frac{1}{q_i}\langle \mathbf{1}|L_1\Pi^i|\boldsymbol{p}\rangle. \tag{5.21}$$

Proceeding similarly with Eq. (5.18), we find

$$D_{\tau|i} = \frac{\langle \mathbf{1}|L_2\Pi^i|\boldsymbol{p}\rangle}{q_i} + \frac{1}{\tau q_i}\int_0^\tau d\tau' \int_0^{\tau'} d\tau''\langle \mathbf{1}|L_1\Pi^i e^{\mathbb{W}(\tau'-\tau'')}L_1\Pi^i|\boldsymbol{p}\rangle - \frac{\mu_i^2 q_i \tau}{2}. \tag{5.22}$$

And to obtain the covariance in Eq. (5.13), we simply subtract the combination $(1-q)D_{\tau|0} + qD_{\tau|1}$ from D_τ in Eq. (5.18). Recalling that $\Pi^0 + \Pi^1 = 1$, this then yields

$$C_\tau = \frac{1}{\tau}\int_0^\tau d\tau' \int_0^{\tau'} d\tau''\langle \mathbf{1}|L_1\Pi^0 e^{\mathbb{W}(\tau'-\tau'')}L_1\Pi^1|\boldsymbol{p}\rangle + \frac{1}{\tau}\int_0^\tau d\tau' \int_0^{\tau'} d\tau''\langle \mathbf{1}|L_1\Pi^1 e^{\mathbb{W}(\tau'-\tau'')}L_1\Pi^0|\boldsymbol{p}\rangle - q(1-q)\mu_0\mu_1\tau.$$

Concerning the timescales of the discontinuous transition, we notice that all diffusion coefficients, D_τ, $D_{\tau|i}$ and C_τ, are subject to a similar dependence, which is ultimately associated with the matrix $e^{\mathbb{W}(\tau-\tau')}$. Thus, one expects that all quantities should scale similarly with τ.

5.4.3 Conditioning on the dynamics

There is a subtle, but crucial difference between conditioning the currents and conditioning the *dynamics*. Eq. (5.8) is an instance of the former: the current is conditioned on which phase the system is in, but $X(t)$ is still free to jump from one phase to the other. Alternatively, one could define a conditional dynamics, where the system is forced to remain only within a certain phase. This could be accomplished, for instance, by splitting the transition matrix $\mathbb{W}$ in Eq. (5.5) in blocks of the form

$$\mathbb{W} = \begin{pmatrix} \mathbb{W}_{00} & \mathbb{W}_{01} \\ \mathbb{W}_{10} & \mathbb{W}_{11} \end{pmatrix}, \tag{5.23}$$

referring to the two subsets $\mathcal{S}_0$ and $\mathcal{S}_1$ of each phase. A conditional *dynamics*, given phase i, is one that is governed by the restricted matrix $\mathbb{W}_{ii}$ (with appropriate adjustments at the boundaries to ensure that it remains a proper transition matrix).

One can similarly adapt Eqs. (5.17) and (5.18) to this case. Let $|\boldsymbol{p}^i\rangle$ denote the steady-state of $\mathbb{W}_{ii}$. For large volumes, since the two phases will be well separated, this will be quite similar to $\frac{1}{q_i}\Pi^i|\boldsymbol{p}\rangle$. Applying Eq. (5.17)

will then yields exactly the same first moment μ_i in Eq. (5.21). Hence, *as far as the first moments are concerned, the distinction between conditional currents and conditional dynamics is thus irrelevant.*

However, for the diffusion coefficients this is absolutely crucial. The reason is associated with the matrix exponential $e^{\mathbb{W}(\tau'-\tau'')}$ in Eq. (5.18). Conditioning on the dynamics would lead instead to a matrix $e^{\mathbb{W}_{ii}(\tau'-\tau'')}$. Since $\mathbb{W}_{ii}$ is essentially $\Pi^i\mathbb{W}\Pi^i$ (except for small modifications at the boundaries), we therefore see that the problem amounts to the difference between $\Pi^i e^{\mathbb{W}(\tau'-\tau'')}\Pi^i$ (conditioning on the currents) and $e^{\Pi^i\mathbb{W}\Pi^i(\tau'-\tau'')}$ (conditioning on the dynamics). The two objects are *drastically* different. The diffusion coefficients obtained by conditioning the dynamics, which we shall henceforth refer to as $\gamma_{\tau|i}$, will thus fundamentally different from the diffusion coefficients $D_{\tau|i}$ in Eq. (5.12).

An intuitive argument as to why this is the case goes as follows. The currents (5.8) are integrated over a certain time interval τ. Hence, its diffusion coefficient will depend on correlations between different instants of time, and these are dramatically affected by the long timescale τ_m introduced by the discontinuous transition. In fact, let us define $Z_t = \sum_{y,z} d_{yz}\delta_{X(t^-),y}\delta_{X(t^+),z}$, so that Eq. (5.8) can be written as

$$\mathcal{J}_{\tau|1} = \int_0^\tau dt\, I_t Z_t. \tag{5.24}$$

The corresponding second moment will thus be

$$E(\mathcal{J}^2_{\tau|1}) = \int_0^\tau dt \int_0^\tau dt'\, E(I_t I_{t'} Z_t Z_{t'}). \tag{5.25}$$

It hence depends, among other things, on the correlations between I_t and $I_{t'}$, which decays very slowly around the transition point. For instance, in the simplest case where one can assume a Markovian 2-state evolution for I_t (as will in fact be considered further in Sec. 5.5), one has

$$C(t-t') = \mathrm{cov}(I_t, I_{t'}) = q(1-q)e^{-(t-t')/\tau_m}, \tag{5.26}$$

which will thus decay very slowly in time. This means that $D_{\tau|i}$ in Eq. (5.12) will depend very sensibly on the interplay between τ and τ_m. Conversely, the diffusion coefficients γ_i, for the conditional dynamics, will not. And hence, even for moderately large τ, one expects it to be τ-independent.

5.5 Minimal Model

Many discontinuous non-equilibrium transitions can be approximated, for large volumes V, by a 2-state model [140]. That is, one reduces the dynamics essentially to the monitoring of the phase indicator I_t. In general, the dynam-

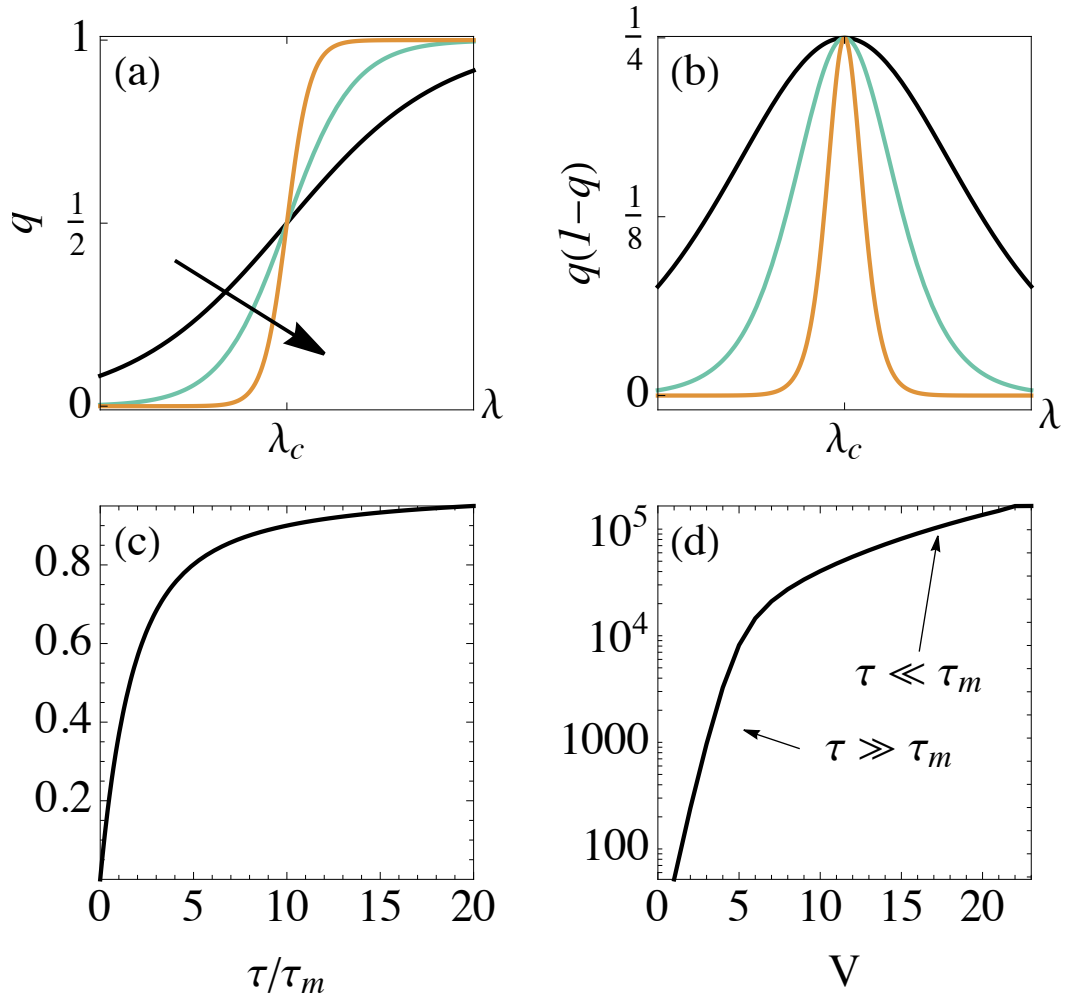

Figure 5.1: Predictions of the minimal model of discontinuous transitions. (a) The probability $q = (1+e^{-cV\Delta\lambda})^{-1}$ of finding the system in phase 1, for increasing volumes (depicted by the arrow). (b) $q(1-q)$, which is non-negligible only in the vicinity of the transition point. (c) The quantity $(e^{-\tau/\tau_m} - 1 + \tau/\tau_m)/(\tau/\tau_m)$ appearing in Eq. (5.32). It tends to unity when $\tau \gg \tau_m$. (d) Prototypical behavior of the diffusion coefficient (5.32) as a function of volume, for a fixed τ. When V is such that $\tau \gg \tau_m$, the diffusion coefficient grows exponentially with V. But for a fixed τ, as V is increased, one must eventually cross the point $\tau \sim \tau_m$, after which the scaling becomes at most polynomial (due to the possible dependences of μ_i, D_i on V). Parameters: $c_0 = c_a = c_b = \lambda_c = 1, \mu_0 = V/2, \mu_1 = 2V, \gamma_0 = \gamma_1 = V$.

ics of I_t will be non-Markovian, as this would represent a hidden Markov chain. Instead, a minimal model is one where the dynamics of I_t can be assumed to be Markovian, which is justified when V is sufficiently large. In this case, instead of the full master equation (5.5), we may restrict the dynamics to

$$\frac{d}{dt}q_i = \sum_{j=0,1} \mathcal{W}_{ij}q_j, \qquad \mathcal{W} = \begin{pmatrix} -a & b \\ a & -b \end{pmatrix}. \tag{5.27}$$

Here a and b represent the rates for the system to jump from phase $0 \to 1$ and $1 \to 0$. The steady-state yields $q \equiv q_1 = E(I_t) = a/(a+b)$. Moreover, the metastability lifetime in this case reads $\tau_m = 1/(a+b)$. Finally, from (5.27) one can compute the two-time correlation function, which is given in Eq. (5.26). And since I_t can take on only two values, once $C(t-t')$ is known we can reconstruct the full joint distribution $\Pr(I_t = i, I_{t'} = i')$, for arbitrary times t, t':

$$\Pr(I_t = i, I_{t'} = i') = \begin{cases} q^2 + C(t-t') & i = i' = 1, \\ (1-q)^2 + C(t-t') & i = i' = 0, \\ q(1-q) - C(t-t') & i \neq i'. \end{cases} \tag{5.28}$$

The key feature of discontinuous transitions is the fact that transitions between phases are seldom when V is large. Close to λ_c, the transition rates a and b will usually behave, up to polynomial corrections, as

$$a \sim e^{-V(c_0 - c_a\Delta\lambda)}, \qquad b \sim e^{-V(c_0 + c_b\Delta\lambda)}, \tag{5.29}$$

where $c_0, c_a, c_b > 0$ are constants and $\Delta\lambda = \lambda - \lambda_c$. Note how the rates are exponentially decreasing with V. Transitions hence become rare when V is large. From (5.29) we also get $\tau_m \sim e^{c_0 V}$, which is the aforementioned exponential dependence. Finally, $q = (1 + e^{-cV\Delta\lambda})^{-1}$, where $c = c_a + c_b > 0$; hence q changes abruptly from 0 to 1 as λ crosses λ_c, as illustrated in Fig. 5.1(a). Since the conditional averages are weakly dependent on $\Delta\lambda$, from Eq. (5.11) we therefore see that J should also change abruptly around λ_c, interpolating from μ_0 to μ_1.

5.5.1 Unconditional diffusion coefficient

As shown in [143], in this two-level model the tilted operator can be written, up to order λ^2, as

$$\mathbb{L}(\lambda) = \begin{pmatrix} -a + \lambda\mu_0 + \lambda^2\gamma_0 & b \\ a & -b + \lambda\mu_1 + \lambda^2\gamma_1 \end{pmatrix} \tag{5.30}$$

$$:= \mathbb{W} + \lambda L_1 + \lambda^2 L_2. \tag{5.31}$$

where γ_i are the diffusion coefficients conditioned on the dynamics, not the currents (as introduced in Sec. 5.4.3).

For the matrix $\mathbb{W}$ defined in Eq. (5.27) we have $\lambda_1 = -1/\tau_m$, $|\boldsymbol{p}\rangle = (1-q, q)$, $|\boldsymbol{x}_1\rangle = (-1, 1)$ and $|\boldsymbol{y}_1\rangle = (-q, 1-q)$. Hence, using the explicit forms of L_1 and L_2 in Eq. (5.31), we get

$$D_\tau = \gamma + q(1-q)(\mu_1 - \mu_0)^2 \, \tau_m f(\tau/\tau_m), \tag{5.32}$$

where $\gamma = (1-q)\gamma_0 + q\gamma_1$ is independent of τ and

$$f(t) = (e^{-t} - 1 + t)/t. \tag{5.33}$$

The interesting part is the last term in Eq. (5.32). First, it depends on $q(1-q)$, which is non-negligible only in the vicinity of the transition point (Fig. 5.1(b)). Second, it depends on the interplay between τ and τ_m through the function f, which is shown in Fig. 5.1(c).

When $\tau \ll \tau_m$ we get $f(\tau/\tau_m) \simeq \tau/2\tau_m$, so that Eq. (5.32) can be approximated to

$$D_\tau \simeq \gamma + q(1-q)(\mu_1 - \mu_0)^2 \tau/2, \qquad \tau \ll \tau_m, \tag{5.34}$$

which is thus *linear* in τ. Conversely, when $\tau \gg \tau_m$, we get

$$D_\tau \simeq \gamma + q(1-q)(\mu_1 - \mu_0)^2 \, \tau_m, \qquad \tau \gg \tau_m, \tag{5.35}$$

which is independent of τ, *but linear in* τ_m. Hence, when V is large, this will become exponentially dominant. As a consequence, the large volume diffusion coefficient will actually become independent of the γ_i, and will instead be governed essentially by the mismatch in *conditional averages* $(\mu_1 - \mu_0)^2$, in agreement with previous studies on Schlögl's model [130].

This offers another explicit illustration of the order of limits issue, which we depict graphically in Fig. 5.1(d): For a given τ, as we increase V the diffusion coefficient will at first increase exponentially according to Eq. (5.35). But if τ is fixed, then a point will always be reached around which $\tau \sim \tau_m$. And beyond this point, the scaling will be given by Eq. (5.34), which is at most polynomial in V (due to a potential polynomial volume dependence of μ_i, γ_i).

Even though these results were developed for a 2-level model, they are still expected to hold for a broad class of discontinuous transitions. The reason is that, as discussed in Ref. [144], the eigenvalues and eigenvectors of the two-level transition matrix (5.27) are connected to some of the eigenvalues and eigenvectors of the full matrix $\mathbb{W}$ in Eq. (5.5). But, in addition, the full $\mathbb{W}$ will also have several other eigenvalues associated to the within-phase dynamics. Thus, the step from Eq. (5.19) to (5.32) only assumes that τ is much larger than all other λ_i, so that within-phase terms can be neglected.

5.5.2 Conditional diffusion coefficient

We can also use this minimal model to relate the diffusion coefficients $D_{\tau|i}$ in Eq. (5.12) with the parameters μ_i, γ_i. To do so, we use Eq. (5.22) with $\mathbb{W}$ now replaced by the two-state matrix $\mathcal{W}$ in Eq. (5.27). As a result, we find

$$D_{\tau|1} = \gamma_1 + \mu_1^2(1-q)\tau_m f(\tau/\tau_m), \tag{5.36}$$

$$D_{\tau|0} = \gamma_0 + \mu_0^2 q\tau_m f(\tau/\tau_m), \tag{5.37}$$

$$C_\tau = -2q(1-q)\mu_0\mu_1\tau_m f(\tau/\tau_m), \tag{5.38}$$

which can be combined together in the form (5.13), to yield Eq. (5.32). All conditional quantities are thus found to scale similarly with τ, according to the function f in Eq. (5.33). This allows us to conclude that even the conditional diffusion coefficients will be dominated by jumps between phases, and will be negligibly affected by the internal fluctuations within each phase. We find this result both relevant and non-trivial.

It is also interesting to notice how the sign of the covariance (5.38) depends only on the signs of μ_0 and μ_1. A positively correlated covariance means that fluctuations above (below) average in one phase tend to lead to fluctuations above (below) the average in the other; and vice-versa for $C < 0$. We see in Eq. (5.38) that the covariance will be negative whenever μ_0, μ_1 have the same sign.

5.6 Applications

Next we shall exemplify our main findings in one representative system displaying discontinuous phase transitions: The 12-state Potts models connected to two baths at different temperatures. The Potts model is defined in a regular lattice and exhibits a nonequilibrium phase transition under a different mechanism. Despite the absence of an exact solution, all main features about the phase transition and statistics about entropy production fluctuations are present.

5.6.1 $Q = 12$-states Potts model

As a second application, we study a $Q = 12$ states Potts model coupled to two thermal baths at different temperatures. The model is defined in a regular 2D lattice with V sites, where each site i assumes one of $Q = 12$

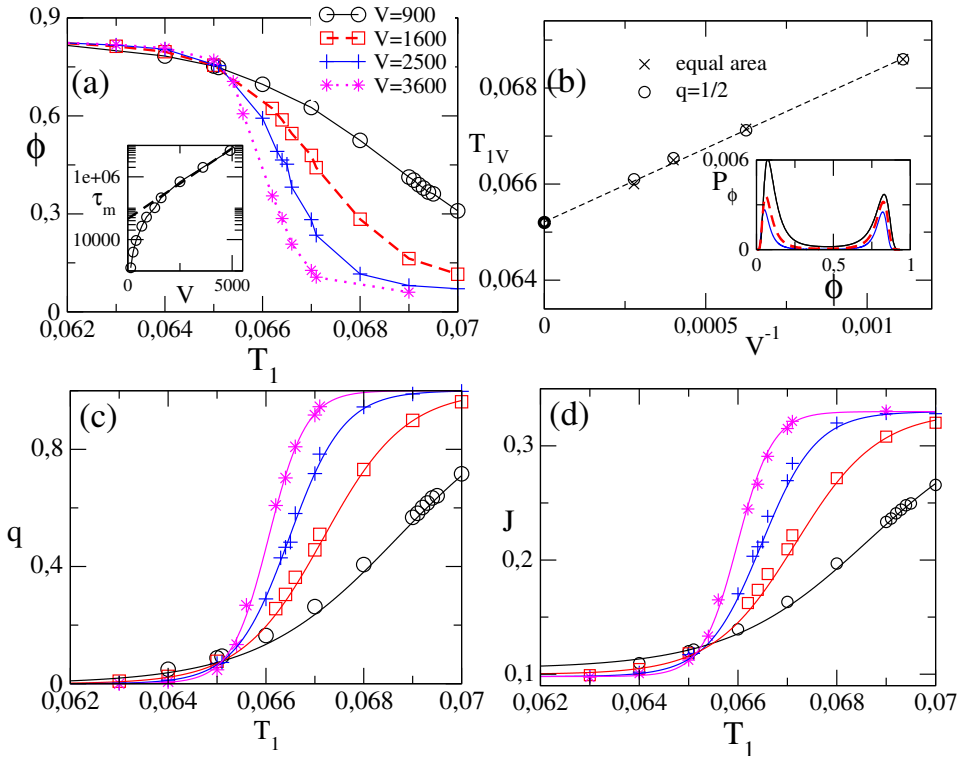

Figure 5.2: Characterization of the $Q = 12$ Potts model in contact with two thermal baths of temperatures T_1 and $T_1 + \Delta T$ (with fixed $\Delta T = 0.9$). (a) Order parameter ϕ vs. T_1 for different volumes V. Inset: metastability lifetime τ_m vs. V. (b) Finite-size analysis of the transition point T_{1V} vs. V^{-1}, yielding the asymptotic value $T_{01} = 0.0651(1)$. Inset: distribution of ϕ at T_{1V}, for different volumes. (c) Phase probability q vs. T_1, again for different volumes. The continuous lines are fits of $q = [1 + Qe^{-Vc(T_1 - T_{10})}]^{-1}$. (d) Average entropy production rate current J [Eq. (5.7)], which follows closely the behavior of q.

values $s_i = 1, \ldots, Q$ and interacts with its $z = 4$ nearest neighbors, with energy $\mathcal{H}(\boldsymbol{s}) = -\sum_{i=1}^{V} \sum_{\delta=1}^{z} \delta_{s_i, s_{i+\delta}}$, where $\boldsymbol{s} = (s_1, \ldots, s_V)$. The equilibrium properties of this model have been studied extensively in [145, 146, 147, 148, 149]. Here, we consider a non-equilibrium version where the even and odd sites of the lattice are coupled to thermal baths at temperatures T_1 and $T_1 + \Delta T$ respectively, forming a checkerboard pattern. For concreteness, we fix $\Delta T = 0.9$. This temperature gradient ensures a steady heat flux from one bath to the other, and hence a non-vanishing production of entropy [29, 150].

The model is simulated using standard Monte Carlo methods. The dynamics is assumed to be governed by Markovian single-site transitions $s_i \to s_i'$, occurring with rate $\omega_{s_i, s_i'} = \min\{1, \exp[-\Delta E_i / T_i]\}$, where $\Delta E_i = \mathcal{H}(\boldsymbol{s}') - \mathcal{H}(\boldsymbol{s})$ and T_i is the temperature of site i. For the current (5.6), we once again focus on the net entropy production rate to the environment which is characterized by increments $\Delta E_i / T_i$ [128, 150].

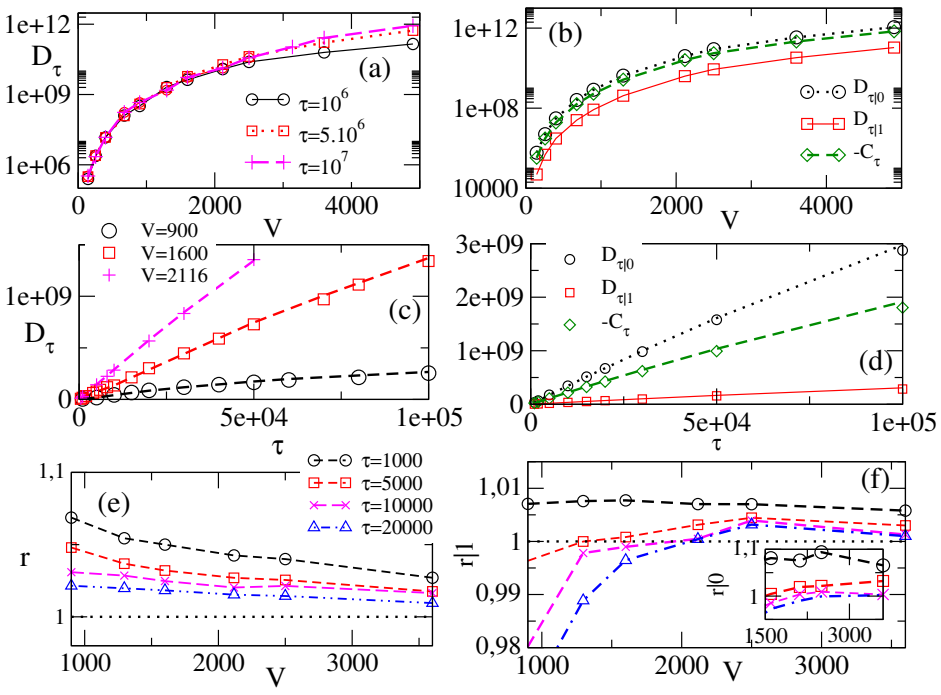

Figure 5.3: Unconditional and conditional diffusion coefficients for the $Q = 12$ Potts model. (a) D_τ vs. V for different values of τ. (b) $D_{\tau|i}$ and C_τ vs. V with $\tau = 5 \times 10^6$. (c) D_τ vs.τ for different V. (d) $D_{\tau|i}$ and C_τ vs. τ for $V = 1600$. Continuous lines in (c) and (d) are the theoretical predictions from Eq. (5.32). (e) The ratio (5.39) between D_τ and the predictions of the minimal model, Eq. (5.32), which tends to unity for large volumes. Curves are for different values of τ. (f) Same, but for $r|0$ (main plot) and $r|1$ (inset). In all curves, for each V, we fix T_1 as the value T_{1V} for which $q = 1/2$. Other details are as in Fig. 5.2.

As in the equilibrium version, the phase transition is expected to be discontinuous for $Q > 4$. Moreover, for $Q = 12$, the discontinuity is expected to become very sharp for sufficient large V, since it involves Q distinct ordered phases coexisting with a single disordered one. The nonequilibrium phase transition can be quantified by the order-parameter $\phi = Q[(\mathcal{N}_{max}/V) - 1]/(Q-1)$, where $\mathcal{N}_{max} = \max\{\mathcal{N}_1, ..., \mathcal{N}_Q\}$ is the maximum number of spins among all Q configurations [148, 151]. Fig. 5.2(a) shows results for ϕ as a function of T_1, for different lattice sizes V. The emergence of a discontinuous transition as V increases is clearly visible. The inset in Fig. 5.2(a) shows the metastability lifetime, which is again found to grow exponentially with V.

The sharp features of discontinuous phase transitions become rounded at the vicinity of the coexistence point, due to finite size effects. To locate the transition point, we resort to the finite size scaling theory [152], establishing that the "pseudo-transition" point T_{1V}, in which both phases have the same weight (equal-area order-parameter probability) reaches its asymptotic value T_{10} according to the relation $T_{1V} - T_{10} \sim V^{-1}$. This is

shown in Fig. 5.2(b), from which we find $T_{10} = 0.0651(1)$.

A histogram of the order parameter ϕ is shown in the inset of Fig. 5.2(b). It shows that there is a clear separation between the two phases, allowing us to define a separator $\phi^* = 1/2$, such that the phase-indicator I_t assumes the value $I_t = 1$ when $\phi(t) > \phi^*$. The resulting phase probability q is presented in Fig. 5.2(c). As in the other models, it presents a sharp transition at $T_{10} = 0.0651(1)$, and is well described by the expression $q = [1 + Qe^{-Vc(T_1 - T_{10})}]^{-1}$. Contrarily to Schlögl's model, however, the curves for different volumes do not cross at $q = 1/2$, but instead at $q \simeq 1/13$. The unconditional current J [Eq. (5.7)] is presented in Fig. 5.2(d). As predicted by Eq. (5.7), it follows very closely the behavior of q [Fig. 5.2(c)], smoothly interpolating between μ_0 and μ_1.

We now turn to an analysis of the unconditional and conditional diffusion coefficients. The results are summarized in Fig. 5.3. To reduce the number of free parameters, we proceed similarly to Schlögl's model, and set, for each volume V, the temperature to T_{1V} (i.e., so that $q = 1/2$). In Fig. 5.4 we repeat the same analysis, but fixing instead the temperature at T_{10} (the thermodynamic limit transition point) for all V. Similar findings are observed.

The unconditional diffusion coefficient D_τ [Eq. (5.7)] is shown in Fig. 5.3(a) for different values of τ. In agreement with the predictions of Eq. (5.32), for each τ the diffusion coefficient initially grows exponentially with V. But for a sufficiently large V, τ_m becomes comparable to τ and D_τ bends downwards. This is exactly the behavior predicted by the minimal model [Fig. 5.1(d)]. The corresponding conditional diffusion coefficients are shown in Fig. 5.3(b). They follow a similar dependence on V as D_τ, which is in agreement with the expectations of Eqs. (5.36)-(5.38).

The dependence of D_τ, $D_{\tau|i}$ and C_τ as a function of τ, for different V, are shown in Figs. 5.3(c),(d). In all cases, when τ is small the diffusion coefficients tend to be linear in τ, in agreement with Eq. (5.34). If V is not too large, then when τ becomes large one recovers instead a τ-independent behavior, as predicted by Eq. (5.35). For large V something similar is expected to occur, although it may require unrealistically large values of τ. For large volumes, these are also well described by the third term in Eq. (5.32) (or (5.36)-(5.37)). We confirm this by plotting in Fig. 5.3(e) the ratio

$$r = \frac{D_\tau}{q(1-q)(\mu_1 - \mu_0)^2 \tau_m f(\tau/\tau_m)}, \tag{5.39}$$

where all quantities in the right-hand side are computed independently from the simulations. One can also consider similar definitions for $r_{0(1)}$. The results for conditional quantities are shown in Fig. 5.3(f). In all cases, the plots clearly show that the ratio seems to tend to unity for sufficiently large V. Since the γ_i are at most

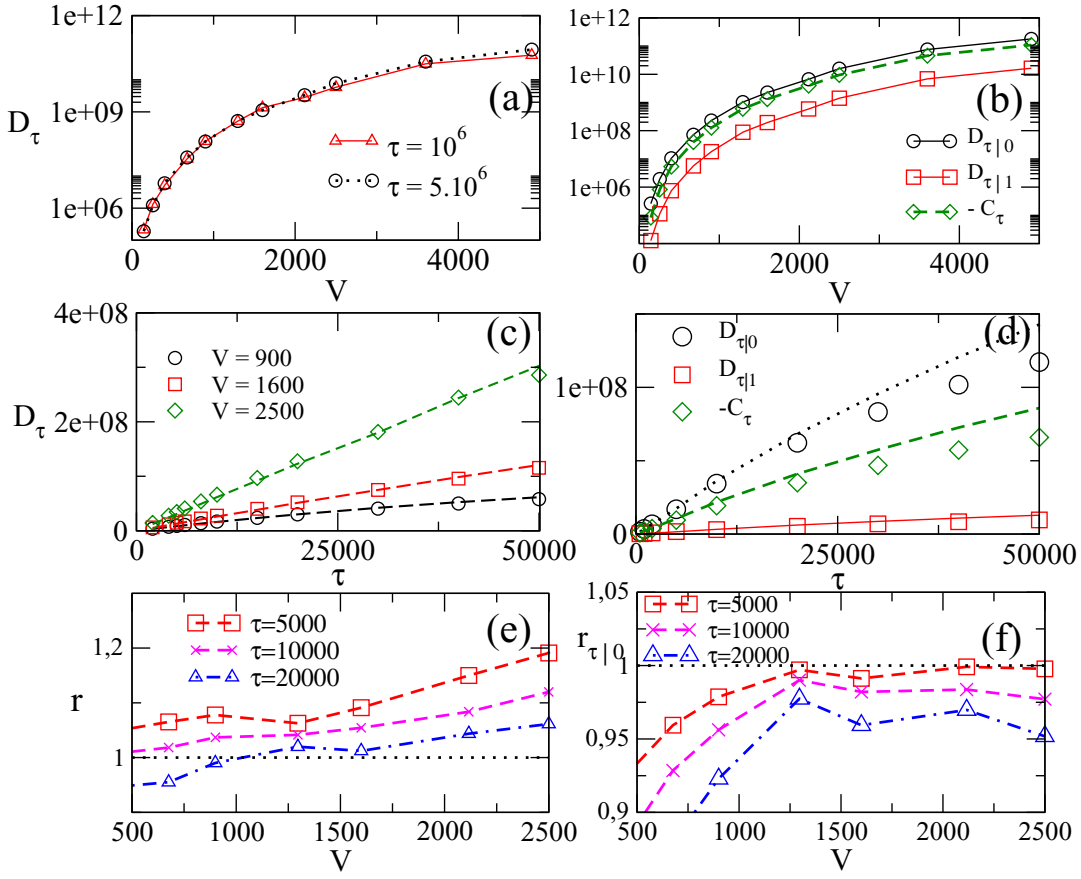

Figure 5.4: Same as Fig. 5.3, but fix T_1 fixed at the thermodynamic limit value $T_{10} = 0.0651(1)$.

polynomial in V, if this ratio tends to $r \to 1$ when V is large, it serves as a confirmation that, for large V, the model effectively behaves as the 2-state minimal model of Sec. 5.5. This strongly indicates that the Potts model will also behave as an effective 2-state minimal model in the thermodynamic limit.

5.7 Conclusions

The statistics of thermodynamic currents is a fundamental issue in nonequilibrium thermodynamics, which has recently received significant interest. In this chapter, we presented a simple and general description of the statistics of thermodynamic currents for systems displaying discontinuous phase transitions. We introduced the idea of conditional statistics, accounting for the currents in each of the coexisting phases. From large deviation theory, general relations for the unconditional and conditional cumulants of a generic current were presented. We also proposed a minimal model, which captures all essential features of the problem. Our ideas were illustrated in one representative system: the Q-states Potts model subject to two baths at different temperatures.

In both cases, the results were found to follow very well the theoretical predictions of the minimal model, illustrating not only its reliability but also the intricate role of distinct scaling times and the volume.

As a final remark, we address some potential extensions of our work. It would be interesting to extend such approach to study the statistics of thermodynamic quantities, such as work. This can be accomplished by extending LDT to time-dependent rates [98, 153] describing the action of an external agent. Similarly, it would also be interesting to tackle the statistics of the efficiency of a thermal engine operating at phase coexistence [154].

Chapter 6

General conclusions

We present a study on the performance of different thermal machines in the context of non-equilibrium thermodynamics. We introduce the idea of collisional approach to Brownian engine, in which the Brownian particle is sequentially placed in contact with different thermal reservoirs and exposed to different external forces (sources of work). We discussed different strategies on how to optimize their performances, among them via the controlling the interaction between the system and the reservoir and the driving force used. We also obtained general expressions for the thermodynamic quantities in these cases, for any driving force. It should be noted that the sequential/collisional approach plays an important role in quantum mechanics and was generalized in this thesis to Brownian particles. With regard to systems described by master equations, the collisional approach was also used in this thesis, extending the work of [93], considering the role of the stage as a strategy to improve the performance of such systems.

In the last part we carried out a study on the statistics mean and variance of entropy production in discontinuous phase transitions. Such a study is important, as it takes into account the role of two times: the integration time and the tunneling time between phases, in which the system needs to cross from one phase to another. We show that the interplay between both times is fundamental. All these features were described considering the coexistence of phases as a two-state model and its generality was verified in different models presenting discontinuous phase transitions. As a perspective for future works, the extension of the collisional approach to different models, especially systems more complex than the one composed of a quantum-dot or even the study of some strategy for converting heat into work in the Brownian particles case. In our case, the inclusion of different temperatures did not improve the performance of the system, because in these systems only work was converted into other work at each stage. An initial study considering a coupling between driving and

velocities was introduced in [155] and possible extensions would be interesting. Another perspective for future works would be the extension of power and efficiency statistics to phase transitions, in order to describe their behavior.

Appendix A

Onsager coefficients and linear regimes

In this appendix, we address the relation between coefficients $\tilde{L}_{ij}$ and Onsager coefficients L_{ij}. Our starting point is the steady state entropy production averaged over one period which is given by,

$$\overline{\Pi} = \frac{2\gamma k_{\mathrm{B}}}{m}\left(\frac{\overline{\dot{Q}}_1}{\Gamma_1} + \frac{\overline{\dot{Q}}_2}{\Gamma_2}\right) = \overline{\Pi}_F + \overline{\Pi}_T. \tag{A.1}$$

The coefficients $\tilde{L}_{ij}$ are straightforwardly obtained from $\overline{\Pi}_F$ performing the integration in Eq. (3.13), which $\langle v_i\rangle(t)$'s are given by Eq. (3.4), as:

$$\begin{aligned}
\tilde{L}_{11} &= \frac{\gamma}{\tau}\left[\frac{\left(e^{2\gamma(\tau-\tau_1)}-1\right)\hat{G}_1(\tau_1)^2}{\Gamma_2\left(e^{\gamma\tau}-1\right)^2} + \frac{\gamma}{\Gamma_1}\int_0^{\tau_1}\frac{2e^{-2\gamma t}\left[\left(e^{\gamma\tau}-1\right)\hat{G}_1(t)+\hat{G}_1(\tau_1)\right]^2}{\left(e^{\gamma\tau}-1\right)^2}\,dt\right]\\
\tilde{L}_{22} &= \frac{\gamma}{\tau}\left[\frac{\left(1-e^{-2\gamma\tau_1}\right)\hat{G}_2(\tau)^2}{\Gamma_1\left(e^{\gamma\tau}-1\right)^2} + \frac{\gamma}{\Gamma_2}\int_{\tau_1}^{\tau}\frac{2e^{-2\gamma t}\left[\left(e^{\gamma\tau}-1\right)\hat{G}_2(t)+\hat{G}_2(\tau)\right]^2}{\left(e^{\gamma\tau}-1\right)^2}\,dt\right],\\
\tilde{L}_{12}+\tilde{L}_{21} &= \frac{2\gamma e^{-\gamma\tau_1}\hat{G}_1(\tau_1)\hat{G}_2(\tau)}{\tau\left(e^{\gamma\tau}-1\right)^2}\left[\frac{\sinh(\gamma\tau_1)}{\Gamma_1}+\frac{\sinh(\gamma(\tau-\tau_1))}{\Gamma_2}\right]\\
&\quad+\frac{2\gamma^2}{\Gamma_1\Gamma_2\tau\left(e^{\gamma\tau}-1\right)}\left[\Gamma_2\hat{G}_2(\tau)\int_0^{\tau_1}\hat{G}_1(t)e^{-2\gamma t}\,dt+\Gamma_1\hat{G}_1(\tau_1)\int_{\tau_1}^{\tau}\hat{G}_2(t)e^{\gamma(\tau-2t)}\,dt\right],
\end{aligned} \tag{A.2}$$

where $\hat{G}_i(t) = \int_{\tau_{i-1}}^{t} g_i(t')dt'$. For equal temperatures $\Gamma_1 = \Gamma_2 = \Gamma$, $\overline{\Pi}$ reduces to the following expression:

$$\begin{aligned}
\overline{\Pi} = \overline{\Pi}_F &= -\frac{2\gamma k_{\mathrm{B}}}{m\Gamma}\left(\overline{\dot{W}}_1+\overline{\dot{W}}_2\right)\\
&= L_{11}X_1^2 + (L_{12}+L_{21})\,X_1X_2 + L_{22}X_2^2.
\end{aligned} \tag{A.3}$$

Hence, for isothermal reservoirs the entropy production can be written in terms of the Onsager coefficients even in the non-linear (force) regime and thereby $\tilde{L}_{ij} = L_{ij}$. Conversely, for the thermal linear regime, it is convenient to express Γ_1 and Γ_2 in terms of the difference of temperatures $\Gamma_1 = \Gamma - \Delta\Gamma$ and $\Gamma_2 = \Gamma + \Delta\Gamma$. In such case, Eq.

(A.1) becomes

$$\overline{\Pi} \approx \frac{2\gamma k_{\mathrm{B}}}{m\Gamma}\left[-\left(\overline{\dot{W}}_1 + \overline{\dot{W}}_2\right) + \left(\overline{\dot{Q}}_1 - \overline{\dot{Q}}_2\right)\frac{\Delta\Gamma}{\Gamma}\right]. \tag{A.4}$$

Let us assume that $\tilde{L}_{ij}$ can be expanded in power series of the temperature difference, $\tilde{L}_{ij} = L^{(0)}_{ij} + L^{(c)}_{ij}\Delta\Gamma$, where $L^{(0)}_{ij}$ is the coefficient for $\Gamma_1 = \Gamma_2 = \Gamma$ and $L^{(c)}_{ij}$ is the first order correction. In terms of such coefficients, the average entropy production $\overline{\Pi}$ is given by

$$\begin{aligned}\overline{\Pi} &= \overline{\Pi}_F + \overline{\Pi}_T \\ &= \left[L^{(0)}_{11}X_1^2 + \left(L^{(0)}_{12} + L^{(0)}_{21}\right)X_1X_2 + L^{(0)}_{22}X_2^2\right] + \\ &+ \left[L^{(c)}_{11}X_1^2 + \left(L^{(c)}_{12} + L^{(c)}_{21}\right)X_1X_2 + L^{(c)}_{22}X_2^2\right]\Delta\Gamma \\ &+ \frac{4L_{\Gamma\Gamma}}{\Gamma^2}(\Delta\Gamma)^2 .\end{aligned} \tag{A.5}$$

By comparing Eqs. (A.4) and (A.5), it follows that

$$L^{(0)}_{11}X_1^2 + \left(L^{(0)}_{12} + L^{(0)}_{21}\right)X_1X_2 + L^{(0)}_{22}X_2^2 = -\frac{2\gamma k_{\mathrm{B}}}{m\Gamma}\left(\overline{\dot{W}}_1 + \overline{\dot{W}}_2\right), \tag{A.6}$$

and hence Onsager coefficients L_{ij}'s correspond to 0-th order coefficients $L^{(0)}_{ij}$'s evaluated from $\overline{\Pi}_F$. Once again, they do not depend on $\Delta\Gamma$, since $\overline{\dot{W}}_i$ does not depend on the temperature at all.

In the true linear regime (both temperature gradient and force strength are small), the correction of $\overline{\Pi}_F$ is of third order ($X_iX_j\Delta\Gamma$), thus it can be neglected. Hence, the entropy production components $\overline{\Pi}_F$ and $\overline{\Pi}_T$ are approximately

$$\overline{\Pi}_F \approx -\frac{2\gamma k_{\mathrm{B}}}{m\Gamma}\left(\overline{\dot{W}}_1 + \overline{\dot{W}}_2\right), \tag{A.7}$$

and

$$\overline{\Pi}_T \approx \frac{4L_{\Gamma\Gamma}}{\Gamma^2}(\Delta\Gamma)^2 , \tag{A.8}$$

respectively. In addition, the coefficients $\tilde{L}_{ij}$ and L_{ij} are approximately equal $\tilde{L}_{ij} \approx L_{ij}$.

Appendix B

Constant drivings

For the machine operating at constant drivings, defined by the forces from Eqs. (3.32) and (3.33), the velocities $\langle v_i \rangle(t)$'s are given by

$$\langle v_1 \rangle(t) = \frac{X_1}{\gamma} + \frac{e^{-\gamma(t-\tau_1)} - e^{-\gamma(t-\tau)})}{e^{\gamma\tau} - 1} \frac{X_1 - X_2}{\gamma}, \tag{B.1}$$

$$\langle v_2 \rangle(t) = \frac{X_2}{\gamma} + \frac{e^{-\gamma(t-\tau-\tau_1)} - e^{-\gamma(t-\tau)}}{e^{\gamma\tau} - 1} \frac{X_1 - X_2}{\gamma}, \tag{B.2}$$

for $i = 1$ and 2, respectively. The associated Onsager coefficients are straightforwardly obtained from Eq. (3.10) and are given by

$$\begin{aligned} L_{11} &= \frac{2\tau_1}{\Gamma_1 \tau} - L_{12}, \\ L_{22} &= \frac{2\tau_2}{\Gamma_2 \tau} - L_{21}, \\ L_{12} &= \frac{4 \operatorname{csch}\left(\frac{\gamma\tau}{2}\right) \sinh\left(\frac{\gamma\tau_1}{2}\right) \sinh\left(\frac{1}{2}\gamma\tau_2\right)}{\gamma\Gamma_1\tau}, \\ L_{21} &= \frac{4 \operatorname{csch}\left(\frac{\gamma\tau}{2}\right) \sinh\left(\frac{\gamma\tau_1}{2}\right) \sinh\left(\frac{1}{2}\gamma\tau_2\right)}{\gamma\Gamma_2\tau}. \end{aligned} \tag{B.3}$$

Furthermore, for isothermal reservoirs, L_{12} and L_{21} are equal for any value of asymmetry parameter $\kappa = \tau_1/\tau_2$.

Appendix C

Linear drivings

Similarly to the constant drivings model, the average velocities for the linear driving model [defined by Eqs. (3.34) and (3.35)] is obtained from Eq. (3.4) and are given by

$$\langle v_1\rangle(t) = \frac{1}{\gamma}\left\{X_1(\gamma t-1)+\frac{e^{-\gamma t}}{e^{\gamma\tau}-1}\left\{X_1\left[e^{\gamma\tau}+e^{\frac{\gamma\kappa\tau}{1+\kappa}}\left(\frac{\gamma\kappa\tau}{1+\kappa}-1\right)\right]-X_2[e^{\frac{\gamma\kappa\tau}{1+\kappa}}+e^{\gamma\tau}\left(\frac{\gamma\tau}{1+\kappa}-1\right)]\right\}\right\}, \tag{C.1}$$

and

$$\langle v_2\rangle(t) = \frac{1}{\gamma}\left\{X_2[1-\gamma\left(t-\frac{\kappa\tau}{1+\kappa}\right)]+\frac{e^{-\gamma(t-\frac{\kappa\tau}{1+\kappa})}}{e^{\gamma\tau}-1}\left\{X_1[e^{\frac{\gamma\tau}{1+\kappa}}+e^{\gamma\tau}\left(\frac{\gamma\kappa\tau}{1+\kappa}-1\right)]-X_2[e^{\frac{\gamma\tau}{1+\kappa}}\left(\frac{\gamma\tau}{1+\kappa}-1\right)+e^{\gamma\tau}]\right\}\right\}. \tag{C.2}$$

Likewise, Onsager coefficients L_{ij}'s are also straightforwardly calculated from Eq. (3.10) and read

$$\begin{aligned}
L_{11} &= \frac{2\gamma^3\tau_1^3+\left[6-3\gamma^2\tau_1^2\right]\coth\left(\frac{\gamma\tau}{2}\right)+6\,\mathrm{csch}\left(\frac{\gamma\tau}{2}\right)\left[\gamma\tau_1\sinh\left(\frac{\gamma(\tau_1-\tau_2)}{2}\right)-\cosh\left(\frac{\gamma(\tau_1-\tau_2)}{2}\right)\right]}{3\gamma\Gamma\tau}.\\
L_{22} &= \frac{2\gamma^3\tau_2^3+\left[6-3\gamma^2\tau_2^2-6\cosh(\gamma\tau_1)\right]\coth\left(\frac{\gamma\tau}{2}\right)+6\gamma\tau_2\,\mathrm{csch}\left(\frac{\gamma\tau}{2}\right)\sinh\left(\frac{\gamma(\tau_2-\tau_1)}{2}\right)+6\sinh(\gamma\tau_1)}{3\gamma\Gamma\tau},\\
L_{12} &= \frac{2}{\gamma\tau\Gamma_1(1-e^{\gamma\tau})}\left[1+\gamma\tau_1-e^{\gamma\tau_1}\right]\left[1-e^{\gamma\tau_2}\left(1-\gamma\tau_2\right)\right],\\
L_{21} &= \frac{2}{\gamma\tau\Gamma_2(1-e^{\gamma\tau})}\left[1+\gamma\tau_2-e^{\gamma\tau_2}\right]\left[1-e^{\gamma\tau_1}\left(1-\gamma\tau_1\right)\right].
\end{aligned} \tag{C.3}$$

Notably, contrasting to the constant drivings case, coefficients L_{12} and L_{21} are different from each other when $\Gamma_1=\Gamma_2$. Only for symmetric switching times ($\tau_1=\tau_2$), it turns out that $L_{12}=L_{21}$.

Appendix D

Large deviation theory results at arbitrary times

In this appendix, we derive the expressions for the first and second current moments from the large deviation theory. Unlike standard treatments, the main difference here is that we focus on finite integration times τ. The starting point is Eq. (5.14), describing the evolution of the entries $G_x(\eta)$ of the moment generating function (MGF). Treating it as a vector $|\boldsymbol{G}(\eta)\rangle$ and from its series expansion in powers of η, we have that

$$|\boldsymbol{G}(\eta)\rangle = |\boldsymbol{p}\rangle + \eta|\boldsymbol{g}_1\rangle + \eta^2|\boldsymbol{g}_2\rangle + \dots, \tag{D.1}$$

where $|\boldsymbol{p}\rangle$ is the steady-state of $\mathbb{W}$. Combining this with the series expansion of the tilted operator, $\mathbb{L}(\eta) = \mathbb{W} + \eta L_1 + \eta^2 L_2$, and collecting terms of the same order in η, we have the following system of equations

$$\frac{d}{d\tau}|\boldsymbol{p}\rangle = \mathbb{W}|\boldsymbol{p}\rangle, \tag{D.2}$$

$$\frac{d}{d\tau}|\boldsymbol{g}_1\rangle = L_1|\boldsymbol{p}\rangle + \mathbb{W}|\boldsymbol{g}_1\rangle, \tag{D.3}$$

$$\frac{d}{d\tau}|\boldsymbol{g}_2\rangle = L_2|\boldsymbol{p}\rangle + L_1|\boldsymbol{g}_1\rangle + \mathbb{W}|\boldsymbol{g}_2\rangle. \tag{D.4}$$

From these, the first and second moments are promptly obtained as

$$E(\mathcal{J}_\tau) = \langle \mathbf{1}|\boldsymbol{g}_1\rangle, \qquad E(\mathcal{J}_\tau^2) = 2\langle \mathbf{1}|\boldsymbol{g}_2\rangle, \tag{D.5}$$

which follow from the definition of the MGF. Eq. (D.2) is automatically satisfied in the steady-state. The solution of Eq. (D.3), with $|\boldsymbol{g}_1(\tau = 0)\rangle = 0$, is given by

$$|\boldsymbol{g}_1(\tau)\rangle = \int_0^\tau d\tau' e^{\mathbb{W}(\tau-\tau')} L_1|\boldsymbol{p}\rangle. \tag{D.6}$$

For concreteness, we assume $\mathbb{W}$ is diagonalizable as discussed above Eq. (5.19). We can then write

$$e^{\mathbb{W}\tau} = |\boldsymbol{p}\rangle\langle\mathbf{1}| + \sum_{i\neq 0} e^{\lambda_i\tau}|\boldsymbol{x}_i\rangle\langle\boldsymbol{y}_i|. \tag{D.7}$$

The eigenvectors satisfy $\langle\mathbf{1}|\boldsymbol{p}\rangle = \langle\boldsymbol{y}_i|\boldsymbol{x}_i\rangle = 1$ and $\langle\mathbf{1}|\boldsymbol{x}_i\rangle = \langle\boldsymbol{y}_i|\boldsymbol{p}\rangle = 0$. Thus, plugging (D.7) in (D.6), we find

$$|\boldsymbol{g}_1(\tau)\rangle = |\boldsymbol{p}\rangle\langle\mathbf{1}|L_1|\boldsymbol{p}\rangle\,\tau + \sum_{i\neq 0}\frac{e^{\lambda_i\tau}-1}{\lambda_i}|\boldsymbol{x}_i\rangle\langle\boldsymbol{y}_i|L_1|\boldsymbol{p}\rangle. \tag{D.8}$$

To obtain the first moment we take the inner product $\langle\mathbf{1}|\boldsymbol{g}_1\rangle$; the second term vanishes and we are left with

$$E(\mathcal{J}_\tau) = \langle\mathbf{1}|L_1|\boldsymbol{p}\rangle\,\tau, \tag{D.9}$$

which yields Eq. (5.17).

Turning now to the second moment, the solution of Eq. (D.4) reads

$$|\boldsymbol{g}_2(\tau)\rangle = \int_0^\tau d\tau' e^{\mathbb{W}(\tau-\tau')}(L_2|\boldsymbol{p}\rangle + L_1|\boldsymbol{g}_1(\tau')\rangle). \tag{D.10}$$

We are only interested in $\langle\mathbf{1}|\boldsymbol{g}_2\rangle$. Using Eq. (D.7), together with the fact that $\langle\mathbf{1}|\boldsymbol{x}_i\rangle = 0$, we are then left only with

$$\langle\mathbf{1}|\boldsymbol{g}_2(\tau)\rangle = \int_0^\tau d\tau'\Big\{\langle\mathbf{1}|L_2|\boldsymbol{p}\rangle + \langle\mathbf{1}|L_1|\boldsymbol{g}_1(\tau')\rangle\Big\}. \tag{D.11}$$

The first term is time-independent and hence will simply give a factor of τ. In the second term we use Eq. (D.8), leading to

$$\langle\mathbf{1}|\boldsymbol{g}_2(\tau)\rangle = \langle\mathbf{1}|L_2|\boldsymbol{p}\rangle\,\tau + \int_0^\tau d\tau'\int_0^{\tau'} d\tau''\langle\mathbf{1}|L_1 e^{\mathbb{W}(\tau'-\tau'')}L_1|\boldsymbol{p}\rangle. \tag{D.12}$$

This, combined with the first moment squared, yields Eq. (5.18).

To obtain the more explicit formula (5.19), we carry out the remaining integral, leading to

$$\begin{aligned}\langle\mathbf{1}|\boldsymbol{g}_2(\tau)\rangle = \langle\mathbf{1}|L_2|\boldsymbol{p}\rangle\,\tau + \langle\mathbf{1}|L_1|\boldsymbol{p}\rangle^2\frac{\tau^2}{2} \\ + \sum_{i\neq 0}\langle\mathbf{1}|L_1|\boldsymbol{x}_i\rangle\langle\boldsymbol{y}_i|L_1|\boldsymbol{p}\rangle\left(\frac{e^{\lambda_i\tau}-1-\lambda_i\tau}{\lambda_i^2}\right).\end{aligned} \tag{D.13}$$

The second term is identified as the first moment squared. Hence,

$$\begin{aligned}E(\mathcal{J}_\tau^2) - E(\mathcal{J}_\tau)^2 = 2\langle\mathbf{1}|L_2|\boldsymbol{p}\rangle\,\tau \\ +2\sum_{i\neq 0}\langle\mathbf{1}|L_1|\boldsymbol{x}_i\rangle\langle\boldsymbol{y}_i|L_1|\boldsymbol{p}\rangle\left(\frac{e^{\lambda_i\tau}-1-\lambda_i\tau}{\lambda_i^2}\right).\end{aligned} \tag{D.14}$$

Dividing by 2τ finally yields Eq. (5.19).

As a final comment, concerning now the computation of Eq. (5.20), which is valid when $\tau \gg \lambda_i$, it is convenient to express the solution in a way which is independent of the full eigendecomposition of $\mathbb{W}$ (and hence more convenient for numerical computations). Let $|\boldsymbol{Q}_1\rangle$ denote the solution of the linear equation

$$\mathbb{W}|\boldsymbol{Q}_1\rangle = \Big(1 - |\boldsymbol{p}\rangle\langle\mathbf{1}|\Big)L_1|\boldsymbol{p}\rangle. \tag{D.15}$$

This equation actually has an infinite number of solutions, which are of the form

$$|\boldsymbol{Q}_1\rangle = \mathbb{W}^+ L_1|\boldsymbol{p}\rangle + |\boldsymbol{p}\rangle\langle\mathbf{1}|\boldsymbol{w}\rangle, \tag{D.16}$$

for any vector $|\boldsymbol{w}\rangle$. Here, recall, $\mathbb{W}^+$ is the Moore-Penrose pseudo-inverse of $\mathbb{W}$. Projecting out the contributions from the subspace $|\boldsymbol{p}\rangle\langle\mathbf{1}|$, we see that

$$\Big(1 - |\boldsymbol{p}\rangle\langle\mathbf{1}|\Big)|\boldsymbol{Q}_1\rangle = \mathbb{W}^+ L_1|\boldsymbol{p}\rangle. \tag{D.17}$$

Hence, Eq. (5.20) can be rewritten as

$$D_\tau = \langle\mathbf{1}|L_2|\boldsymbol{p}\rangle - \langle\mathbf{1}|L_1|\boldsymbol{Q}_1\rangle - \langle\mathbf{1}|L_1|\boldsymbol{p}\rangle\langle\mathbf{1}|\boldsymbol{Q}_1\rangle. \tag{D.18}$$

This form of the diffusion coefficient is more familiar in the LDT literature, as compared with Eq. (5.20). It has the advantage that it requires solving a single linear equation (D.15), which is computationally much cheaper than fully diagonalizing $\mathbb{W}$.

Appendix E

Published articles

In this appendix we show the first pages of all the published articles in which I participated during the course of my PhD. The articles [75, 94, 95] about the energetic performance of Brownian Particles Machines, part of this results are presented in the chapter 3. As well as the first page of the published article [136] about current fluctuations in nonequilibrium discontinuous phase transitions, associated with the results shown in the chapter 5. Lastly, the first page of the article [156] associated with the results discussed in chapter 4 is shown. This article last one is available in the arXiv platform (https://doi.org/10.48550/arXiv.2305.03813) and is currently in the process of being published.

Thermodynamics of collisional models for Brownian particles: General properties and efficiency

Angel L. L. Stable, C. E. Fernández Noa, William G. C. Oropesa, and C. E. Fiore
Universidade de São Paulo, Instituto de Física, Rua do Matão, 1371, 05508-090 São Paulo, São Paulo, Brasil

(Received 1 May 2020; accepted 2 September 2020; published 2 October 2020)

We introduce the idea of *collisional models* for Brownian particles, in which a particle is sequentially placed in contact with distinct thermal environments and external forces. Thermodynamic properties are exactly obtained, irrespective of the number of reservoirs involved. In the presence of external forces, the entropy production presents a bilinear form in which Onsager coefficients are exactly calculated. Analysis of Brownian engines based on sequential thermal switchings is proposed and considerations about their efficiencies are investigated, taking into account distinct external forces protocols. Our results shed light to an alternative route for obtaining efficient thermal engines based on finite times Brownian machines.

DOI: 10.1103/PhysRevResearch.2.043016

I. INTRODUCTION

Stochastic thermodynamics has proposed a general and unified scheme for addressing central issues in thermodynamics [1–5]. It includes not only an extension of concepts from equilibrium to nonequilibrium systems but also it deals with the existence of new definitions and bounds [6–9], general considerations about the efficiency of engines at finite time operations [1–3], and others aspects. In all cases, the concept of entropy production [1,4,10] plays a central role, being a quantity continuously produced in nonequilibrium steady states (NESS), whose main properties and features have been extensively studied in the last years, including its usage for typifying phase transitions [11–14].

Basically, a NESS can be generated under two fundamental ways: From fixed thermodynamic forces [15,16] or from time-periodic variation of external parameters [17–20]. In this contribution, we address a different kind of periodic driving, suitable for the description of engineered reservoirs, at which a system interacts sequentially and repeatedly with distinct environments [21–23]. Commonly referred as *collisional models*, they have been inspired by the assumption that in many cases (e.g., the original Brownian motion) a particle collides only with few molecules of the environment and then the subsequent collision will occur with another fraction of uncorrelated molecules. Collisional models have been viewed as more realistic frameworks in certain cases, encompassing not only particles interacting with a small fraction of the environment but also those presenting distinct drivings over each member of system [24–27] or even species yielding a weak coupling with the reservoir. More recently, they have been (broadly) extended for quantum systems for mimicking the environment, represented by a weak interaction between the system and a sequential collection of uncorrelated particles [28–30].

With the above in mind, we introduce the concept of repeated interactions for Brownian particles. More specifically, a particle under the influence of a given external force is placed in contact with a reservoir during the time interval and afterwards it is replaced by an entirely different (and independent) set of interactions. Exact expressions for thermodynamic properties are derived and the entropy production presents a bilinear form, in which Onsager coefficients are obtained as function of period. Considerations about the efficiency are undertaken and a suited regime for the system operating as an efficient thermal machine is investigated.

The present study sheds light for fresh perspectives in nonequilibrium thermodynamics, including the possibility of experimental buildings of heat engines based on Brownian dynamics [31–36] with sequential reservoirs. Also, they provide us the extension and validation of recent bounds between currents and entropy production, the so called thermodynamic uncertainty relations (TURs) [8,9,37–41], which has aroused a recent and great interest.

This paper is organized as follows: Secs. II and III present the model description and its exact thermodynamic properties. In Sec. IV we extend analysis for external forces and considerations about efficiency are performed in Sec. V. Conclusions and perspectives are drawn in Sec. VI.

II. MODEL AND FOKKER-PLANCK EQUATION

We are dealing with a Brownian particle with mass m sequentially placed in contact with N different thermal reservoirs. Each contact has a duration of τ/N and occurs during the intervals $\tau_{i-1} \leqslant t < \tau_i$, where $\tau_i = i\tau/N$ for $i = 1, .., N$, in which the particle evolves in time according to the following Langevin equation:

$$m\frac{dv_i}{dt} = -\alpha_i v_i + F_i(t) + B_i(t), \tag{1}$$

where quantities v_i, α_i, and $F_i(t)$ denote the particle velocity, the viscous constant and external force, respectively. From

Efficient asymmetric collisional Brownian particle engines

C. E. Fernández Noa,[1] Angel L. L. Stable,[1] William G. C. Oropesa,[1] Alexandre Rosas,[2] and C. E. Fiore[1]
[1]*Instituto de Física da Universidade de São Paulo, 05508-090 São Paulo, São Paulo, Brazil*
[2]*Departamento de Física, CCEN, Universidade Federal da Paraíba, Caixa Postal 5008, 58059-900 João Pessoa, Brazil*

(Received 2 August 2021; accepted 15 November 2021; published 2 December 2021)

The construction of efficient thermal engines operating at finite times constitutes a fundamental and timely topic in nonequilibrium thermodynamics. We introduce a strategy for optimizing the performance of Brownian engines, based on a collisional approach for unequal interaction times between the system and thermal reservoirs. General (and exact) expressions for thermodynamic properties and their optimized values are obtained, irrespective of the driving forces, asymmetry, temperatures of reservoirs, and protocol to be maximized. Distinct routes for the engine optimization, including maximizations of output power and efficiency with respect to the asymmetry, the force, and both of these, are investigated. For the isothermal work-to-work converter and/or a small difference in temperature between reservoirs, they are solely expressed in terms of Onsager coefficients. Although the symmetric engine can operate very inefficiently depending on the control parameters, the usage of distinct contact times between the system and each reservoir not only can enhance the machine performance (signed by an optimal tuning ensuring the largest gain) but also enlarges substantially the machine regime operation. The present approach can pave the way for the construction of efficient Brownian engines operating at finite times.

DOI: 10.1103/PhysRevResearch.3.043152

I. INTRODUCTION

A long-standing dilemma in thermodynamics and related areas concerns the issue of mitigating the impact of thermal noise or wasted heat in order to improve the machine performance. This constitutes a highly relevant problem, not only for theoretical purposes but also for the construction of experimental setups [1–3]. Giving that the machine performance is commonly dependent on particular chemical compositions and operation conditions, notably for small-scale engines, the role of fluctuations being crucial for such engines, distinct approaches have been proposed and investigated in the realm of stochastic and quantum thermodynamics [4,5]. A second fundamental point concerns the fact that, even if all sources of dissipation could be mitigated, the performance of any thermal machine would still be limited by Carnot efficiency, which requires the occurrence of infinitely slow quasistatic processes, and consequently the engine operates at null power. In contrast, realistic systems operate at finite time and power. Such a conundrum (control or mitigation of dissipation and engine optimization) has contributed to the discovery of several approaches based on the maximization of power output instead of the efficiency [4–20].

Thermal machines based on Brownian particles have been successfully studied not only for theoretical purposes [6,7,15,21] but also for the building of reliable experimental setups [22–27]. They are also remarkable for depicting the limitations of classical thermodynamics and disclose the scales at which thermal fluctuations become relevant. In several situations, thermal machines involve isothermal transformations [22,23,25]. Such a class of processes are fundamental in thermodynamics since they are minimally dissipative. However, isothermal transformations are slow, demanding a sufficiently large number of stages for achieving the desired final state. For this reason, distinct protocols, such as increasing the coupling between the system and the thermal bath, have been undertaken for speeding it up and simultaneously controlling the increase in dissipation [28–32].

Here, we introduce a strategy for optimizing the performance of irreversible Brownian machines operating in isothermal parts via control of the interaction time between the system and the environment. Our approach is based on a Brownian particle sequentially placed in contact with distinct thermal baths and subject to external forces [33] for unequal times. Such a description, also referred to as collisional, has been successfully employed in different contexts, such as systems that interact only with a small fraction of the environment and those presenting distinct drivings over each member of the system [34–37]. Depending on the parameters of the model (period, driving, and difference of temperatures), the symmetric version can operate very inefficiently. Our aim is to show that the machine performance improves substantially by tuning properly the interaction time between the particle and each reservoir. Besides the increase in the power and/or efficiency, the asymmetry in the contact time also enlarges the regime of operation of the machine substantially. Contrasting with previous works [29–32], the optimization is solely

Thermodynamics and efficiency of sequentially collisional Brownian particles: The role of drivings

Fernando S. Filho,[1] Bruno A. N. Akasaki,[1] Carlos E. F. Noa,[1] Bart Cleuren,[2] and Carlos E. Fiore[1]
[1]*Universidade de São Paulo, Instituto de Física, Rua do Matão, 1371, 05508-090 São Paulo, SP, Brasil*
[2]*UHasselt, Faculty of Sciences, Theory Lab, Agoralaan, 3590 Diepenbeek, Belgium*

(Received 13 June 2022; accepted 30 September 2022; published 24 October 2022)

Brownian particles placed sequentially in contact with distinct thermal reservoirs and subjected to external driving forces are promising candidates for the construction of reliable engine setups. In this contribution, we address the role of driving forces for enhancing the collisional machine performance. Analytical expressions for thermodynamic quantities such as power output and efficiency are obtained for general driving schemes. A proper choice of these driving schemes substantially increases both power output and efficiency and extends the working regime. Maximizations of power and efficiency, whether with respect to the strength of the force, driving scheme, or both have been considered and exemplified for two kind of drivings: generic power-law and harmonic (sinusoidal) drivings.

DOI: 10.1103/PhysRevE.106.044134

I. INTRODUCTION

The construction of nanoscale engines has received a great deal of attention and recent technological breakthroughs have made feasible not only the realization of distinct setups composed of quantum dots [1], colloidal particles [2–5], single and coupled systems [6–8] but also coarse-grained approaches for systems presenting different degrees of freedom [9,10]. In contrast with their macroscopic counterparts, their main features are strongly influenced by fluctuations when operating at the nanoscale, having several features described within the framework of stochastic thermodynamics [11–16].

Recently a novel approach, coined collisional, has been put forward as a candidate for the realization of reliable thermal engines [17,18] and novel engine setups [19–21]. They consist of sequentially placing the system (a Brownian particle) in contact with distinct thermal reservoirs and subjected to external driving forces during each stage (stroke) of the cycle. Each stage is characterized by the temperature of the connected thermal reservoir and the external driving force. The time needed to switch between the thermal baths at the end of each stage is neglected. Despite its reliability in distinct situations, such as systems interacting only with a small fraction of the environment and those presenting distinct drivings over each member of the system [22–25], the engine can operate rather inefficiently depending on the way it is projected (temperatures, kind of driving, and duration of each stroke). Hence the importance for strategies to enhance its performance [20,21]. Among the distinct approaches, we cite those based on the maximization of power [1,6,14,26–33], efficiency [20,34,35], low or finite dissipation [36,37] and even the assumption of maximization via the largest dissipation [38].

This paper deals with the above points but it focuses on a different direction, namely, the optimization of the engine performance by fine-tuning the driving at each stroke. Such an idea is illustrated in a collisional Brownian machine, which has been considered as a working substance in several works, both from the theoretical [7,39–43] and experimental points of view [3,35,44–46]. The collisional description allows us to derive general (and exact) expressions for thermodynamic quantities, such as output power and efficiency, irrespective of the kind of driving [20]. To exploit the consequences of a distinct driving each stroke and possible optimizations, two representative examples will be considered: generic harmonic and power-law drivings. The former consists of a simpler and feasible way to drive Brownian particles out of equilibrium [35,45,47–49] and providing simultaneous maximizations of the engine [7]. Since the engine performance is substantially reduced for linear drivings when compared with constant ones [19,20], generic power-law drivings have been considered not only for generalizing the machine performance beyond constant and linear drivings but also to exploit the possibility of obtaining a gain by changing its form at each stroke.

This paper is organized as follows: Section II presents the model and the main expressions for the thermodynamic quantities. Efficiency and optimization is discussed in detail for both classes of drivings in Sec. III. Conclusions and perspectives are addressed in Sec. IV.

II. THERMODYNAMICS AND MAIN EXPRESSIONS

We focus on the simplest projection of an engine composed of only two strokes and returning to the initial step after one cycle. The time it takes to complete one cycle is set to τ, with each stroke $\in\{1, 2\}$ lasting a time $\tau/2$. During stroke i the Brownian particle of mass m is in contact with a thermal bath at temperature T_i and described by the Langevin equation.[1]

$$\frac{dv_i(t)}{dt} = -\gamma_i v_i(t) + \tilde{f}_i(t) + \zeta_i(t), \tag{1}$$

[1]Eq. (1) is formally identical to description of the overdamped harmonic oscillator subject to the harmonic force $\tilde{f}_h = -\bar{k}x$ just by replacing $x \to v$, $\bar{k}/\alpha \to \gamma_i$, $1/\alpha \to \gamma_i/m$.

Current fluctuations in nonequilibrium discontinuous phase transitions

C. E. Fiore,[1,*] Pedro E. Harunari,[1,2,†] C. E. Fernández Noa,[1] and Gabriel T. Landi[1,‡]
[1]*Instituto de Física da Universidade de São Paulo, 05314-970 São Paulo, Brazil*
[2]*Complex Systems and Statistical Mechanics, Physics and Materials Science Research Unit, University of Luxembourg, Luxembourg L-1511, G.D. Luxembourg*

(Received 7 September 2021; accepted 29 November 2021; published 17 December 2021)

Discontinuous phase transitions out of equilibrium can be characterized by the behavior of macroscopic stochastic currents. But while much is known about the average current, the situation is much less understood for higher statistics. In this paper, we address the consequences of the diverging metastability lifetime—a hallmark of discontinuous transitions—in the fluctuations of arbitrary thermodynamic currents, including the entropy production. In particular, we center our discussion on the *conditional* statistics, given which phase the system is in. We highlight the interplay between integration window and metastability lifetime, which is not manifested in the average current, but strongly influences the fluctuations. We introduce conditional currents and find, among other predictions, their connection to average and scaled variance through a finite-time version of large deviation theory and a minimal model. Our results are then further verified in two paradigmatic models of discontinuous transitions: Schlögl's model of chemical reactions, and a 12-state Potts model subject to two baths at different temperatures.

DOI: 10.1103/PhysRevE.104.064123

I. INTRODUCTION

In microscopic systems, currents of heat, work, and entropy production must be treated as random variables, which fluctuate over different runs of an experiment [1,2]. This represents a paradigm shift in thermodynamics, and has already led to fundamental advancements in the field, such as fluctuation theorems [3–8] and, more recently, the discovery of thermodynamic uncertainty relations [9–13]. It also entails practical consequences, e.g., in the design of Brownian engines [14–17], molecular motors [18–21], information-driven devices [22,23], and bacterial baths [24]. In these systems, both the output power [13,25] and the efficiency [26–29] may fluctuate significantly, leading to possible violations of macroscopic predictions, such as the Carnot limit [14].

A scenario of particular interest is that of nonequilibrium steady states (NESSs), which occur when a system is placed in contact with multiple reservoirs at different temperatures T_i and/or chemical potentials μ_i. NESSs are characterized by finite currents of energy and matter, and thus also a finite entropy production rate σ_t [1,30–33]. At the stochastic level, these become fluctuating quantities, associated to a probability distribution. Understanding the behavior of said distributions constitutes a major area of research, as they form the basis for extending the laws of the thermodynamics towards the microscale, providing insights in nontrivial properties of nonequilibrium physics. Of particular interest is their behavior across nonequilibrium phase transitions [34]. Most of our understanding, however, is centered on the average current. For instance, the average entropy production rate has been found to be always finite around the transition point, with the first derivative either diverging, in continuous transitions [35–41], or presenting a jump in discontinuous ones [38,39,42]. These clear signatures suggest, in fact, that the average entropy production could even be used to classify the type of transition. Conversely, the behavior of higher order statistics, such as the variance, is much less understood.

Cumulants of thermodynamic currents are usually assessed via numerical approaches, such as Monte Carlo simulations [39], or large deviation theory (LDT) [7,43–47]. In both cases, cumulants are computed from long-time sample averages, integrated over a time window τ. Ultimately, one is interested in taking $\tau \to \infty$, at least in principle. But in systems presenting discontinuous transitions this can become an issue, since the phase coexistence is characterized by states with very long metastability lifetimes τ_m. In fact, τ_m increases exponentially with the system volume V, which is a consequence of the discontinuous nature of the transition (for continuous transitions these divergences are algebraic). As a consequence, the order of the limits $\tau \to \infty$ and $V \to \infty$ becomes nontrivial [48].

In this paper we approach this issue by introducing the idea of conditional currents, given which phase the system is in. We focus, in particular, on the diffusion coefficient (scaled variance). We formulate a finite-time large deviation theory, which neatly highlights the nontrivial interplay between τ and τ_m. This is then specialized to a minimal two-state model, that is able to capture the key features of the problem and also provides useful predictions. These are then tested on two paradigmatic examples of discontinuous transitions: Schlögl's model of chemical kinetics, and a 12-state Potts model subject to two baths at different temperatures.

This paper is organized as follows: Section II presents the main concepts and assumptions considered. The conditional

*fiorecarlos.cf@gmail.com
†pedroharunari@gmail.com
‡gtlandi@gmail.com

Thermodynamics of a collisional quantum-dot machine: the role of stages.

C. E. Fernández Noa,[1,2] C. E. Fiore,[1] F. F. S. Filho,[1] B. Wijns,[2] and B. Cleuren[2]

[1] *Universidade de São Paulo, Instituto de Física, Rua do Matão, 1371, 05508-090 São Paulo, SP, Brasil*
[2] *UHasselt, Faculty of Sciences, Theory Lab, Agoralaan, 3590 Diepenbeek, Belgium*

(Dated: July 13, 2023)

Sequential (or collisional) engines have been put forward as an alternative candidate for the realisation of reliable engine setups. Despite this, the role of the different stages and the influence of the intermediate reservoirs is not well understood. We introduce the idea of conveniently adjusting/choosing intermediate reservoirs at engine devices as a strategy for optimizing its performance. This is done by considering a minimal model composed of a quantum-dot machine sequentially exposed to distinct reservoirs at each stage, and for which thermodynamic quantities (including power and efficiency) can be obtained exactly from the framework of stochastic thermodynamics, irrespective to the number of stages. Results show that a significant gain can be obtained by increasing the number of stages and conveniently choosing their parameters.

I. INTRODUCTION

Stochastic engines are devices that convert a given amount of energy, say heat**,** into work or vice-versa. In contrast to macroscopic engines, they operate at the nanoscale and consequently the relevant thermodynamic quantities are subjected to fluctuations at the microscopic level, above all in power and efficiency. Although an ideal engine is always desired to operate at high power, high efficiency and low (power) fluctuations, these conditions can never be satisfied simultaneously. For this reason the development of distinct approaches/trade-offs has been strongly levered in the last years, such as by including the variation of external parameters [1], cyclic operations under quasistatic conditions [2], interaction between particles [3, 4], dynamics based on control via shortcuts to adiabaticy [5–7], to isothermality [8], maximization of power [9–21] and efficiency [4, 22] and more recently the strategies based on synchronized operation under ordered arrangements [23] or Pareto optimal cycles for power, efficiency and fluctuations [24].

Sequential (or collisional) engines have been put forward as an alternative candidate for the realisation of reliable thermal engines [25, 26] and novel engine setups [27–30]. They consist of sequentially placing the system/engine in contact with distinct thermal reservoirs and subjected to external driving forces during each stage (stroke) of the cycle. Each stage is characterized by the connected thermal reservoir. The time needed to switch between the thermal baths at the beginning/end of each stage is neglected. Despite its reliability in distinct situations [31–34], the conditions to be imposed in order to provide a better performance have not been fully understood and for this reason distinct (and recent) approaches for enhancing its performance have been proposed and analyzed. Among them, we cite the convenient choices of the duration of each stroke [28, 30] and driving [29, 35].

In this contribution, we address a less explored strategy for improving the performance of collisional engines: the number of stages and the reservoir parameters for each stage. The system we consider is a particle pump model introduced in references [25, 26], consisting of a two-level system sequentially brought into contact with distinct reservoirs allowing for the exchange of particles among reservoirs and the generation of a power output. Quantum dot devices are one of the most prominent system in the realm of stochastic and quantum thermodynamics, as in theoretical [36–39] and experimental [40] studies. Due to its simplicity, it presents several advantages such as an exact solution irrespective of the number of strokes and model parameters [36–39]. And so it provides full access to all relevant quantities. Another advantage concerns that they can be projected to function either as heat or pump engines rather than Brownian engines, which only can be operated as work-to-work converters depending on the kind of external driving used as the work source [4, 27–29]. A careful analysis over the space of parameters for distinct intermediate stages reveals that a remarkable gain can be obtained by increasing the number of stages and a suitable choice of parameters.

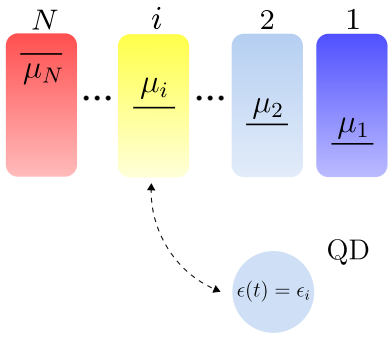

FIG. 1. Sketch of a Quantum-dot setup sequentially exposed to N distinct thermal baths, each one at the interval $\tau_{i-1} \leq t < \tau_i = i\tau/N$ characterized by chemical potential μ_i and temperature $T_i = T$.

This paper is structured as follows: In Sec. II, the thermodynamic considerations are derived irrespective of the number of strokes and exemplified for distinct stages. The engine performance when the stages are varied is investigated in Sec. III and conclusions are drawn in Sec. IV.

Bibliography

[1] F. S. Gnesotto, F. Mura, J. Gladrow, and C. P. Broedersz, "Broken detailed balance and non-equilibrium dynamics in living systems: a review," *Reports on Progress in Physics*, vol. 81, p. 066601, apr 2018.

[2] R. Rao and M. Esposito, "Nonequilibrium thermodynamics of chemical reaction networks: Wisdom from stochastic thermodynamics," *Phys. Rev. X*, vol. 6, p. 041064, Dec 2016.

[3] D. M. Busiello, S. Liang, F. Piazza, and P. De Los Rios, "Dissipation-driven selection of states in non-equilibrium chemical networks," *Communications Chemistry*, vol. 4, no. 1, p. 16, 2021.

[4] D. Kolisnyk and G. Schaller, "Performance boost of a collective qutrit refrigerator," *Phys. Rev. Appl.*, vol. 19, p. 034023, Mar 2023.

[5] S. Kamimura, H. Hakoshima, Y. Matsuzaki, K. Yoshida, and Y. Tokura, "Quantum-enhanced heat engine based on superabsorption," *Phys. Rev. Lett.*, vol. 128, p. 180602, May 2022.

[6] M. A. Macovei, "Performance of the collective three-level quantum thermal engine," *Phys. Rev. A*, vol. 105, p. 043708, Apr 2022.

[7] L. Onsager, "Reciprocal relations in irreversible processes. i.," *Physical Review*, vol. 37, no. 4, p. 405 – 426, 1931.

[8] L. Onsager, "Reciprocal relations in irreversible processes. ii," *Physical Review*, vol. 38, no. 12, p. 2265 – 2279, 1931.

[9] I. Prigogine and P. V. Rysselberghe, "Introduction to thermodynamics of irreversible processes," *Journal of The Electrochemical Society*, vol. 110, p. 97C, apr 1963.

[10] D. J. Evans, E. G. D. Cohen, and G. P. Morriss, "Probability of second law violations in shearing steady states," *Physical Review Letters*, vol. 71, no. 1 5, pp. 2401–2404, 1993.

[11] G. Gallavotti and E. G. D. Cohen, "Dynamical ensembles in stationary states," *Journal of Statistical Physics*, vol. 80, pp. 931–970, 9 1995.

[12] J. Kurchan, "Fluctuation theorem for stochastic dynamics," *Journal of Physics A: Mathematical and General*, vol. 31, no. 16, p. 3719, 1998.

[13] J. L. Lebowitz and H. Spohn, "A gallavotti–cohen-type symmetry in the large deviation functional for stochastic dynamics," *Journal of Statistical Physics*, vol. 95, no. 1, pp. 333–365, 1999.

[14] D. J. Evans and D. J. Searles, "Equilibrium microstates which generate second law violating steady states," *Phys. Rev. E*, vol. 50, pp. 1645–1648, Aug 1994.

[15] C. Jarzynski, "Nonequilibrium equality for free energy differences," *Physical Review Letters*, vol. 78, no. 14, p. 2690, 1997.

[16] C. Jarzynski, "Equilibrium free-energy differences from nonequilibrium measurements: A master-equation approach," *Phys. Rev. E*, vol. 56, pp. 5018–5035, Nov 1997.

[17] G. E. Crooks, "Entropy production fluctuation theorem and the nonequilibrium work relation for free energy differences," *Phys. Rev. E*, vol. 60, pp. 2721–2726, Sep 1999.

[18] G. E. Crooks, "Path-ensemble averages in systems driven far from equilibrium," *Phys. Rev. E*, vol. 61, pp. 2361–2366, Mar 2000.

[19] T. Hatano and S.-i. Sasa, "Steady-state thermodynamics of langevin systems," *Phys. Rev. Lett.*, vol. 86, pp. 3463–3466, Apr 2001.

[20] K. Sekimoto, "Kinetic characterization of heat bath and the energetics of thermal ratchet models," *Journal of the Physical Society of Japan*, vol. 66, no. 5, pp. 1234–1237, 1997.

[21] K. Sekimoto, "Langevin Equation and Thermodynamics," *Progress of Theoretical Physics Supplement*, vol. 130, pp. 17–27, 01 1998.

[22] C. Maes and K. Netočný, "Time-reversal and entropy," *Journal of Statistical Physics*, vol. 110, pp. 269–310, jan 2003.

[23] C. Maes, "On the origin and use of fluctuation relations on the entropy," *Séminaire Poincaré*, vol. 2, pp. 29–62, Dec 2003.

[24] U. Seifert, "Stochastic thermodynamics: principles and perspectives," *The European Physical Journal B*, vol. 64, no. 3, pp. 423–431, 2008.

[25] K. Brandner, K. Saito, and U. Seifert, "Thermodynamics of micro- and nano-systems driven by periodic temperature variations," *Phys. Rev. X*, vol. 5, p. 031019, Aug 2015.

[26] K. Proesmans and C. Van den Broeck, "Onsager coefficients in periodically driven systems," *Phys. Rev. Lett.*, vol. 115, p. 090601, Aug 2015.

[27] K. Proesmans, B. Cleuren, and C. V. den Broeck, "Linear stochastic thermodynamics for periodically driven systems," *Journal of Statistical Mechanics: Theory and Experiment*, vol. 2016, p. 023202, feb 2016.

[28] K. Proesmans and C. E. Fiore, "General linear thermodynamics for periodically driven systems with multiple reservoirs," *Phys. Rev. E*, vol. 100, p. 022141, Aug 2019.

[29] T. Tomé and M. J. de Oliveira, "Entropy production in nonequilibrium systems at stationary states," *Phys. Rev. Lett.*, vol. 108, p. 020601, Jan 2012.

[30] T. Tomé and M. J. de Oliveira, "Stochastic approach to equilibrium and nonequilibrium thermodynamics," *Phys. Rev. E*, vol. 91, p. 042140, Apr 2015.

[31] M. Bauer, K. Brandner, and U. Seifert, "Optimal performance of periodically driven, stochastic heat engines under limited control," *Phys. Rev. E*, vol. 93, p. 042112, Apr 2016.

[32] K. Proesmans, B. Cleuren, and C. Van den Broeck, "Power-efficiency-dissipation relations in linear thermodynamics," *Phys. Rev. Lett.*, vol. 116, p. 220601, Jun 2016.

[33] I. Iyyappan and M. Ponmurugan, "Relations between the efficiency, power and dissipation for linear irreversible heat engine at maximum trade-off figure of merit," *Journal of Statistical Mechanics: Theory and Experiment*, vol. 2018, p. 033202, mar 2018.

[34] J. M. R. Parrondo, J. M. Horowitz, and T. Sagawa, "Thermodynamics of information," *Nature Physics*, vol. 11, pp. 131–139, Feb 2015.

[35] D. Mandal, K. Klymko, and M. R. DeWeese, "Entropy production and fluctuation theorems for active matter," *Phys. Rev. Lett.*, vol. 119, p. 258001, Dec 2017.

[36] L. Dabelow, S. Bo, and R. Eichhorn, "Irreversibility in active matter systems: Fluctuation theorem and mutual information," *Phys. Rev. X*, vol. 9, p. 021009, Apr 2019.

[37] A. C. Barato and U. Seifert, "Thermodynamic uncertainty relation for biomolecular processes," *Physical review letters*, vol. 114, no. 15, p. 158101, 2015.

[38] T. Tomé and M. J. De Oliveira, *Stochastic dynamics and irreversibility*. Springer, 2015.

[39] B. A. N. Akasaki, M. J. de Oliveira, and C. E. Fiore, "Entropy production and heat transport in harmonic chains under time-dependent periodic drivings," *Phys. Rev. E*, vol. 101, p. 012132, Jan 2020.

[40] T. Tomé and M. J. de Oliveira, "Entropy production in irreversible systems described by a Fokker-Planck equation," *Phys. Rev. E*, vol. 82, p. 021120, Aug 2010.

[41] J. Schnakenberg, "Network theory of microscopic and macroscopic behavior of master equation systems," *Reviews of Modern physics*, vol. 48, no. 4, p. 571, 1976.

[42] C. E. F. Noa, P. E. Harunari, M. J. de Oliveira, and C. E. Fiore, "Entropy production as a tool for characterizing nonequilibrium phase transitions," *Physical Review E*, vol. 100, no. 1, p. 012104, 2019.

[43] J. M. Encinas, P. E. Harunari, M. M. de Oliveira, and C. E. Fiore, "Fundamental ingredients for discontinuous phase transitions in the inertial majority vote model," *Scientific Reports*, vol. 8, p. 9338, 2018.

[44] H. B. Callen, "Thermodynamics and an introduction to thermostatistics," 1998.

[45] I. Prigogine, *Introduction to thermodynamics of irreversible processes*. Interscience New York, 1965.

[46] S. De Groot and P. Mazur, *Irreversible Processes: Non-Equilibrium Thermodynamics*. North-Holland, Amsterdam, 1962.

[47] U. Seifert, "Stochastic thermodynamics, fluctuation theorems and molecular machines," *Reports on progress in physics*, vol. 75, no. 12, p. 126001, 2012.

[48] C. Van den Broeck, "Thermodynamic efficiency at maximum power," *Physical Review Letters*, vol. 95, no. 19, p. 190602, 2005.

[49] G. Verley, M. Esposito, T. Willaert, and C. Van den Broeck, "The unlikely Carnot efficiency.," *Nature communications*, vol. 5, p. 4721, 1 2014.

[50] T. Schmiedl and U. Seifert, "Efficiency at maximum power: An analytically solvable model for stochastic heat engines," *Europhysics Letters*, vol. 81, no. 2, p. 20003, 2007.

[51] M. Esposito, K. Lindenberg, and C. Van den Broeck, "Universality of efficiency at maximum power," *Phys. Rev. Lett.*, vol. 102, p. 130602, Apr 2009.

[52] B. Cleuren, B. Rutten, and C. Van den Broeck, "Universality of efficiency at maximum power," *The European Physical Journal Special Topics*, vol. 224, no. 5, pp. 879–889, 2015.

[53] M. Esposito, R. Kawai, K. Lindenberg, and C. Van den Broeck, "Quantum-dot carnot engine at maximum power," *Physical Review E*, vol. 81, no. 4, p. 041106, 2010.

[54] U. Seifert, "Efficiency of autonomous soft nanomachines at maximum power," *Physical Review Letters*, vol. 106, no. 2, p. 020601, 2011.

[55] Y. Izumida and K. Okuda, "Efficiency at maximum power of minimally nonlinear irreversible heat engines," *Europhysics Letters*, vol. 97, no. 1, p. 10004, 2012.

[56] N. Golubeva and A. Imparato, "Efficiency at maximum power of interacting molecular machines," *Physical Review Letters*, vol. 109, no. 19, p. 190602, 2012.

[57] V. Holubec, "An exactly solvable model of a stochastic heat engine: optimization of power, power fluctuations and efficiency," *Journal of Statistical Mechanics: Theory and Experiment*, vol. 2014, no. 5, p. P05022, 2014.

[58] K. Proesmans, B. Cleuren, and C. Van den Broeck, "Power-efficiency-dissipation relations in linear thermodynamics," *Physical review letters*, vol. 116, no. 22, p. 220601, 2016.

[59] Z. Tu, "Efficiency at maximum power of feynman's ratchet as a heat engine," *Journal of Physics A: Mathematical and Theoretical*, vol. 41, no. 31, p. 312003, 2008.

[60] S. Ciliberto, "Experiments in stochastic thermodynamics: Short history and perspectives," *Physical Review X*, vol. 7, no. 2, p. 021051, 2017.

[61] M. V. S. Bonança, "Approaching carnot efficiency at maximum power in linear response regime," *Journal of Statistical Mechanics: Theory and Experiment*, vol. 2019, p. 123203, dec 2019.

[62] B. Rutten, M. Esposito, and B. Cleuren, "Reaching optimal efficiencies using nanosized photoelectric devices," *Physical Review B*, vol. 80, no. 23, p. 235122, 2009.

[63] K. Proesmans and C. Van den Broeck, "The underdamped brownian duet and stochastic linear irreversible thermodynamics," *Chaos: An Interdisciplinary Journal of Nonlinear Science*, vol. 27, no. 10, p. 104601, 2017.

[64] K. Proesmans, Y. Dreher, M. c. v. Gavrilov, J. Bechhoefer, and C. Van den Broeck, "Brownian duet: A novel tale of thermodynamic efficiency," *Phys. Rev. X*, vol. 6, p. 041010, Oct 2016.

[65] I. A. Martínez, É. Roldán, L. Dinis, D. Petrov, J. M. Parrondo, and R. A. Rica, "Brownian carnot engine," *Nature physics*, vol. 12, no. 1, pp. 67–70, 2016.

[66] V. Blickle and C. Bechinger, "Realization of a micrometre-sized stochastic heat engine," *Nature Physics*, vol. 8, no. 2, pp. 143–146, 2012.

[67] P. A. Quinto-Su, "A microscopic steam engine implemented in an optical tweezer," *Nature communications*, vol. 5, no. 1, pp. 1–7, 2014.

[68] S. Krishnamurthy, S. Ghosh, D. Chatterji, R. Ganapathy, and A. Sood, "A micrometre-sized heat engine operating between bacterial reservoirs," *Nature Physics*, vol. 12, no. 12, pp. 1134–1138, 2016.

[69] A. Kumar and J. Bechhoefer, "Nanoscale virtual potentials using optical tweezers," *Applied Physics Letters*, vol. 113, no. 18, p. 183702, 2018.

[70] M. Esposito, R. Kawai, K. Lindenberg, and C. Van den Broeck, "Efficiency at maximum power of low-dissipation carnot engines," *Phys. Rev. Lett.*, vol. 105, p. 150603, Oct 2010.

[71] T. Schmiedl and U. Seifert, "Optimal finite-time processes in stochastic thermodynamics," *Phys. Rev. Lett.*, vol. 98, p. 108301, Mar 2007.

[72] N. Pancotti, M. Scandi, M. T. Mitchison, and M. Perarnau-Llobet, "Speed-ups to isothermality: Enhanced quantum thermal machines through control of the system-bath coupling," *Phys. Rev. X*, vol. 10, p. 031015, Jul 2020.

[73] N. Piccione, G. De Chiara, and B. Bellomo, "Power maximization of two-stroke quantum thermal machines," *Phys. Rev. A*, vol. 103, p. 032211, Mar 2021.

[74] P. Abiuso and M. Perarnau-Llobet, "Optimal cycles for low-dissipation heat engines," *Phys. Rev. Lett.*, vol. 124, p. 110606, Mar 2020.

[75] A. L. L. Stable, C. E. F. Noa, W. G. C. Oropesa, and C. E. Fiore, "Thermodynamics of collisional models for brownian particles: General properties and efficiency," *Phys. Rev. Research*, vol. 2, p. 043016, Oct 2020.

[76] C. H. Bennett, "The thermodynamics of computation—a review," *International Journal of Theoretical Physics*, vol. 21, no. 12, pp. 905–940, 1982.

[77] K. Maruyama, F. Nori, and V. Vedral, "Colloquium: The physics of maxwell's demon and information," *Reviews of Modern Physics*, vol. 81, no. 1, p. 1, 2009.

[78] T. Sagawa, "Thermodynamic and logical reversibilities revisited," *Journal of Statistical Mechanics: Theory and Experiment*, vol. 2014, no. 3, p. P03025, 2014.

[79] S. Liepelt and R. Lipowsky, "Operation modes of the molecular motor kinesin," *Phys. Rev. E*, vol. 79, p. 011917, Jan 2009.

[80] B. Altaner, A. Wachtel, and J. Vollmer, "Fluctuating currents in stochastic thermodynamics. ii. energy conversion and nonequilibrium response in kinesin models," *Phys. Rev. E*, vol. 92, p. 042133, Oct 2015.

[81] J. M. Horowitz and M. Esposito, "Work producing reservoirs: Stochastic thermodynamics with generalized gibbs ensembles," *Phys. Rev. E*, vol. 94, p. 020102, Aug 2016.

[82] P. E. Harunari, F. S. Filho, C. E. Fiore, and A. Rosas, "Maximal power for heat engines: Role of asymmetric interaction times," *Phys. Rev. Research*, vol. 3, p. 023194, Jun 2021.

[83] T. Feldmann and R. Kosloff, "Performance of discrete heat engines and heat pumps in finite time," *Phys. Rev. E*, vol. 61, pp. 4774–4790, May 2000.

[84] V. Holubec and A. Ryabov, "Cycling tames power fluctuations near optimum efficiency," *Phys. Rev. Lett.*, vol. 121, p. 120601, Sep 2018.

[85] H. Vroylandt, M. Esposito, and G. Verley, "Collective effects enhancing power and efficiency," *EPL (Europhysics Letters)*, vol. 120, p. 30009, nov 2017.

[86] I. N. Mamede, P. E. Harunari, B. A. N. Akasaki, K. Proesmans, and C. E. Fiore, "Obtaining efficient thermal engines from interacting brownian particles under time-periodic drivings," *Phys. Rev. E*, vol. 105, p. 024106, Feb 2022.

[87] D. Guéry-Odelin, A. Ruschhaupt, A. Kiely, E. Torrontegui, S. Martínez-Garaot, and J. G. Muga, "Shortcuts to adiabaticity: Concepts, methods, and applications," *Rev. Mod. Phys.*, vol. 91, p. 045001, Oct 2019.

[88] S. Deffner and M. V. Bonança, "Thermodynamic control—an old paradigm with new applications," *EPL (Europhysics Letters)*, vol. 131, no. 2, p. 20001, 2020.

[89] X.-H. Zhao, Z.-N. Gong, and Z. C. Tu, "Low-dissipation engines: Microscopic construction via shortcuts to adiabaticity and isothermality, the optimal relation between power and efficiency," Dec 2022.

[90] G. A. Forão, F. Filho, D. M. Busiello, B. Cleuren, C. E. Fiore, *et al.*, "Powerful ordered collective heat engines," *arXiv preprint arXiv:2301.06591*, 2023.

[91] P. A. Erdman, A. Rolandi, P. Abiuso, M. Perarnau-Llobet, and F. Noé, "Pareto-optimal cycles for power, efficiency and fluctuations of quantum heat engines using reinforcement learning," *Phys. Rev. Res.*, vol. 5, p. L022017, Apr 2023.

[92] A. Rosas, C. Van den Broeck, and K. Lindenberg, "Stochastic thermodynamics for a periodically driven single-particle pump," *Phys. Rev. E*, vol. 96, p. 052135, Nov 2017.

[93] A. Rosas, C. Van den Broeck, and K. Lindenberg, "Three-stage stochastic pump: Another type of onsager-casimir symmetry and results far from equilibrium," *Phys. Rev. E*, vol. 97, p. 062103, Jun 2018.

[94] C. E. F. Noa, A. L. L. Stable, W. G. C. Oropesa, A. Rosas, and C. E. Fiore, "Efficient asymmetric collisional brownian particle engines," *Phys. Rev. Research*, vol. 3, p. 043152, Dec 2021.

[95] F. S. Filho, B. A. N. Akasaki, C. E. F. Noa, B. Cleuren, and C. E. Fiore, "Thermodynamics and efficiency of sequentially collisional brownian particles: The role of drivings," *Phys. Rev. E*, vol. 106, p. 044134, Oct 2022.

[96] E. Šubrt and P. Chvosta, "Exact analysis of work fluctuations in two-level systems," *Journal of Statistical Mechanics: Theory and Experiment*, vol. 2007, p. P09019, sep 2007.

[97] P. Chvosta, V. Holubec, A. Ryabov, M. Einax, and P. Maass, "Thermodynamics of two-stroke engine based on periodically driven two-level system," *Physica E: Low-dimensional Systems and Nanostructures*, vol. 42, no. 3, pp. 472–476, 2010. Proceedings of the international conference Frontiers of Quantum and Mesoscopic Thermodynamics FQMT '08.

[98] G. Verley, C. Van den Broeck, and M. Esposito, "Modulated two-level system: Exact work statistics," *Physical Review E*, vol. 88, p. 032137, 9 2013.

[99] P. E. Harunari, C. E. Fiore, and K. Proesmans, "Exact statistics and thermodynamic uncertainty relations for a periodically driven electron pump," *Journal of Physics A: Mathematical and Theoretical*, vol. 53, p. 374001, aug 2020.

[100] W. Khan, P. P. Potts, S. Lehmann, C. Thelander, K. A. Dick, P. Samuelsson, and V. F. Maisi, "Efficient and continuous microwave photoconversion in hybrid cavity-semiconductor nanowire double quantum dot diodes," *Nature communications*, vol. 12, no. 1, p. 5130, 2021.

[101] O. Kedem and S. R. Caplan, "Degree of coupling and its relation to efficiency of energy conversion," *Trans. Faraday Soc.*, vol. 61, pp. 1897–1911, 1965.

[102] L. P. Bettmann, M. J. Kewming, and J. Goold, "Thermodynamics of a continuously monitored double-quantum-dot heat engine in the repeated interactions framework," *Physical Review E*, vol. 107, no. 4, p. 044102, 2023.

[103] F. Ritort, "The nonequilibrium thermodynamics of small systems," *Comptes Rendus Physique*, vol. 8, no. 5, pp. 528–539, 2007. Work, dissipation, and fluctuations in nonequilibrium physics.

[104] M. Esposito, U. Harbola, and S. Mukamel, "Nonequilibrium fluctuations, fluctuation theorems, and counting statistics in quantum systems," *Reviews of Modern Physics*, vol. 81, pp. 1665–1702, 12 2009.

[105] G. E. Crooks, "Nonequilibrium Measurements of Free Energy Differences for Microscopically Reversible Markovian Systems," *Journal of Statistical Physics*, vol. 90, pp. 1481–1487, 1998.

[106] M. Campisi, P. Hänggi, and P. Talkner, "Colloquium: Quantum fluctuation relations: Foundations and applications," *Reviews of Modern Physics*, vol. 83, pp. 771–791, 7 2011.

[107] P. Pietzonka, A. C. Barato, and U. Seifert, "Universal bounds on current fluctuations," *Physical Review E*, vol. 93, p. 052145, 2016.

[108] T. R. Gingrich, J. M. Horowitz, N. Perunov, and J. L. England, "Dissipation Bounds All Steady-State Current Fluctuations," *Physical Review Letters*, vol. 116, no. 12, p. 120601, 2016.

[109] P. Pietzonka, F. Ritort, and U. Seifert, "Finite-time generalization of the thermodynamic uncertainty relation," *Physical Review E*, vol. 96, no. 1, p. 012101, 2017.

[110] P. Pietzonka and U. Seifert, "Universal trade-off between power, efficiency and constancy in steady-state heat engines," *Physical Review Letters*, vol. 120, no. 19, p. 190602, 2017.

[111] K. Kinosita, R. Yasuda, H. Noji, and K. Adachi, "A rotary molecular motor that can work at near 100% efficiency," *Philosophical Transactions of the Royal Society of London. Series B: Biological Sciences*, vol. 355, no. 1396, pp. 473–489, 2000.

[112] S. Liepelt and R. Lipowsky, "Kinesin's network of chemomechanical motor cycles," *Phys. Rev. Lett.*, vol. 98, p. 258102, Jun 2007.

[113] A. Lau, D. Lacoste, and K. Mallick, "Nonequilibrium fluctuations and mechanochemical couplings of a molecular motor," *Physical review letters*, vol. 99, no. 15, p. 158102, 2007.

[114] J. V. Koski, V. F. Maisi, J. P. Pekola, and D. V. Averin, "Experimental realization of a szilard engine with a single electron," *Proceedings of the National Academy of Sciences*, vol. 111, no. 38, pp. 13786–13789, 2014.

[115] S. Toyabe, T. Sagawa, M. Ueda, E. Muneyuki, and M. Sano, "Experimental demonstration of information-to-energy conversion and validation of the generalized jarzynski equality," *Nature physics*, vol. 6, no. 12, pp. 988–992, 2010.

[116] P. Pietzonka and U. Seifert, "Universal trade-off between power, efficiency, and constancy in steady-state heat engines," *Phys. Rev. Lett.*, vol. 120, p. 190602, May 2018.

[117] T. Denzler and E. Lutz, "Power fluctuations in a finite-time quantum carnot engine," *arXiv preprint arXiv:2007.01034*, 2020.

[118] G. Verley, T. Willaert, C. Van den Broeck, and M. Esposito, "Universal theory of efficiency fluctuations," *Physical Review E*, vol. 90, no. 5, p. 052145, 2014.

[119] M. Polettini, G. Verley, and M. Esposito, "Efficiency statistics at all times: Carnot limit at finite power," *Physical review letters*, vol. 114, no. 5, p. 050601, 2015.

[120] T. Denzler and E. Lutz, "Efficiency fluctuations of a quantum heat engine," *Phys. Rev. Research*, vol. 2, p. 032062, Sep 2020.

[121] M. Esposito and C. Van Den Broeck, "Three faces of the second law. I. Master equation formulation," *Physical Review E - Statistical, Nonlinear, and Soft Matter Physics*, vol. 82, p. 011143, 2010.

[122] C. Van den Broeck and M. Esposito, "Three faces of the second law. II. Fokker-Planck formulation," *Physical Review E*, vol. 82, p. 011144, 7 2010.

[123] J. Marro and R. Dickman, *Nonequilibrium Phase Transitions in Lattice Models*. Cambridge: Cambridge University Press, 1st ed., 1999.

[124] T. Herpich and M. Esposito, "Universality in driven potts models," *Physical Review E*, vol. 99, no. 2, p. 022135, 2019.

[125] B. O. Goes, C. E. Fiore, and G. T. Landi, "Quantum features of entropy production in driven-dissipative transitions," *Physical Review Research*, vol. 2, no. 1, p. 013136, 2020.

[126] P. S. Shim, H. M. Chun, and J. D. Noh, "Macroscopic time-reversal symmetry breaking at a nonequilibrium phase transition," *Physical Review E*, vol. 93, p. 012113, 2016.

[127] L. Crochik and T. Tomé, "Entropy production in the majority-vote model," *Physical Review E - Statistical, Nonlinear, and Soft Matter Physics*, vol. 72, p. 057103, 2005.

[128] Y. Zhang and A. C. Barato, "Critical behavior of entropy production and learning rate: Ising model with an oscillating field," *Journal of Statistical Mechanics: Theory and Experiment*, vol. 2016, p. 113207, 2016.

[129] T. Herpich, J. Thingna, and M. Esposito, "Collective power: minimal model for thermodynamics of nonequilibrium phase transitions," *Physical Review X*, vol. 8, no. 3, p. 031056, 2018.

[130] B. Nguyen and U. Seifert, "Exponential volume dependence of entropy-current fluctuations at first-order phase transitions in chemical reaction networks," *Physical Review E*, vol. 102, p. 022101, 8 2020.

[131] L. Levitov and G. Lesovik, "Charge distribution in quantum shot noise," *JETP letters*, vol. 58, no. 3, pp. 230–235, 1993.

[132] C. Flindt, C. Fricke, F. Hohls, T. Novotny, K. Netocny, T. Brandes, and R. J. Haug, "Universal oscillations in counting statistics," *Proceedings of the National Academy of Sciences*, vol. 106, pp. 10116–10119, 6 2009.

[133] H. Touchette, "The large deviation approach to statistical mechanics," *Physics Reports*, vol. 478, no. 1-3, pp. 1–69, 2009.

[134] Z. Koza, "General technique of calculating the drift velocity and diffusion coefficient in arbitrary periodic systems," *Journal of Physics A: Mathematical and General*, vol. 32, pp. 7637–7651, 11 1999.

[135] F. Baras, M. M. Mansour, and J. E. Pearson, "Microscopic simulation of chemical bistability in homogeneous systems," *The Journal of Chemical Physics*, vol. 105, pp. 8257–8261, 11 1996.

[136] C. E. Fiore, P. E. Harunari, C. E. F. Noa, and G. T. Landi, "Current fluctuations in nonequilibrium discontinuous phase transitions," *Phys. Rev. E*, vol. 104, p. 064123, Dec 2021.

[137] P. E. Harunari, M. M. de Oliveira, and C. E. Fiore, "Partial inertia induces additional phase transition in the majority vote model," *Phys. Rev. E*, vol. 96, p. 042305, Oct 2017.

[138] D. Landau and K. Binder, *A guide to Monte Carlo simulations in statistical physics*. Cambridge university press, 2021.

[139] N. G. van Kampen, *Stochastic Processes in Physics and Chemistry*. North-Holland Personal Library, 2007.

[140] P. Hanggi, H. Grabert, P. Talkner, and H. Thomas, "Bistable systems: Master equation versus fokker-planck modeling," *Physical Review A*, vol. 29, no. 1, p. 371, 1984.

[141] M. Esposito, U. Harbola, and S. Mukamel, "Entropy fluctuation theorems in driven open systems: Application to electron counting statistics," *Phys. Rev. E*, vol. 76, p. 031132, Sep 2007.

[142] A. Imparato and L. Peliti, "The distribution function of entropy flow in stochastic systems," vol. 2007, pp. L02001–L02001, feb 2007.

[143] P. Pietzonka, K. Kleinbeck, and U. Seifert, "Extreme fluctuations of active brownian motion," *New Journal of Physics*, vol. 18, p. 052001, may 2016.

[144] M. Vellela and H. Qian, "Stochastic dynamics and non-equilibrium thermodynamics of a bistable chemical system: The Schlögl model revisited," *Journal of the Royal Society Interface*, vol. 6, no. 39, pp. 925–940, 2009.

[145] F. Y. Wu, "The potts model," *Rev. Mod. Phys.*, vol. 54, pp. 235–268, Jan 1982.

[146] D. Kim, "1/q-expansion for the magnetization discontinuity of potts model in two dimensions," *Physics Letters A*, vol. 87, no. 3, pp. 127–129, 1981.

[147] R. Baxter, "Magnetisation discontinuity of the two-dimensional potts model," *Journal of Physics A: Mathematical and General*, vol. 15, no. 10, p. 3329, 1982.

[148] C. E. Fiore and M. G. E. da Luz, "Exploiting a semi-analytic approach to study first order phase transitions," *The Journal of Chemical Physics*, vol. 138, no. 1, p. 014105, 2013.

[149] C. E. Fiore and M. G. E. da Luz, "General approach for studying first-order phase transitions at low temperatures," *Phys. Rev. Lett.*, vol. 107, p. 230601, Nov 2011.

[150] T. Martynec, S. H. L. Klapp, and S. A. M. Loos, "Entropy production at criticality in a nonequilibrium potts model," *New Journal of Physics*, vol. 22, p. 093069, sep 2020.

[151] M. S. S. Challa, D. P. Landau, and K. Binder, "Finite-size effects at temperature-driven first-order transitions," *Phys. Rev. B*, vol. 34, pp. 1841–1852, Aug 1986.

[152] M. M. de Oliveira, M. G. E. da Luz, and C. E. Fiore, "Finite-size scaling for discontinuous nonequilibrium phase transitions," *Phys. Rev. E*, vol. 97, p. 060101, Jun 2018.

[153] L. Bertini, R. Chetrite, A. Faggionato, and D. Gabrielli, "Level 2.5 Large Deviations for Continuous-Time Markov Chains with Time Periodic Rates," *Annales Henri Poincaré*, vol. 19, pp. 3197–3238, 10 2018.

[154] H. Vroylandt, M. Esposito, and G. Verley, "Efficiency fluctuations of stochastic machines undergoing a phase transition," *Phys. Rev. Lett.*, vol. 124, p. 250603, Jun 2020.

[155] I. N. Mamede, A. L. L. Stable, and C. E. Fiore, "Obtaining efficient collisional engines via velocity-dependent drivings," *Phys. Rev. E*, vol. 106, p. 064125, Dec 2022.

[156] C. E. Fernandez Noa, C. E. Fiore, F. F. S. Filho, B. Wijns, and B. Cleuren, "Thermodynamics of a collisional quantum-dot machine: the role of stages," *arXiv e-prints*, p. arXiv:2305.03813, May 2023.